

Branes, Quivers, and the Affine Grassmannian

Antoine Bourget,[♮] Julius F. Grimminger,[♮] Amihay Hanany,[♮] Marcus Sperling,[♮] and Zhenghao Zhong[♮]

[♮]*Theoretical Physics Group, The Blackett Laboratory, Imperial College London, Prince Consort Road London, SW7 2AZ, UK*

[♮]*Yau Mathematical Sciences Center, Tsinghua University, Haidian District, Beijing, 100084, China*

E-mail: a.bourget@imperial.ac.uk, julius.grimminger17@imperial.ac.uk,
a.hanany@imperial.ac.uk, marcus.sperling@univie.ac.at,
zhenghao.zhong14@imperial.ac.uk

ABSTRACT: Brane systems provide a large class of gauge theories that arise in string theory. This paper demonstrates how such brane systems fit with a somewhat exotic geometric object, called the affine Grassmannian. This gives a strong motivation to study physical aspects of the affine Grassmannian. Explicit quivers are presented throughout the paper, and a quiver addition algorithm to generate the affine Grassmannian is introduced. An important outcome of this study is a set of quivers for new elementary slices.

Contents

1	Introduction	1
2	The Affine Grassmannian	5
2.1	Formal power series	5
2.2	Groups valued in formal power series	6
2.3	Lattices and the Affine Grassmannian	7
2.4	Explicit description of the $\mathrm{SL}(2, \mathbb{C})$ and $\mathrm{PSL}(2, \mathbb{C})$ affine Grassmannians	8
2.5	Orbits in the Affine Grassmannian	10
2.6	Slices in the affine Grassmannian	12
3	Quivers and Hasse diagrams	14
3.1	General formula for slices	16
3.2	Hasse diagrams for Affine Grassmannians at ranks 1 and 2	17
3.3	Quivers for Quasi-Minimal Singularities	31
4	Branes	34
4.1	The A -type affine Grassmannian	35
4.1.1	The A_1 affine Grassmannian	38
4.1.2	The A_2 affine Grassmannian	40
4.2	The B -type affine Grassmannian	43
4.2.1	The B_1 affine Grassmannian	45
4.2.2	The B_2 affine Grassmannian	46
4.3	The C -type affine Grassmannian	49
4.3.1	The C_1 affine Grassmannian	50
4.3.2	The C_2 affine Grassmannian	52
4.4	The D -type affine Grassmannian	55
4.4.1	The D_2 affine Grassmannian	57
5	Quiver addition	63
5.1	Algorithm	63
5.2	Examples with simply laced quivers	65
5.3	Examples with non simply laced quivers	69
6	Hilbert series of transverse slices	69
6.1	Hilbert series for infinite-dimensional transverse slices	69
6.2	A note on Infinity	74
7	Outlook	75

A	Branes, ON Planes and Quivers	76
A.1	ON^+	80
A.2	ON^-	80
A.3	$\widetilde{\text{ON}}^-$	81
A.4	Leaf Closures and Transverse Slices in Brane Systems	82

1 Introduction

Branes play a crucial role in our current understanding of string theory. Their world-volume low energy effective action has been occupying numerous papers and is still used as an essential tool in studying a whole variety of string backgrounds. Furthermore, the existence of brane systems opens up a window to the study of theories when an effective Lagrangian either does not exist or is beyond reach. This again increases the level of understanding in a significant way.

This paper is devoted to yet another conceptual advancement in the study of brane systems in string theory. It has to do with a somewhat exotic object – and so far less studied within the string theory community – the affine Grassmannian [1–6]. This object plays a prominent role in the so-called geometric Satake correspondence in the geometric Langlands program [7, 8], which is partly responsible for the considerable interest it has attracted in mathematics in the past two decades. A close inspection reveals that the affine Grassmannian is also precisely the type of object one should study when trying to understand brane systems, hence making it an important element in physical systems.

As is argued below, brane systems of the type of Hanany-Witten setups [9] fit into the affine Grassmannian, and they do so in a host of space-time dimensions ranging from 6 to 3, and possibly even lower. A definition of the affine Grassmannian, suitable to a physics audience is presented below, together with examples and explanations. Special attention is paid to slices in the affine Grassmannian [10–12] which turn out to fit with the physical setting, namely each slice is a moduli space vacua of an interacting theory, with or without a Lagrangian; or viewed from the brane perspective, a Kraft-Procesi transition [13, 14] between two phases of the brane system [15, 16]. The connection between Coulomb branches viewed as moduli spaces of singular monopoles [9, 17–19] and slices in the affine Grassmannians was made in [12, 20, 21], using previous developments [22–28]. The mathematical properties of the slices in connection with symplectic geometry and the relation with quiver theories have been further studied in [11, 29–31].

We note that so far we do not have a brane construction for the affine Grassmannian of exceptional groups. Slices in these affine Grassmannians can nevertheless be studied using quivers. This involves a new algorithm of quiver addition, which is explained in detail below.

Let us turn to Hasse diagrams [32]. Hasse diagrams are a depiction of a partial order. They are a useful tool for characterizing the phase structure of a given theory. In such diagrams, consisting of nodes connected by edges, each node represents a fixed set of

massless states of the physical system. Tuning moduli without moving to a different phase corresponds to changing the effective masses of massive particles, while keeping the set of massless states fixed. When the set of massless states of one phase, call it phase a , is contained in the set of massless states of another phase, call it phase b , we assign the order $b < a$. Suppose there exists no phase c such that $b < c < a$ then a and b are connected by an edge due to the partial order $b < a$. The edge connecting node a to node b represents the minimal set of moduli one needs to tune in order to move from phase a to phase b . The tuned moduli form a conical singularity and supersymmetry dictates the type of such a singularity. For $3d \mathcal{N} = 4$ Coulomb branches, and Higgs branches of theories with 8 supercharges in dimensions 3 – 6, this singularity is a symplectic singularity [33], or a hyper Kähler cone – as more commonly referred to in the physics literature.

As Hasse diagrams for moduli spaces are composed of nodes and edges, it is natural to put some additional structure by embedding such a diagram into a lattice. Indeed, it is one of the features of the affine Grassmannian of a Lie group G , that the Hasse diagram for any slice originates from such a lattice, making the conceptual understanding of such Hasse diagram much easier. The leaves of the affine Grassmannian (called Schubert cells)¹ are in one-to-one correspondence with dominant coweights. Transverse slices between two leaves are in one-to-one correspondence with lattice vectors that connect one node to another. These lattice vectors, in turn, are spanned by positive coroots, and if the linear combination is non-negative then there exists a directed path between one point and another; hence, inducing a natural partial order in the lattice [34]. Therefore, slices in the affine Grassmannian are particularly nice, as their Hasse diagrams can be understood as all directed paths between two points in the principal Weyl chamber. The fact that this structure fits beautifully with brane systems is not surprising, as brane systems can be viewed as algebraic objects. This just emphasizes the point that slices in the affine Grassmannian form very interesting physical systems. The stratification of the slices in the affine Grassmannian into symplectic leaves can be related to monopole bubbling [35–38].

The simplest affine Grassmannian is that of $\mathrm{SL}(2, \mathbb{C})$, where the Hasse diagram is a semi infinite linear diagram. Each slice in the affine Grassmannian of $\mathrm{SL}(2, \mathbb{C})$ is an SQCD type moduli space (specifically its Coulomb branch) with a unitary gauge group as opposed to special unitary. Hasse diagrams of SQCD theories were already shown to be linear in [32, Table 1]. One important point made in the present paper is that this line is actually connecting two points on the principal Weyl chamber of $\mathrm{SL}(2, \mathbb{C})$. It is reassuring to see that for the simplest possible, and most studied, gauge theories – SQCD – there is a correspondence with the simplest possible affine Grassmannian – the affine Grassmannian of $\mathrm{SL}(2, \mathbb{C})$. If one identifies SQCD theories with the more mathematical name, framed A_1 quiver theories, then it is easy to see the generalization. A slice in the affine Grassmannian of the group G is given by the Coulomb branch of a framed Dynkin diagram of type G .

It is useful to introduce a simple characterisation of a moduli space by an integer number, for example the dimension or the number of leaves. A new measure of the simplicity

¹We note that these Schubert cells may be of odd complex dimension, and their closure hence not a symplectic singularity. The transverse slice between two Schubert cells, however, is a symplectic singularity.

of a moduli space is given by the following integer number: For a generic moduli space \mathcal{M} with a Hasse diagram \mathfrak{H} one can define the *disposition*² $\mathfrak{D}(n)$ of a node $n \in \mathfrak{H}$ as the number of minimal degenerations of the corresponding leaf,

$$\mathfrak{D}(n) = \text{number of minimal degenerations of } n. \quad (1.1)$$

One can further define the disposition $\mathfrak{D}(\mathcal{M})$ of a moduli space as the maximal disposition over all nodes in its Hasse diagram,

$$\mathfrak{D}(\mathcal{M}) = \max_{n \in \mathfrak{H}} (\mathfrak{D}(n)) . \quad (1.2)$$

One would say that a moduli space with a smaller disposition is simpler than a moduli space with a bigger disposition. The disposition of the affine Grassmannian is the rank of the group. The disposition of a slice in the affine Grassmannian is hence bounded from above by the rank of G . The disposition of the Coulomb branch or Higgs branch of SQCD is 1; the lowest possible. The disposition of the entire moduli space of SQCD is 2. In general it is much easier to obtain and generalise Hasse diagrams with a low disposition. However, Hasse diagrams for slices in the affine Grassmannian can be well understood due to their embedding into the coweight lattice, even when the disposition is very high.

Another important integer number is the minimal number of generators of the chiral ring, call it g . A striking feature of any slice in the affine Grassmannian of a group G is the fact that $g/\dim(G)$ is again an integer number.

One should further make a distinction between finite dimensional Lie groups and infinite dimensional generalizations. By analogy with the finite dimensional case, one would identify (the Coulomb branch of) a framed affine quiver with a slice in the affine Grassmannian of the affine Lie group. Naturally, the structure of the moduli space, and consequently its Hasse diagram, become significantly more complex. The disposition for a generic slice in the affine Grassmannian of an affine group appears not to be bounded from above. Consequently, if the group is infinite dimensional one expects a much more complicated moduli space than that of a finite dimensional group. Prominent examples of slices in the affine Grassmannian of affine groups are moduli spaces of instantons. While they are well studied spaces in physics, we see that they are much more challenging objects than slices in the affine Grassmannian of finite groups.

The present paper focuses on slices in the affine Grassmannian of a finite dimensional Lie group, which in this sense are simpler than moduli spaces of instantons. This is reflected in several ways. Many of the slices are complete intersections. Many of these are closures of nilpotent orbits. The generators of the chiral ring are simple and, as argued above, the Hasse diagram for slices of algebras of finite type is simpler than the Hasse diagram for the moduli space of instantons. These features make these moduli spaces more tractable objects and, hence, simpler to study.

In the long run, the lessons learned from the affine Grassmannian of finite dimensional groups will hopefully help us to tackle more difficult moduli spaces.

²We propose the name disposition to mean the tendency of the theory to gain more massless states in several inequivalent ways.

Slice	Framed quiver	Unframed quiver
a_n		
b_n		
c_n		
d_n		
e_6		
e_7		
e_8		

Slice	Framed quiver	Unframed quiver
f_4		
g_2		
ac_n		
ag_2		
cg_2		
$h_{n,k}$		
$\bar{h}_{n,k}$		
A_n		

Table 1. Most up-to-date, but incomplete list of unitary quivers without loops for elementary slices usable in the quiver subtraction algorithm. In each case we provide two quivers, a framed version and an equivalent unframed version, where a $U(1)$ should be ungauged on the long node. For a_n , b_n , c_n , d_n , ac_n , $h_{n,k}$ and $\bar{h}_{n,k}$ there are n gauge nodes in the framed quiver and $n + 1$ gauge nodes in the unframed quiver. Notice that $h_{n,1} = \mathbb{H}^n$, $h_{n,2} = c_n$, $h_{2,3} = cg_2$, $\bar{h}_{n,1} = a_n$, $\bar{h}_{n,2} = ac_n$, and $\bar{h}_{2,3} = ag_2$.

A nice by-product of studying the affine Grassmannian is the encounter of the so-called *quasi-minimal singularities* introduced in [10], which are elementary slices that do not appear in the study of nilpotent orbits. This is an important update to our arsenal of quivers to be used in quiver subtraction. We display all unitary quivers without loops which we know to be elementary slices in Table 1. The classification of these slices is still an open problem, and every new addition is hence very exciting.

Plan of the paper In Section 2, we provide a lightening review of the construction of the affine Grassmannian, and put forward the important concepts of orbits, stratification and transverse slices. In Section 3, we construct quivers for the transverse slices and compute them explicitly for rank 1 and 2 groups, along with the Hasse diagrams. This allows to identify new quivers for the quasi-minimal singularities. We then show how this construction can be reproduced using brane setups with orientifolds for the classical groups in Section 4, and for any group using the new algorithm of quiver addition in Section 5. Finally, we end with an analysis of the generators of the infinite dimensional transverse slices using Hilbert series in Section 6.

2 The Affine Grassmannian

In this section, we give the definitions that apply to the discussions in this paper. Our notations are summarized at the end of this section in Table 3.

Our description tries to avoid excessive technicalities as it is aimed at physicists primarily. For instance, we describe the affine Grassmannian as an infinite dimensional variety and not as an ind-scheme; we also identify schemes with their underlying topological space. For a more formal treatment, we refer to [1, 39–43]. A summary of the main properties of the affine Grassmannian is presented in [22, Section 2]. For a very explicit treatment with examples, see [44, 45]. For an introduction in the context of gauge theory, see [46, 47].

2.1 Formal power series

We define three important structures that underlie all the construction of the affine Grassmannian, reviewed below. We use throughout a formal variable t .

- First, we have the ring of formal power series in t , denoted $\mathbb{C}[[t]]$. Here formal means that we do not worry about convergence issues. For examples of elements of $\mathbb{C}[[t]]$, let us mention the polynomials in t , the rational functions like $\frac{1}{1-t} = \sum_{i=0}^{\infty} t^i$, transcendental functions like $e^t = \sum_{i=0}^{\infty} t^i/i!$, or non-convergent series like $\sum_{i=0}^{\infty} t^i i!$. Note that the important condition is that an element of $\mathbb{C}[[t]]$ is a formal series in t with only non-negative powers of t . Geometrically, $\mathbb{C}[[t]]$ can be seen as the ring of functions on the unit complex disk $D = \{z \in \mathbb{C} \mid |z| < 1\}$. Equivalently, the unit disk D is the spectrum of $\mathbb{C}[[t]]$.
- The second object we consider is the ring of polynomials in t^{-1} , denoted $\mathbb{C}[t^{-1}]$. We draw the attention of the reader on two differences with $\mathbb{C}[[t]]$: here the powers of t are ≤ 0 , and the series expansion needs to terminate (a polynomial has a finite degree).

- Finally, we need the field of fractions of $\mathbb{C}[[t]]$, denoted $\mathbb{C}((t))$. This can be defined as the set of all fractions $f(t)/g(t)$ for $f(t), g(t) \in \mathbb{C}[[t]]$ with $g(t) \neq 0$. Equivalently, this is the set of formal series that can be written in the form $\sum_{i=N}^{\infty} a_i t^i$ for some $N \in \mathbb{Z}$ and $a_i \in \mathbb{C}$. The spectrum of $\mathbb{C}((t))$ is the punctured disk $D^* = \{z \in \mathbb{C} \mid 0 < |z| < 1\}$.

The ring $\mathbb{C}[[t]]$ is a *discrete valuation ring*, where the valuation is given by the degree of the lowest non-zero monomial. More generally for

$$f = \sum_{i=N}^{\infty} f_i t^i \in \mathbb{C}((t)) \quad (2.1)$$

with $N \in \mathbb{Z}$ and $f_N \neq 0$, the valuation is $\nu(f) = N$. As the name indicates, $\mathbb{C}((t))$ is a field, so every non-zero element is invertible. We remark that $\mathbb{C}[[t]]$ is the ring of integers of $\mathbb{C}((t))$, and that the multiplicative group $\mathbb{C}[[t]]^*$ of invertible elements in $\mathbb{C}[[t]]$ is

$$\mathbb{C}[[t]]^* = \left\{ \sum_{i=0}^{\infty} a_i t^i \mid a_i \in \mathbb{C} \text{ and } a_0 \neq 0 \right\}. \quad (2.2)$$

Finally, the only invertible elements in $\mathbb{C}[t^{-1}]$ are the non-zero constants.

2.2 Groups valued in formal power series

The groups $G((t))$

For any characteristic 0 field K , $\mathrm{GL}(n, K)$ is the group of invertible $n \times n$ matrices with entries in K . As mentioned in the previous subsection, $\mathbb{C}((t))$ is a field and we can use it to consider the group $\mathrm{GL}(n, \mathbb{C}((t)))$ of invertible $n \times n$ matrices with entries in $\mathbb{C}((t))$. Such a matrix is invertible if and only if its determinant is not identically zero. More generally, let G be an algebraic subgroup of $\mathrm{GL}(n, \mathbb{C})$, which means that

$$G = \{M \in \mathrm{GL}(n, \mathbb{C}) \mid P_j(M) = 0\} \quad (2.3)$$

for a certain collection of polynomials P_j , $j = 1, \dots, J$. This includes the classical groups $\mathrm{SL}(n, \mathbb{C})$, $\mathrm{SO}(n, \mathbb{C})$, $\mathrm{Sp}(2n, \mathbb{C})$,³ and also the exceptional groups. We then define

$$G((t)) := \{M \in \mathrm{GL}(n, \mathbb{C}((t))) \mid P_j(M) = 0\}. \quad (2.4)$$

Example For $G = \mathrm{SL}(2, \mathbb{C})$, we have

$$G((t)) := \left\{ \begin{pmatrix} a(t) & b(t) \\ c(t) & d(t) \end{pmatrix} \mid a(t), b(t), c(t), d(t) \in \mathbb{C}((t)) \text{ and } a(t)d(t) - b(t)c(t) = 1 \right\}. \quad (2.5)$$

³Note that $\mathrm{Sp}(2n, \mathbb{C})$ denotes the symplectic group of rank n over the complex numbers.

The groups $G[[t]]$ and $G[t^{-1}]$

We can mimic this construction with $\mathbb{C}((t))$ replaced with $\mathbb{C}[[t]]$. One can consider the group $\mathrm{GL}(n, \mathbb{C}[[t]])$ of matrices with coefficients in $\mathbb{C}[[t]]$ and which are invertible in $\mathbb{C}[[t]]$. Note that a necessary and sufficient condition for this to be the case is that the determinant should belong to $\mathbb{C}[[t]]^*$, i.e. have a series expansion with non-zero coefficient of degree 0. Up to this subtlety, the definition of $G[[t]]$ goes exactly as before:

$$G[[t]] := \{M \in \mathrm{GL}(n, \mathbb{C}[[t]]) \mid P_j(M) = 0\}. \quad (2.6)$$

Similarly, one can construct $G[t^{-1}]$, bearing in mind that by the remark above $\mathrm{GL}(n, \mathbb{C}[t^{-1}])$ is characterized by the property that the determinant is a non-vanishing constant.

The groups $G_1[t^{-1}]$

Finally, we define

$$G_1[t^{-1}] := \{M \in G[t^{-1}] \mid M|_{t \rightarrow \infty} = \mathbf{1}\}. \quad (2.7)$$

In other words, $G_1[t^{-1}]$ is the subgroup of $G[t^{-1}]$ where the degree 0 term in the series expansion of the elements are the identity matrix.

2.3 Lattices and the Affine Grassmannian

In this section, we finally give the definition of the affine Grassmannian for the group G . This involves spaces of lattices, so we begin as a warm-up with a brief reminder about lattices.

Consider a vector space V of dimension n . A *lattice* in V is a discrete subgroup of V which is isomorphic to \mathbb{Z}^n . One way to construct a lattice explicitly is as follows: pick a basis (v_1, \dots, v_n) of V , and consider the set of all linear combinations with integer coefficients:

$$\mathcal{L} = \left\{ \sum_{i=1}^n a_i v_i \mid a_i \in \mathbb{Z} \right\}. \quad (2.8)$$

So a basis of V defines a unique lattice $\mathcal{L} \subset V$, but the converse is not true: many different bases give the same lattice. Two bases correspond to the same lattice if and only if one is obtained from the other by multiplication by a matrix in $\mathrm{GL}(n, \mathbb{Z})$, the set of invertible matrices with integer coefficients and whose inverse also has integer coefficients. On the other hand, the set of all bases of V can be identified with the set $\mathrm{GL}(n, \mathbb{R})$, once a reference basis is picked: one just writes the components of the basis vectors as *columns* of the matrix. We now turn to the crucial point of the argument: we have chosen to write the basis vectors as columns of the matrix $M \in \mathrm{GL}(n, \mathbb{R})$; then for any $P \in \mathrm{GL}(n, \mathbb{Z})$, the matrix MP corresponds to the same lattice, as the columns of MP are linear combinations with integer coefficients of the columns of M . However PM does not a priori give the same lattice! Therefore the set of inequivalent lattices is

$$\text{Set of inequivalent lattices in } V = \mathrm{GL}(n, \mathbb{R}) / \mathrm{GL}(n, \mathbb{Z}), \quad (2.9)$$

where the quotient is taken on the *right*. Multiplication on the *left* gives instead an action of $\mathrm{GL}(n, \mathbb{Z})$ on the set of lattices. In the context of the affine Grassmannian, it is this action which generates the orbits we are interested in.

We now repeat the above discussion but replace our base field \mathbb{R} by $\mathbb{C}((t))$ and the integers \mathbb{Z} by $\mathbb{C}[[t]]$. A *lattice* \mathcal{L} in $V = \mathbb{C}((t))^n$ is a free $\mathbb{C}[[t]]$ -submodule of rank n . A lattice is fully specified by a basis, in other words an $n \times n$ matrix of elements of $\mathbb{C}((t))$ with non-zero determinant, or equivalently a matrix in $\mathrm{GL}(n, \mathbb{C}((t)))$. We identify the basis vectors with the *columns* of the matrix. Multiplying such a matrix on the *right* by a matrix in $\mathrm{GL}(n, \mathbb{C}[[t]])$ gives a matrix representing the same lattice. On the other hand, multiplication on the *left* by a matrices in $\mathrm{GL}(n, \mathbb{C}[[t]])$ gives a family of possibly inequivalent lattices, that we call the *orbit* of the initial lattice. We can identify the set of lattices as the set of equivalence classes of elements of $\mathrm{GL}(n, \mathbb{C}((t)))$ with equivalence relation given by multiplication on the right by $\mathrm{GL}(n, \mathbb{C}[[t]])$.

Definition The affine Grassmannian Gr_G for the group $G = \mathrm{GL}(n, \mathbb{C})$ is, as a set, the set of all lattices in $\mathbb{C}((t))^n$. By the remark above, we have

$$\mathrm{Gr}_{\mathrm{GL}(n, \mathbb{C})} \simeq \mathrm{GL}(n, \mathbb{C}((t))) / \mathrm{GL}(n, \mathbb{C}[[t]]). \quad (2.10)$$

More generally, for a group G we define

$$\mathrm{Gr}_G \simeq G((t)) / G[[t]]. \quad (2.11)$$

This can be seen as an infinite dimensional variety. The group $G[[t]]$ acts on the left on the points of the affine Grassmannian Gr_G , thus generating *orbits*, which are Zariski open algebraic sets. The closure of the orbits are finite dimensional (generically singular) projective varieties.

2.4 Explicit description of the $\mathrm{SL}(2, \mathbb{C})$ and $\mathrm{PSL}(2, \mathbb{C})$ affine Grassmannians

In this subsection, we leave our general discussion to illustrate it with explicit computations at rank 1. Some of these computations can be found in [1, Proposition 2.6].

Points of $\mathrm{Gr}_{\mathrm{SL}(2, \mathbb{C})}$

In this paragraph, we set $G = \mathrm{SL}(2, \mathbb{C})$. The group $G((t))$ has been explicitly written in (2.5). A matrix in this set represents a lattice as:

$$\Lambda \left[\begin{pmatrix} a & b \\ c & d \end{pmatrix} \right] = \left\{ u(t) \begin{pmatrix} a(t) \\ c(t) \end{pmatrix} + v(t) \begin{pmatrix} b(t) \\ d(t) \end{pmatrix} \mid u, v \in G[[t]] \right\}. \quad (2.12)$$

For any matrix $R \in G[[t]]$, it is clear with this description that

$$\Lambda \left[\begin{pmatrix} a & b \\ c & d \end{pmatrix} \right] = \Lambda \left[\begin{pmatrix} a & b \\ c & d \end{pmatrix} R \right]. \quad (2.13)$$

The points in Gr_G are equivalence classes of matrices

$$M = \begin{pmatrix} a & b \\ c & d \end{pmatrix} \in G((t)) \quad \text{under} \quad M \sim MR, \quad R = \begin{pmatrix} \alpha & \beta \\ \gamma & \delta \end{pmatrix} \in G[[t]]. \quad (2.14)$$

This relation is non-trivial because R is restricted to lie in $G[[t]]$, so $\alpha(t)$, $\beta(t)$, $\gamma(t)$ and $\delta(t)$ can not have negative powers of t , while $a(t)$, $b(t)$, $c(t)$ and $d(t)$ may have negative powers. We can see this in action explicitly by trying to implement Gaussian elimination. Let us assume for definiteness that the most singular coefficient of M (the coefficient with lowest valuation) is d , and set $\lambda = -2\nu(d) \geq 0$ (recall that the valuation was defined below equation (2.1)). We can write $d = t^{-\lambda/2}d_0$ where $\nu(d_0) = 0$. The first step of Gaussian elimination uses

$$R_1 = \begin{pmatrix} d_0 & 0 \\ -ct^{\lambda/2} & d_0^{-1} \end{pmatrix} \in G[[t]] \quad \text{giving} \quad MR_1 = \begin{pmatrix} t^{\lambda/2} & bd_0^{-1} \\ 0 & t^{-\lambda/2} \end{pmatrix} \quad (2.15)$$

Then for the second step one can write

$$bd_0^{-1} = \left(\sum_{i=\nu(b)}^{\lambda/2-1} x_i t^i \right) + t^{\lambda/2} b' \quad (2.16)$$

where $\nu(b') \geq 0$, so that we obtain

$$R_2 = \begin{pmatrix} 1 & -b' \\ 0 & 1 \end{pmatrix} \in G[[t]] \quad \text{giving} \quad MR_1 R_2 = \begin{pmatrix} t^{\lambda/2} & \sum_{i=-\lambda/2}^{\lambda/2-1} x_i t^i \\ 0 & t^{-\lambda/2} \end{pmatrix} \quad (2.17)$$

So the points in Gr_G are parametrized by $\lambda \in 2\mathbb{N}$, and then for a given λ by λ complex numbers $(x_{-\lambda/2}, x_{-\lambda/2+1}, \dots, x_{\lambda/2-1})$.

Orbits

We now describe the orbits under the right action of $G[[t]]$. From the point of view of Gaussian elimination, this means we can now combine rows of the matrix M together. It is clear from the explicit representative (2.17) that all the points of Gr_G corresponding to the same $\lambda \in 2\mathbb{N}$ form a single orbit, and conversely points corresponding to $\lambda \neq \lambda'$ belong to different orbits. Therefore, the orbits, which we denote by $[\text{Gr}_G]^\lambda$, are labeled by $\lambda \in 2\mathbb{N}$, and can be defined by a distinguished element M_λ :

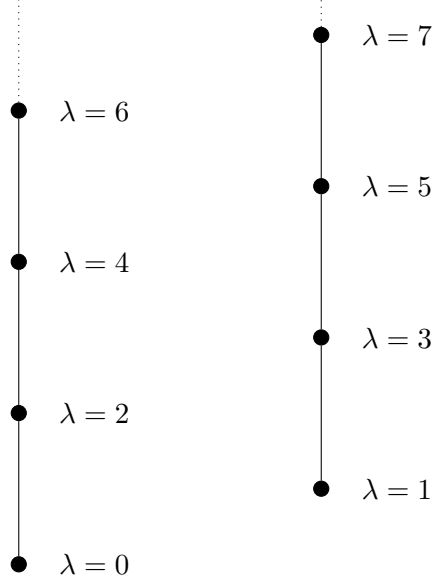
$$[\text{Gr}_G]^\lambda = G[[t]] \cdot M_\lambda, \quad M_\lambda = \begin{pmatrix} t^{\lambda/2} & 0 \\ 0 & t^{-\lambda/2} \end{pmatrix}. \quad (2.18)$$

Elements of $2\mathbb{N}$ can be seen as the positive coweights of G .

Consider an orbit $[\text{Gr}_G]^\lambda$. For every $u \in \mathbb{C}^*$, we have

$$\begin{pmatrix} 0 & u \\ -u^{-1} & tu^{-1} \end{pmatrix} M_\lambda \begin{pmatrix} u^{-1} & 0 \\ u^{-1}t^{\lambda-1} & u \end{pmatrix} = \begin{pmatrix} t^{\lambda/2-1} & u^2 t^{-\lambda/2} \\ 0 & t^{-\lambda/2+1} \end{pmatrix} \quad (2.19)$$

which when $u \rightarrow 0$ reaches the orbit $[\text{Gr}_G]^{\lambda-2}$. This shows that the orbit $[\text{Gr}_G]^\lambda$ is open and contains $[\text{Gr}_G]^{\lambda-2}$ in its closure. Therefore there is a partial order in the orbits defined by closure inclusions. The difference between the coweights labeling two adjacent orbits, $\lambda - (\lambda - 2) = 2$, can be interpreted as the positive coroot in G .



Component $I = 0 \in \mathbb{Z}_2$ Component $I = 1 \in \mathbb{Z}_2$

Figure 1. Hasse diagram for the orbits in the affine Grassmannian of $\mathrm{PSL}(2, \mathbb{C})$.

Points and orbits of $\mathrm{Gr}_{\mathrm{PSL}(2, \mathbb{C})}$

In this paragraph we discuss $\mathrm{PSL}(2, \mathbb{C})$, seen as $\mathrm{GL}(2, \mathbb{C})$ quotiented by scalar matrices. In $\mathrm{GL}(2, \mathbb{C})$, the difference with the previous analysis is that the determinant condition is lifted, so the orbits can be labeled by two integers a and b , with $a \geq b$. In $\mathrm{PSL}(2, \mathbb{C})$ though we have

$$\begin{pmatrix} t^a & 0 \\ 0 & t^b \end{pmatrix} \sim \begin{pmatrix} t^{a-b} & 0 \\ 0 & 1 \end{pmatrix}, \quad (2.20)$$

so the orbits can be labeled by $\lambda = a - b \in \mathbb{N}$. A computation analog to (6.4) shows that again the orbit $[\mathrm{Gr}_{\mathrm{PSL}(2, \mathbb{C})}]^{\lambda-2}$ lies in the closure of $[\mathrm{Gr}_{\mathrm{PSL}(2, \mathbb{C})}]^\lambda$. There are two connected components in $\mathrm{Gr}_{\mathrm{PSL}(2, \mathbb{C})}$: one is the union of all the orbits $[\mathrm{Gr}_{\mathrm{PSL}(2, \mathbb{C})}]^\lambda$ for $\lambda \in 2\mathbb{N}$, which gives $\mathrm{Gr}_{\mathrm{SL}(2, \mathbb{C})}$, and the other is the union of all the orbits $[\mathrm{Gr}_{\mathrm{PSL}(2, \mathbb{C})}]^\lambda$ for λ odd. The complex dimension of $[\mathrm{Gr}_{\mathrm{PSL}(2, \mathbb{C})}]^\lambda$ is λ in all cases, so it is even in one component and odd in the other. This is summarized in Figure 1.

2.5 Orbits in the Affine Grassmannian

We now come back to the general discussion and spell out how the observations of the previous subsections generalize to an arbitrary (semisimple complex algebraic) group G . An important role is played by the coweights and the coroots of G , so we begin with a reminder of a few definitions.

Let us pick a maximal torus and a Borel subgroup $T \subset B \subset G$, with Lie algebras $\mathfrak{h} \subset \mathfrak{b} \subset \mathfrak{g}$. A character of G is a homomorphism $T \rightarrow \mathbb{C}^*$ while a cocharacter is a homomorphism $\mathbb{C}^* \rightarrow T$. The differentials of characters are weights, while the differentials of cocharacters are coweights. We call Λ the coweight lattice of G and Λ_0 the coroot lattice of G . The goal of this subsection is to define a collection of elements $M_\lambda \in G((t))$ generalizing (2.18) from which we will build orbits in the affine Grassmannian, so it is natural to require that λ be a *coweight*, and not a weight. The coweights of G can be used to label the (highest-weight) irreducible representations of the Langlands dual group G^\vee . We use the Killing form to identify the space of weights and the space of coweights. The Borel subalgebra \mathfrak{b} fixes a set of simple roots, which in turn defines a set of fundamental weights in the usual fashion. We call λ^+ (respectively Λ_0^+) the set of linear combinations with nonnegative integer coefficients of the fundamental coweights (resp. simple coroots). Any weight or coweight can then be expressed in the basis of the fundamental weights $(\varpi_i)_{i=1,\dots,r}$, and we denote a (co)weight by its coordinates in this basis

$$\lambda = \sum_{i=1}^r \lambda_i \varpi_i. \quad (2.21)$$

The coweights are partially ordered as follows. For λ and μ two coweights,

$$\lambda \leq \mu \iff \begin{array}{l} \mu - \lambda \text{ is a linear combination of} \\ \text{simple coroots with coefficients in } \mathbb{N} \end{array} \iff \mu - \lambda \in \Lambda_0^+. \quad (2.22)$$

This partial order defines a Hasse diagram for the dominant coweights. This Hasse diagram has connected components labeled by classes Λ/Λ_0 .

Definition Given a coweight λ we have a corresponding homomorphism $\mathbb{C}^* \rightarrow T$. Denoting by $t \in \mathbb{C}^*$ the formal variable, the image of this homomorphism is called $M_\lambda(t) := M_\lambda$.

We have identified the affine Grassmannian of G with the space

$$\mathrm{Gr}_G = G((t))/G[[t]], \quad (2.23)$$

where a matrix in $G((t))$ specifies a lattice by giving an explicit basis, and the quotient by $G[[t]]$ eliminating the arbitrariness in the choice of such a basis. We also recall that given a matrix $M \in G((t))$, multiplying on the right by an element of $G[[t]]$ gives the same lattice, as we just said, but multiplying on the left gives a different lattice. We can then denote points and orbits in the affine Grassmannian as follows:

- $M \cdot G[[t]]$ is the point in Gr_G corresponding to M
- $G[[t]] \cdot M \cdot G[[t]]$ is the orbit of that point in Gr_G .

Given a coweight λ of G , we can build a full orbit in the affine Grassmannian, which is denoted:

$$[\mathrm{Gr}_G]^\lambda = G[[t]] \cdot M_\lambda \cdot G[[t]]. \quad (2.24)$$

Two coweight λ and λ' which belong to the same Weyl group orbit give the same orbit in the affine Grassmannian, $[\mathrm{Gr}_G]^\lambda = [\mathrm{Gr}_G]^{\lambda'}$, so we can restrict our attention to the orbits $[\mathrm{Gr}_G]^\lambda$ for λ dominant. It turns out these orbits provide a partition of the affine Grassmannian, which can be written as a disjoint union

$$\mathrm{Gr}_G = \bigcup_{\lambda \in \Lambda^+} [\mathrm{Gr}_G]^\lambda . \quad (2.25)$$

The (Zariski) closure of $[\mathrm{Gr}_G]^\lambda$ is

$$\overline{[\mathrm{Gr}_G]^\lambda} = [\mathrm{Gr}_G]^{\leq \lambda} = \bigcup_{\mu \in \Lambda^+, \mu \leq \lambda} [\mathrm{Gr}_G]^\mu . \quad (2.26)$$

Therefore, the partial order on the dominant coweights Λ^+ provides the Hasse diagram for the $G[[t]]$ orbits in the affine Grassmannian Gr_G . There is one Hasse diagram for each connected component of Gr_G , and by construction we have

$$\pi_0(\mathrm{Gr}_G) = \Lambda/\Lambda_0 = \pi_1(G) . \quad (2.27)$$

Elements of this group will be denoted by an index I . We now introduce the notion of lowest dominant coweights. A coweight Ω is a lowest dominant coweight if it is dominant, and if in addition there is no other dominant coweight ω such that $\omega < \Omega$. There are as many components in the affine Grassmannian of G as there are lowest dominant coweights of G ; we call them Ω_I , where the index $I \in \pi_1(G)$. We list the lowest dominant coweights for simple groups in Table 2.

The $[\mathrm{Gr}_G]^\lambda$ are called *Schubert cells* and the $[\mathrm{Gr}_G]^{\leq \lambda}$ are called *Schubert varieties*. The Schubert cell $[\mathrm{Gr}_G]^\lambda$ is a smooth variety of dimension

$$\dim_{\mathbb{C}} [\mathrm{Gr}_G]^\lambda = \langle 2\rho, \lambda \rangle , \quad (2.28)$$

where ρ is the Weyl vector [41, Prop 2.1.5]. The Schubert varieties can be singular spaces, but are well behaved: the singularities are always normal, Gorenstein and Cohen-Macaulay [41, Theorem 2.1.21]. Their complex dimension can be even or odd, but the parity of the complex dimension remains the same in a given connected component of Gr_G .

2.6 Slices in the affine Grassmannian

One can use other groups than $G[[t]]$ to generate orbits. In particular, we can use $G[t^{-1}]$ to generate the orbit

$$[\mathrm{Gr}_G]_\lambda := G[t^{-1}] \cdot M_\lambda \cdot G[[t]] , \quad (2.29)$$

which is called an *opposite Schubert cell*. From this one can build an (infinite dimensional but finite codimensional) *opposite Schubert variety*

$$[\mathrm{Gr}_G]_{\geq \lambda} := \bigcup_{\mu \in \Lambda^+, \mu \geq \lambda} [\mathrm{Gr}_G]_\mu . \quad (2.30)$$

G	$\pi_1(G) = Z(G^\vee)$	Ω_I
$\mathrm{PSL}(n+1, \mathbb{C})$	\mathbb{Z}_{n+1}	$\Omega_0 = [0, \dots, 0]$ $\Omega_l = [0, \dots, 0, \underbrace{1, 0, \dots, 0}_{l-1}]$
$\mathrm{SO}(2n+1, \mathbb{C})$	\mathbb{Z}_2	$\Omega_0 = [0, 0, \dots, 0]$ $\Omega_1 = [1, 0, \dots, 0]$
$\mathrm{PSp}(2n, \mathbb{C})$	\mathbb{Z}_2	$\Omega_0 = [0, \dots, 0, 0]$ $\Omega_1 = [0, \dots, 0, 1]$
$\mathrm{PSO}(4n, \mathbb{C})$	$\mathbb{Z}_2 \times \mathbb{Z}_2$	$\Omega_{(0,0)} = [0, 0, \dots, 0, 0, 0]$ $\Omega_{(1,1)} = [1, 0, \dots, 0, 0, 0]$ $\Omega_{(1,0)} = [0, 0, \dots, 0, 1, 0]$ $\Omega_{(0,1)} = [0, 0, \dots, 0, 0, 1]$
$\mathrm{PSO}(4n+2, \mathbb{C})$	\mathbb{Z}_4	$\Omega_0 = [0, 0, \dots, 0, 0, 0]$ $\Omega_1 = [0, 0, \dots, 0, 1, 0]$ $\Omega_2 = [1, 0, \dots, 0, 0, 0]$ $\Omega_3 = [0, 0, \dots, 0, 0, 1]$
E_6/\mathbb{Z}_3	\mathbb{Z}_3	$\Omega_0 = [0, 0, 0, 0, 0, 0]$ $\Omega_1 = [1, 0, 0, 0, 0, 0]$ $\Omega_2 = [0, 0, 0, 0, 1, 0]$
E_7/\mathbb{Z}_2	\mathbb{Z}_2	$\Omega_0 = [0, 0, 0, 0, 0, 0, 0]$ $\Omega_1 = [1, 0, 0, 0, 0, 0, 0]$
E_8	trivial	$\Omega_0 = [0, 0, 0, 0, 0, 0, 0, 0]$
F_4	trivial	$\Omega_0 = [0, 0, 0, 0]$
G_2	trivial	$\Omega_0 = [0, 0]$

Table 2. Lowest dominant coweights Ω_I (given in the basis of fundamental coweights) for centerless simple groups G . We denote elements of $\pi_1(G) = Z(G^\vee) I$. To each Ω_I there is a component labelled I in the affine Grassmannian of G .

Note that $[\mathrm{Gr}_G]_\lambda \cap [\mathrm{Gr}_G]^\lambda = G \cdot M_\lambda \cdot G[[t]]$ is not reduced to a point. This motivates the introduction of a last type of orbits, in which G does not act at degree 0, namely

$$[\mathcal{W}_G]_\lambda := G_1[t^{-1}] \cdot M_\lambda \cdot G[[t]]. \quad (2.31)$$

The intersection of these orbits with Schubert cells and Schubert varieties give the the spaces which are the main focus of this paper:

$$[\mathcal{W}_G]_\lambda^\mu = [\mathcal{W}_G]_\lambda \cap [\mathrm{Gr}_G]^\mu \quad \text{and} \quad \overline{[\mathcal{W}_G]_\lambda}^\mu = [\mathcal{W}_G]_\lambda \cap \overline{[\mathrm{Gr}_G]^\mu} \quad (2.32)$$

The spaces $\overline{[\mathcal{W}_G]_\lambda}^\mu$ intersect $[\mathrm{Gr}_G]^\nu$ transversely for any $\lambda \leq \nu \leq \mu$, and are called the *slices* in the affine Grassmannian. They are varieties with symplectic singularities [11, 33], with

dimension

$$\dim_{\mathbb{C}} \overline{[\mathcal{W}_G]_{\lambda}}^{\mu} = \langle 2\rho, \mu - \lambda \rangle. \quad (2.33)$$

In particular, when $\mu - \lambda$ is a simple coroot α^{\vee} , the two orbits $[\mathrm{Gr}_G]^{\mu}$ and $[\mathrm{Gr}_G]^{\lambda}$ are adjacent in the Hasse diagram, the elementary transverse slice has complex dimension is 2, and one can show that [11, Example 2.2]

$$\overline{[\mathcal{W}_G]_{\lambda}}^{\lambda + \alpha^{\vee}} = \mathbb{C}^2 / \mathbb{Z}_{2 + \langle \lambda, \alpha \rangle} = A_{1 + \langle \lambda, \alpha \rangle}. \quad (2.34)$$

This shows that the “generic” elementary slice in the affine Grassmannian is a Kleinian singularity of type A . More generally, elementary slices correspond to pairs of adjacent coweights according to the partial order (2.22). This problem has been studied in detail in [10, 34, 48], and the conclusion is that the elementary transverse slices fall into three categories [10]:

- Kleinian singularities of type A , (2.34), when $\mu - \lambda$ is a simple coroot. These are denoted A_n .
- Closure of minimal nilpotent orbits, when $\mu - \lambda$ is the short dominant coroot of the subalgebra defined by the nonvanishing of $\mu - \lambda$. These are denoted a_n , b_n , c_n , d_n , e_6 , e_7 , e_8 , f_4 and g_2 .
- *Quasi-minimal* singularities,⁴ which can be of three types:
 1. An infinite family called ac_n , for $n \geq 2$;
 2. The ag_2 singularity;
 3. The cg_2 singularity.

The existence of the elementary slices other than Kleinian of type A is caused by geometric constraints in the Weyl chambers when approaching walls. The disposition \mathfrak{D} ⁵ of the affine Grassmannian Gr_G is $r = \mathrm{rank}(G)$. Close to a codimension d wall of the Weyl chamber, the disposition of a generic coweight decreases to $r - d$.

In the next section we will see this at work in the affine Grassmannian at rank 2. The quasi-minimal singularities will be studied in detail in Section 3.3.

3 Quivers and Hasse diagrams

In this section we explore the affine Grassmannian, or rather the slices in the affine Grassmannian, of simple groups. The two coweights which define a slice can be used to produce a quiver, whose Coulomb branch is the slice.

⁴The terminology comes from [10].

⁵The Disposition \mathfrak{D} of a leaf and a moduli space is defined in (1.1) and (1.2) respectively in the Introduction.

Notation	Explanation
$\mathbb{C}[t]$	Ring of polynomials in t
$\mathbb{C}[[t]]$	Ring of formal power series in t
$\mathbb{C}((t))$	Field of formal Laurent series in t , also field of fractions of $\mathbb{C}[[t]]$
G	Simple algebraic subgroup of $\mathrm{GL}(n, \mathbb{C})$
\mathfrak{g}	Lie algebra of G
$C_{\mathfrak{g}}$	Cartan matrix of \mathfrak{g}
Λ	Coweight lattice of G
Λ_0	Coroot lattice of G
$(\alpha_i)_{i=1,\dots,r}, (\alpha_i^\vee)_{i=1,\dots,r}$	Simple roots and simple coroots of \mathfrak{g}
$(\varpi_i)_{i=1,\dots,r}, (\varpi_i^\vee)_{i=1,\dots,r}$	Fundamental weights and fundamental coweights of G
ρ	Weyl vector, half-sum of the positive roots
$G[t]$	Group G “with coefficients in $\mathbb{C}[t]$ ”
$G[[t]]$	Group G “with coefficients in $\mathbb{C}[[t]]$ ”
$G((t))$	Group G “with coefficients in $\mathbb{C}((t))$ ”
$G_1[t^{-1}]$	Subgroup of $G[t^{-1}]$ where the t^0 part is the identity of G
$\mathrm{Gr}_G = G((t))/G[[t]]$	Affine Grassmannian of G
M_λ	Image in $G((t))$ of the coweight $\lambda \in \Lambda$
$[\mathrm{Gr}_G]^\lambda = G[[t]] \cdot M_\lambda \cdot G[[t]]$	Schubert cell associated to dominant coweight λ , a smooth variety of complex dimension $\langle 2\rho, \lambda \rangle$
$\overline{[\mathrm{Gr}_G]}^\lambda = \bigsqcup_{\sigma \leq \lambda} [\mathrm{Gr}_G]^\sigma$	Schubert variety, the Zariski closure of the Schubert cell $[\mathrm{Gr}_G]^\lambda$, of dimension $\langle 2\rho, \lambda \rangle$
$[\mathrm{Gr}_G]_\lambda = G[t^{-1}] \cdot M_\lambda \cdot G[[t]]$	Opposite Schubert Cell (infinite-dimensional)
$[\mathcal{W}_G]_\lambda = G_1[t^{-1}] \cdot M_\lambda \cdot G[[t]]$	Transverse slice to Schubert cell in Gr_G (infinite dimensional)
$\overline{[\mathcal{W}_G]}_\lambda^\mu = [\mathcal{W}_G]_\lambda \cap \overline{[\mathrm{Gr}_G]}^\mu$	Transverse slice from μ to λ , a symplectic singularity of complex dimension $\langle 2\rho, \mu - \lambda \rangle$

Table 3. Summary of the notations.

3.1 General formula for slices

From now on we assume that G is simple with rank r , so that its Lie algebra can be characterized by a connected Dynkin diagram. In [12, 20], following the series of works [22, 24, 27, 28] the slices in the affine Grassmannian Gr_G have been identified with Coulomb branches of certain 3d $\mathcal{N} = 4$ good quiver gauge theories. In this subsection, we summarize this connection and give explicit formulas.

From slice to quiver. Let λ and μ be two coweights. We assume that

- μ is dominant.
- $\mu - \lambda$ is in the positive coroot lattice.

Then we can construct a quiver \mathcal{Q}_λ^μ as follows:

- There are r gauge nodes, connected as in the Dynkin diagram of \mathfrak{g} , with node ranks

$$k_i = \langle \varpi_i, \mu - \lambda \rangle. \quad (3.1)$$

When λ and μ are identified with their components in the basis of fundamental weights, the vector of gauge nodes ranks is $\mathbf{k} = C_{\mathfrak{g}}^{-1} \cdot (\mu - \lambda)$.

- There are r flavor nodes, connected to the r gauge nodes, with ranks given by

$$N_i = \langle \alpha_i^\vee, \mu \rangle. \quad (3.2)$$

When μ is identified with its components in the basis of fundamental weights, $\mathbf{N} = \mu$.

Note that the condition that $\mu - \lambda$ be in the positive coroot lattice guarantees precisely that \mathbf{k} is an element of \mathbb{N}^r .

From good quiver to slice. Consider a *good* quiver such that the gauge nodes form the Dynkin diagram of a simple Lie algebra \mathfrak{g} . We denote by $\mathbf{k} = (k_i)_{i=1,\dots,r}$ the ranks of the gauge nodes and $\mathbf{N} = (N_i)_{i=1,\dots,r}$ the ranks of the flavor nodes, with r the rank of \mathfrak{g} . To this quiver we associate two coweights:

- The coweight μ is given by the flavor nodes, $\mu = \sum_{i=1}^r n_i \varpi_i$;
- The coweight λ is given by⁶ $\lambda = \mathbf{N} - C_{\mathfrak{g}} \cdot \mathbf{k}$.

⁶Note that the components of the coweight λ gives the *balance* of the gauge nodes of the quiver. The assumption that the quiver is good implies that λ is dominant.

Example. For instance if one considers the algebra C_2 and coweights expressed in the basis of fundamental weights⁷ $\lambda = [2, 0]$ and $\mu = [2, 2]$, with the matrix $C_{\mathfrak{g}} = \begin{pmatrix} 2 & -1 \\ -2 & 2 \end{pmatrix}$ one gets $\mu - \lambda = [0, 2]$. This is in the positive coroot lattice, and $C_{\mathfrak{g}}^{-1} \cdot (\mu - \lambda) = [1, 2]$ so the quiver is

$$\mathbf{Q}_{\lambda}^{\mu} = \begin{array}{c} \square \quad \square \\ | \quad | \\ \circ \rightleftarrows \circ \\ 1 \quad 2 \end{array}. \quad (3.3)$$

Note that the gauge node on the right is balanced, corresponding to the vanishing component of λ .

If instead one considers $\lambda = [0, 1]$ and $\mu = [2, 2]$, then $\mu - \lambda = [2, 1]$ is not in the positive coroot lattice. Accordingly, $C_{\mathfrak{g}}^{-1} \cdot (\mu - \lambda) = [\frac{5}{2}, 3]$ is not a vector of integers and no quiver can be defined.

Note that it is not necessary that the coweight λ be dominant. For instance consider the following pair:

$$\lambda = [-1, 2] \quad \mu = [4, 6] \quad \mathbf{Q}_{\lambda}^{\mu} = \begin{array}{c} \square \quad \square \\ | \quad | \\ \circ \rightleftarrows \circ \\ 7 \quad 9 \end{array}. \quad (3.4)$$

Note that the node on the right is under-balanced.

Generalized Slices. When λ is not dominant, the construction of the quiver $\mathbf{Q}_{\lambda}^{\mu}$ still makes sense. The quiver is not good in the sense of [49], and its Coulomb branch does not correspond to a slice in Gr_G . However the Coulomb branch of $\mathbf{Q}_{\lambda}^{\mu}$ can be identified with the generalized slices of [12].

Explicit quivers The quivers $\mathbf{Q}_{\lambda}^{\mu}$ for algebras of classical types are gathered in Table 4. We use the following explicit form for the inverse of the Cartan matrix for $\mathfrak{g} = A_n$:

$$C_{\mathfrak{g}}^{-1} = \left(\min(i, j) - \frac{ij}{n+1} \right)_{1 \leq i, j \leq n}. \quad (3.5)$$

3.2 Hasse diagrams for Affine Grassmannians at ranks 1 and 2

In this subsection, we use the description reviewed above to construct the bottom part of the Hasse diagrams for complex simple groups of ranks 1 and 2. This can be achieved by focusing only on the centerless groups associated to the Lie algebra (the affine Grassmannian for groups with non-trivial center are obtained by taking only the relevant connected components). This is presented in Figures 2 to 13.

⁷For conventions regarding the C_2 algebra, see Figure 9.

Caption for Figures 2-13. For each Lie algebra, we first draw a diagram with our Lie algebra conventions. This diagram represents both the Cartan subalgebra and its dual, identified via the Killing form. The red arrows represent the roots, the black arrow represent the fundamental weights. The simple roots and coroots, and the fundamental weights and coweight are explicitly labeled. The dots denote the coweight lattice, where different colors are used for different elements of the group (2.27), and therefore correspond to different connected components in (the Hasse diagram of) the affine Grassmannian. The Weyl chamber, defined by the fundamental coweights, is shaded in gray.

Then for each element of the group (2.27) we draw a Hasse diagram for the few lowest orbits in the corresponding component of the affine Grassmannian. The dots in the Hasse diagram are the coweights and correspond to orbits (2.24), while the lines connect adjacent coweights according to the partial order (2.22). Dotted lines indicate that the Hasse diagram is infinite.

A connected component can be labeled by a lowest coweight Ω_I . In that component, next to each dot corresponding to a coweight μ , we draw the quiver $\mathbf{Q}_{\Omega_I}^\mu$. The Coulomb branch of this quiver is the transverse slice to the orbit at the origin of the Hasse diagram, $[\overline{\mathcal{W}_G}]_{\Omega_I}^\mu$. Finally, next to each line we indicate the nature of the elementary transverse slice, using the notations specified at the end of Section 2.6.

Disposition and quasi-minimal slices. From the Hasse diagrams presented in this section, one can observe that the appearance of slices beyond Kleinian singularities of type A is related to space constraints close to the walls of the Weyl chamber. In the A_2 case, a non-zero coweight λ always has at least one coweight μ such that $\mu - \lambda$ is a simple coroot. This is related to the basic geometric fact that the Weyl chamber has an angle of $\frac{\pi}{3}$ at the origin, which is the angle for equilateral triangles.

In the B_2 case, the Weyl chamber has an angle $\frac{\pi}{4}$ at the origin. Adding any simple coroot to the coweight ϖ_1^\vee in Figure 6 gives a coweight outside the Weyl chamber. In order to stay in the Weyl chamber, one has to add the non simple coroot $\alpha_1^\vee + \alpha_2^\vee$. This leads to an elementary slice with quasi-minimal singularity in Figure 8. The same obviously applies to the C_2 case.

Finally in the G_2 case, there are two non-zero coweights which are such that adding any simple coroot gives a coweight outside the Weyl chamber, namely ϖ_2^\vee and $2\varpi_2^\vee$. This gives rise to two elementary slices with quasi-minimal singularities in Figure 13.

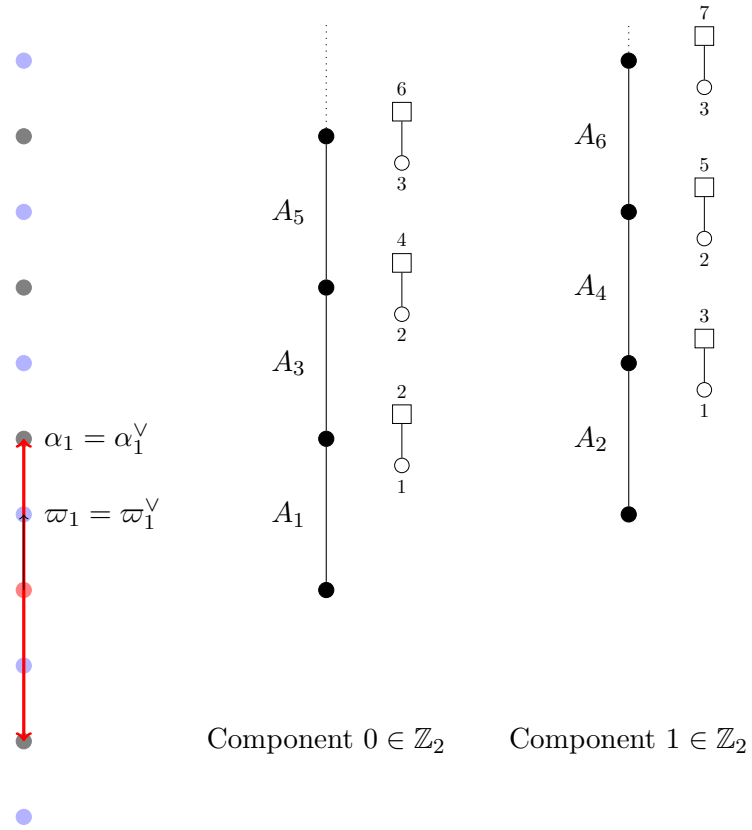


Figure 2. Bottom of the Hasse diagram for $\text{PSL}(2, \mathbb{C})$. See detailed caption on page 18.

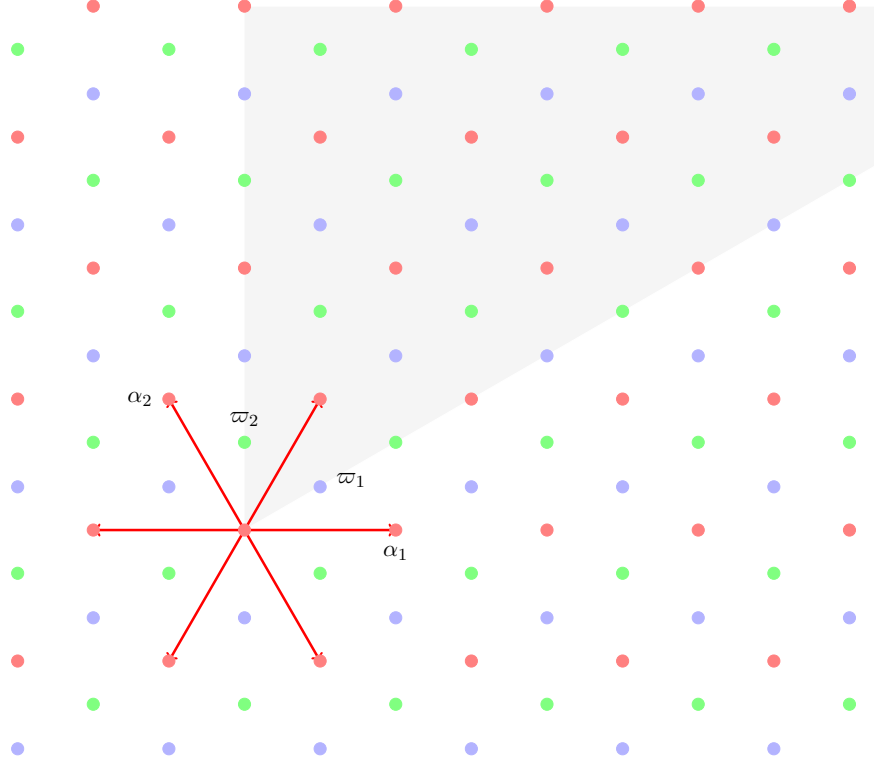


Figure 3. Summary of A_2 data. See detailed caption on page 18. The red dots correspond to the coroot lattice Λ_0 , while the blue dots are the lattice $\Lambda_0 + \varpi_1$ and the green dots are the lattice $\Lambda_0 + \varpi_2$.

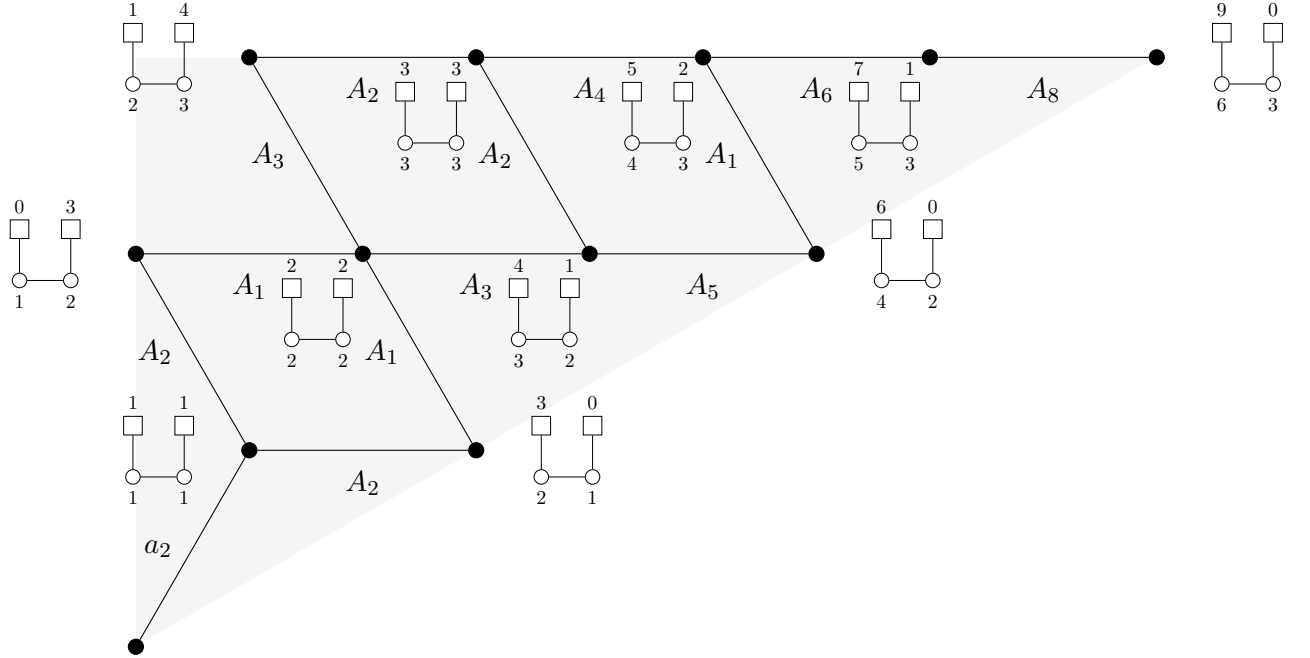


Figure 4. Bottom of the Hasse diagram for $\mathrm{PSL}(3, \mathbb{C})$, component $0 \in \mathbb{Z}_3$. See detailed caption on page 18.

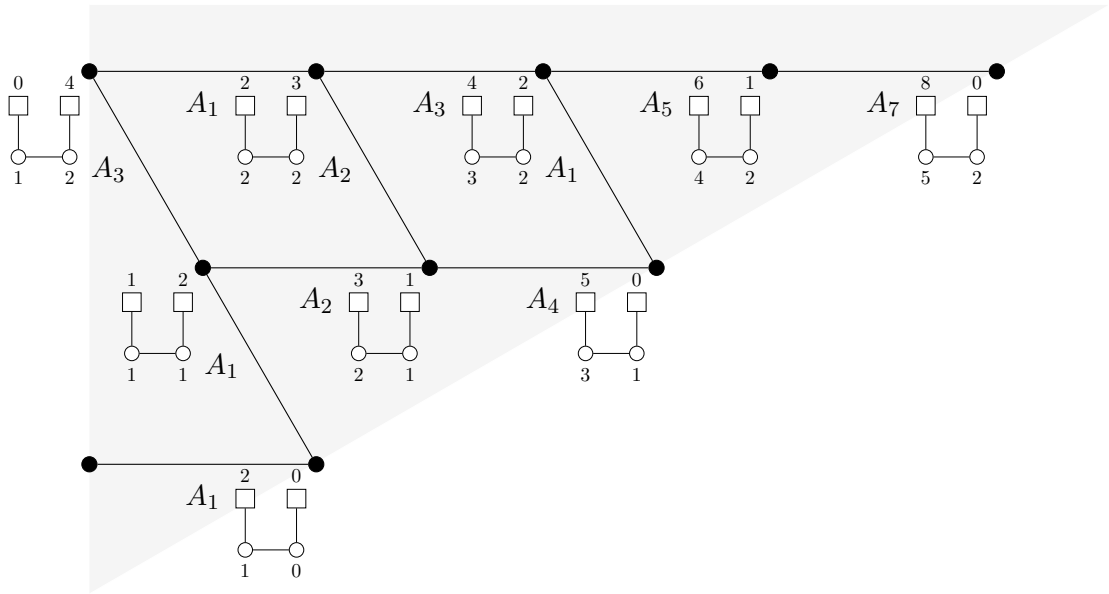


Figure 5. Bottom of the Hasse diagram for $\text{PSL}(3, \mathbb{C})$, component $1 \in \mathbb{Z}_3$. See detailed caption on page 18. The third component $-1 \in \mathbb{Z}_3$ is obtained by symmetry.

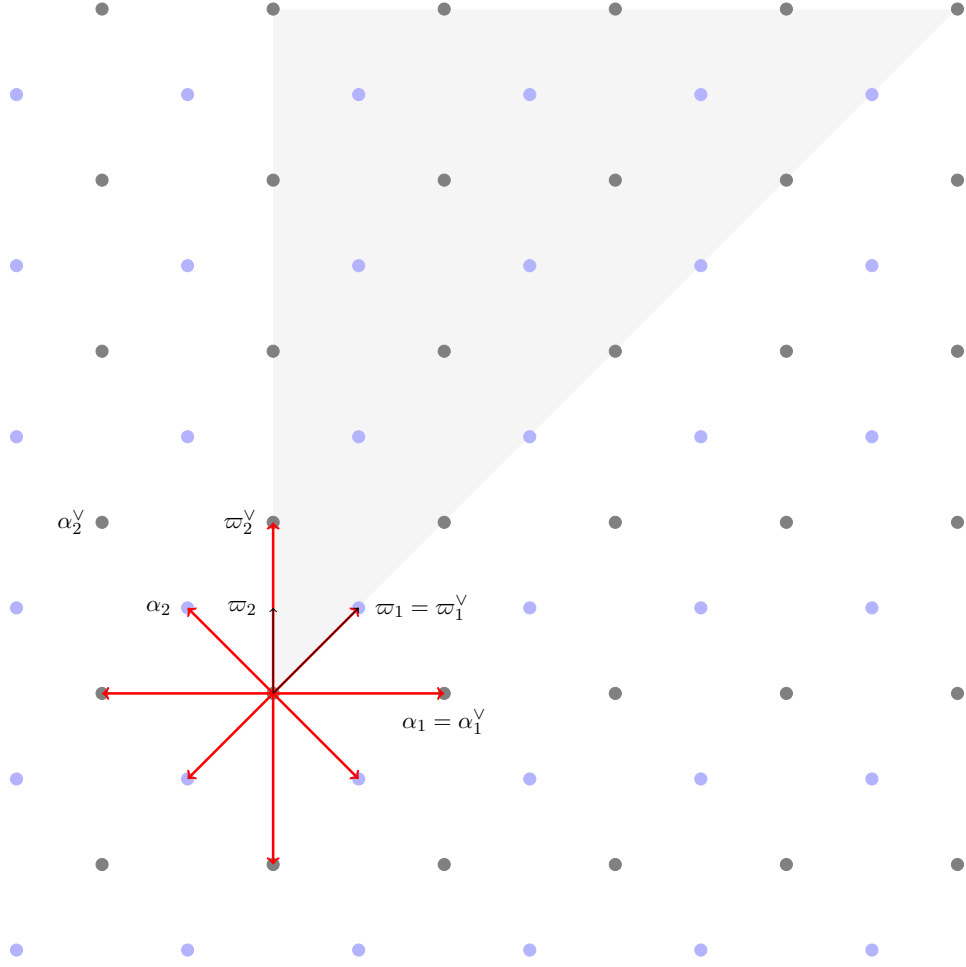


Figure 6. Summary of B_2 data. See detailed caption on page 18. The black dots correspond to the coroot lattice Λ_0 , while the blue dots are the lattice $\Lambda_0 + \varpi_1^\vee$.

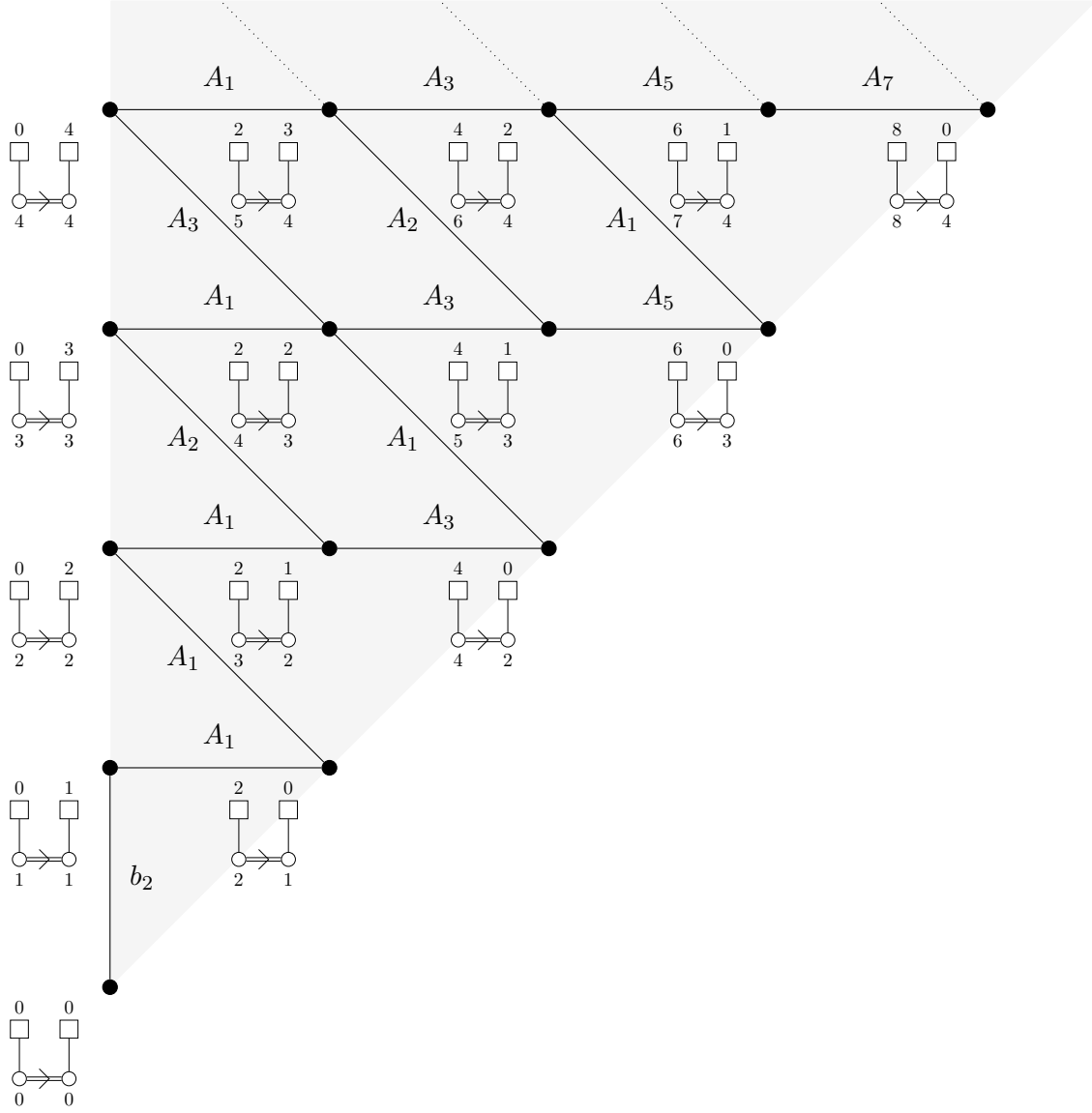


Figure 7. Bottom of the Hasse diagram for $\text{PSO}(5, \mathbb{C})$, component $0 \in \mathbb{Z}_2$. See detailed caption on page 18.

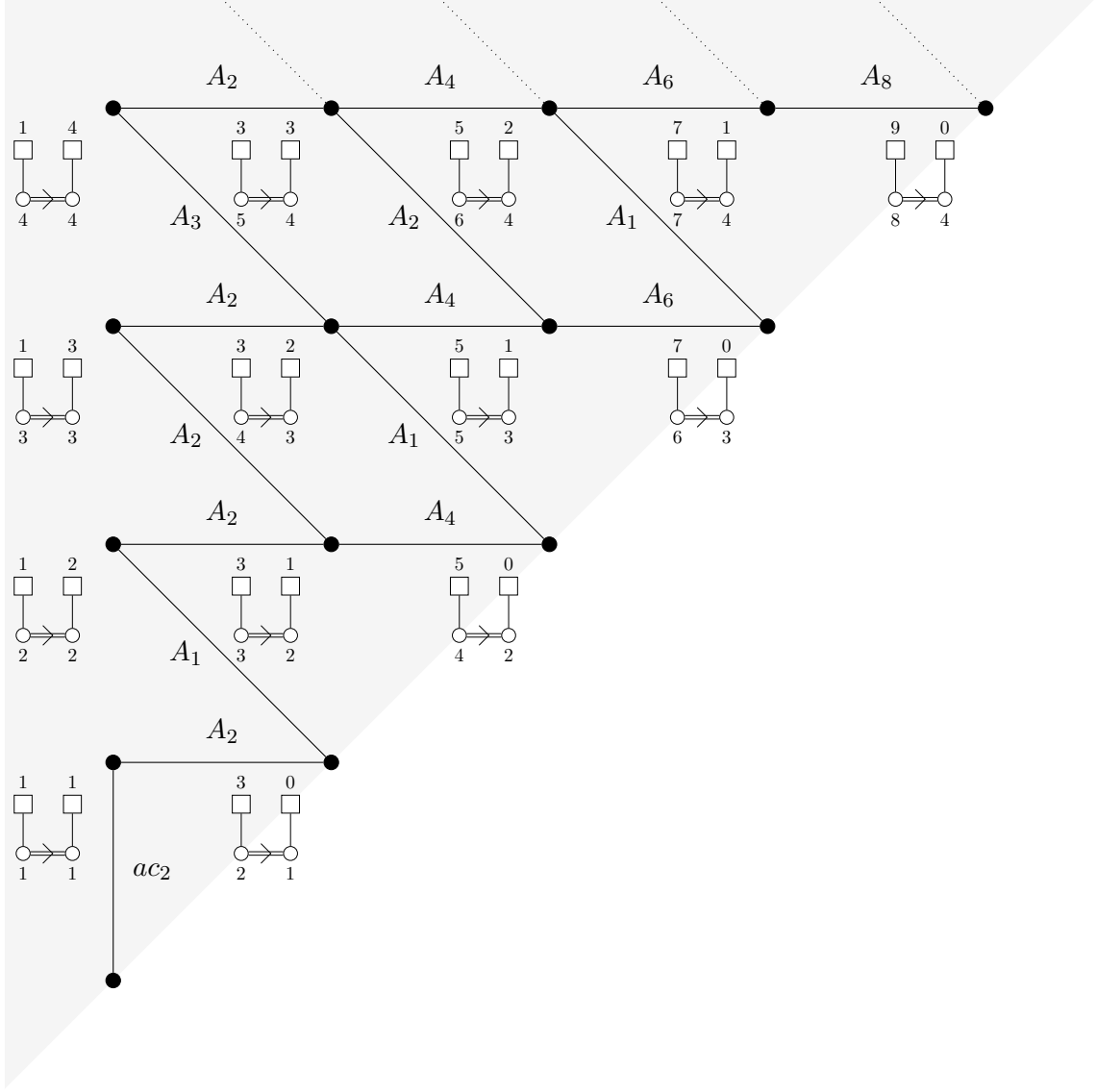


Figure 8. Bottom of the Hasse diagram for $\text{PSO}(5, \mathbb{C})$, component $1 \in \mathbb{Z}_2$. See detailed caption on page 18.

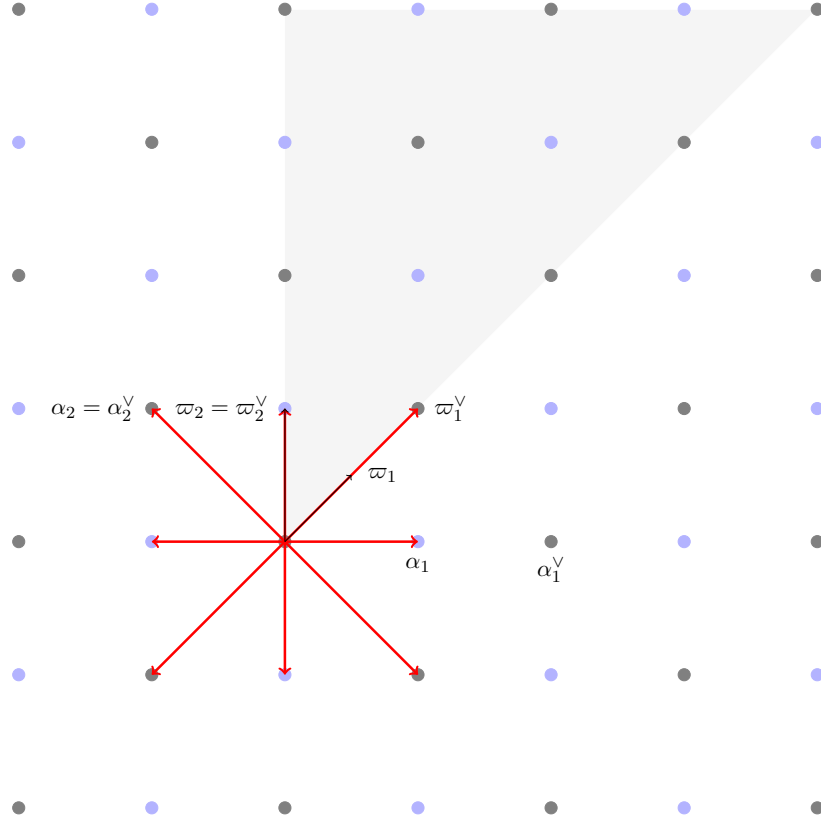


Figure 9. Summary of C_2 data. See detailed caption on page 18. The black dots correspond to the coroot lattice Λ_0 , while the blue dots are the lattice $\Lambda_0 + \varpi_2^\vee$.

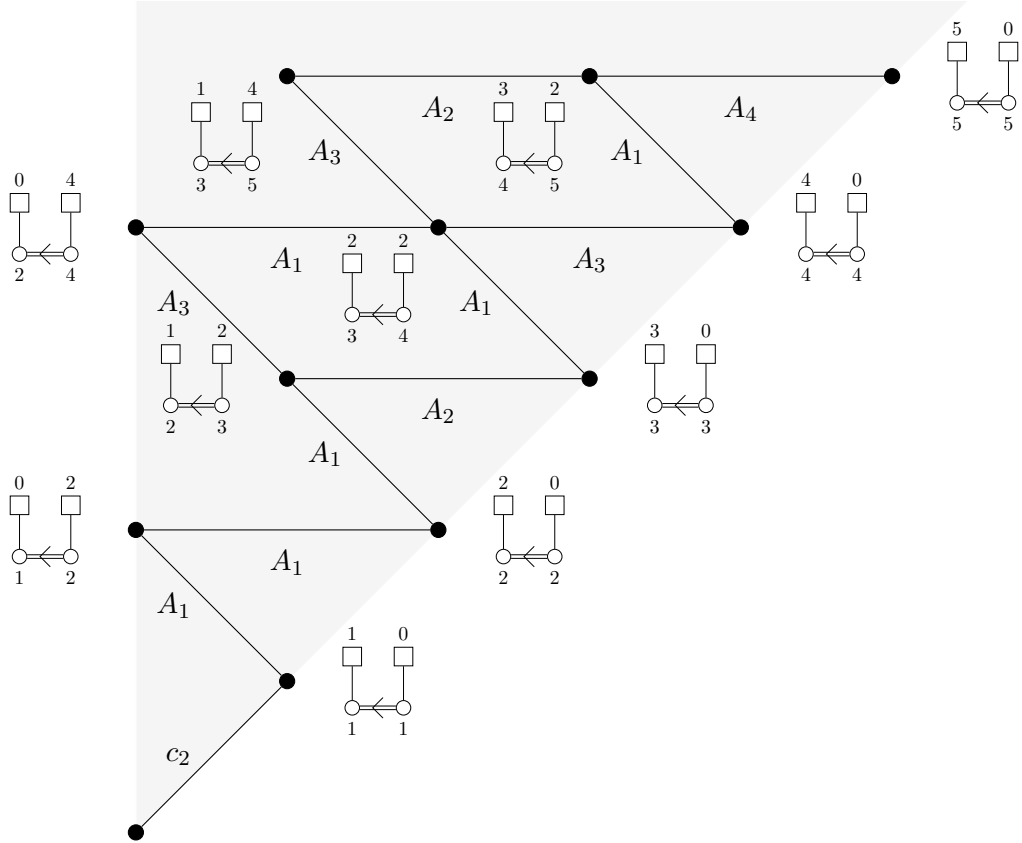


Figure 10. Bottom of the Hasse diagram for $\mathrm{Sp}(4, \mathbb{C})$, component $0 \in \mathbb{Z}_2$. See detailed caption on page 18.

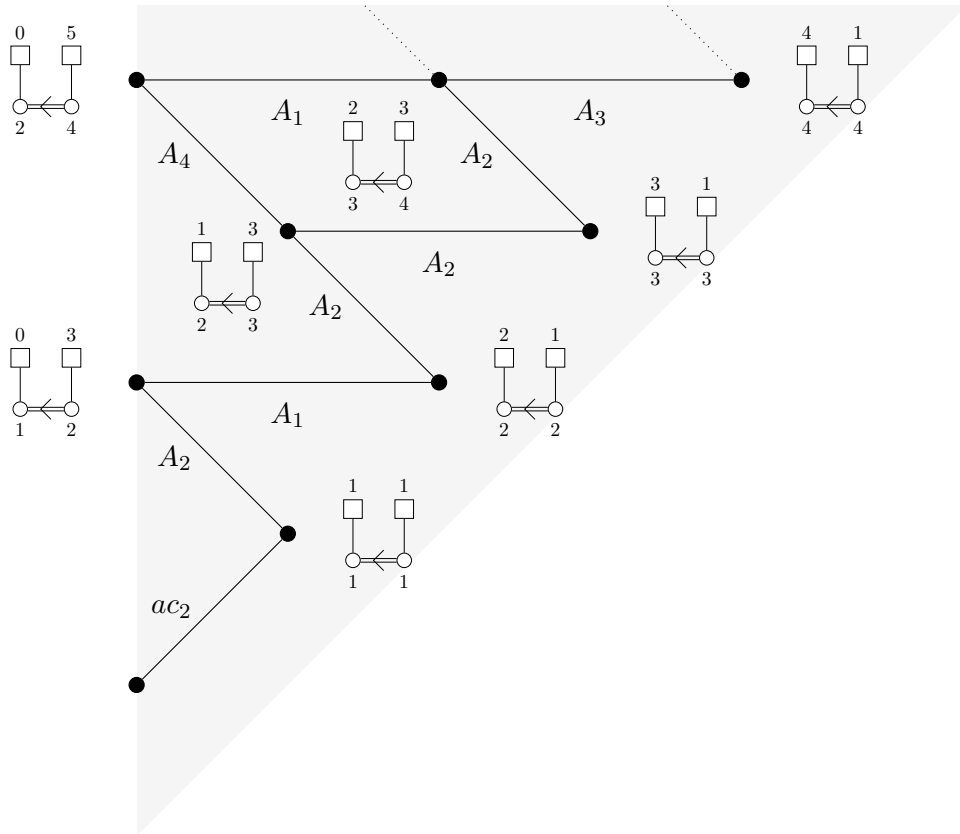


Figure 11. Bottom of the Hasse diagram for $\mathrm{Sp}(4, \mathbb{C})$, component $1 \in \mathbb{Z}_2$. See detailed caption on page 18.

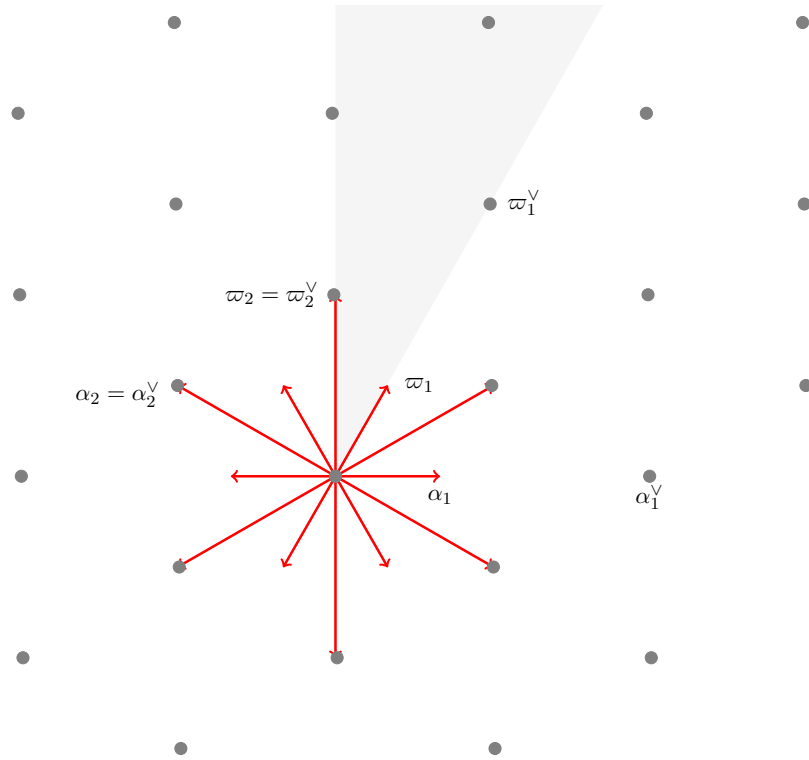
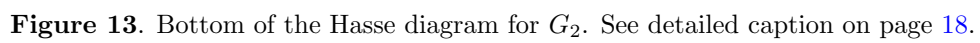


Figure 12. Summary of G_2 data. See detailed caption on page 18.



Algebra	Quiver
A_n	
B_n	
C_n	
D_n	

Table 4. For algebras of classical types, we depict the quivers Q_λ^μ where $\mu = \sum_{i=1}^n \mu_i \varpi_i$ and $\lambda = \sum_{i=1}^n \lambda_i \varpi_i$ are coweights with μ dominant and $\nu := \mu - \lambda$ in the positive coroot lattice. If λ is dominant, their 3d $\mathcal{N} = 4$ Coulomb branch is the transverse slice $[\overline{\mathcal{W}}_G]_\lambda^\mu$.

3.3 Quivers for Quasi-Minimal Singularities

In this section we focus on the elementary slices in the affine Grassmannian that did not make an appearance in [32], corresponding to the quasi-minimal singularities reviewed in Section 2.6:

- The ac_n slices are the lowest slices in the component of $\text{Gr}_{\text{Sp}(n)}$ not connected to the identity.
- The slices cg_2 and ag_2 , which appear in Gr_{G_2} , and were identified in Figure 13.

In this section, we study magnetic quivers for these elementary slices, which are crucial in the algorithm of quiver subtraction and quiver addition, see Section 5. They are deduced from the coweights that are used to define them, using the formulas of Section 3.1. The quivers are gathered in Table 1.

We start with the ac_n singularity. It is the Coulomb branch of the quivers

$$ac_n: \quad \begin{array}{c} 1 \square \quad \quad \quad \square 1 \\ | \quad \quad \quad | \\ \bigcirc \text{---} \bigcirc \text{---} \dots \text{---} \bigcirc \text{---} \bigcirc \text{---} \bigcirc \\ 1 \quad 1 \quad \dots \quad 1 \quad 1 \quad 1 \end{array} \quad (3.6)$$

$\underbrace{\hspace{15em}}_n$

The global symmetry is $\mathfrak{su}(n) \times \mathfrak{u}(1)$, which is consistent with the rightmost node being overbalanced, while the other nodes are balanced and form the A_{n-1} Dynkin diagram. The Coulomb branch Hilbert series can be neatly encapsulated in the form of a highest weight generating function (HWG) [50]:

$$\begin{aligned} \text{HWG} &= \frac{1 - \mu_1^2 \mu_{n-1}^2 t^6}{(1 - t^2)(1 - \mu_1 \mu_{n-1} t^2)(1 - \frac{\mu_1^2 t^3}{q})(1 - q \mu_{n-1}^2 t^3)} \\ &= \text{PE} \left[t^2 + \mu_1 \mu_{n-1} t^2 + (q \mu_1^k + q^{-1} \mu_{n-1}^k) t^{k+1} - \mu_1^k \mu_{n-1}^k t^{2k+2} \right] \end{aligned} \quad (3.7)$$

where μ_i and q are Dynkin fugacities of $\mathfrak{su}(n)$ and $\mathfrak{u}(1)$ respectively. From the HWG we can also obtain the unrefined Hilbert series. For ac_2 , the unrefined Hilbert series is:

$$\text{HS} = \frac{1 + 2t^2 + 4t^3 + 2t^4 + t^6}{(1 - t)^2(1 - t^2)^2(1 + t + t^2)^2} \quad (3.8)$$

In addition, we also provide the refined plethystic logarithm (PL) of the Hilbert series which encodes representation content of the generators and relations in the Coulomb branch in Table 5.

For G_2 affine Grassmannian, we have two new elementary slices which are the ag_2 and cg_2 . For ag_2 , the quiver takes the form:

$$ag_2: \quad \begin{array}{c} 1 \square \quad \square 1 \\ | \quad \quad | \\ \bigcirc \text{---} \bigcirc \\ 1 \quad 1 \end{array} \quad (3.9)$$

with global symmetry $\mathfrak{su}(2) \times \mathfrak{u}(1)$. The HWG takes the form:

$$\begin{aligned} \text{HWG} &= \frac{(1 - \mu^6 t^8)}{(1 - t^2)(1 - \mu^2 t^2)(1 - \frac{\mu^3 t^4}{q})(1 - \mu^3 q t^4)} \\ &= \text{PE}[t^2 + \mu^2 t^2 + (q + q^{-1})\mu^3 t^4 - \mu^6 t^8] \end{aligned} \quad (3.10)$$

where μ and q are the Dynkin fugacities of $\mathfrak{su}(2)$ and $\mathfrak{u}(1)$ respectively. The unrefined Hilbert series is

$$\text{HS} = \frac{1 + 2t^2 + 8t^4 + 2t^6 + t^8}{(1 - t^2)^2(1 - t^4)^2} \quad (3.11)$$

and the refined PL is given in Table 6. For cq_2 the quiver takes the form:

cg_2 :

(3.12)

where the global symmetry is $\mathfrak{su}(2) \times \mathfrak{u}(1)$. The HWG is:

$$\begin{aligned} \text{HWG} &= \frac{1 + \mu^2 t^2 + \mu^4 t^4}{(1 - t^2) \left(1 - \frac{\mu^3 t^3}{q}\right) (1 - q \mu^3 t^3)} \\ &= \text{PE}[t^2 + \mu^2 t^2 + (q + q^{-1}) \mu^3 t^3 - \mu^6 t^6] \end{aligned} \quad (3.13)$$

where μ and q are the Dynkin fugacities of $\mathfrak{su}(2)$ and $\mathfrak{u}(1)$ respectively. The unrefined Hilbert series takes the form:

$$\text{HS} = \frac{1 - 2t + 5t^2 - 2t^3 + t^4}{(1-t)^4(1+t+t^2)^2} \quad (3.14)$$

with the refined PL given in Table 5.

These three singularities, along with Kleinian singularities and closures of minimal nilpotent orbits are all the singularities that occur as elementary slices in affine Grassmannians. However, this does not mean we have a complete list of *all possible* elementary slices for symplectic singularities. In [51], we introduced a two parameter family $h_{n,k} \cong \mathbb{H}^n/\mathbb{Z}_k$ of singularities which generalizes the c_n singularities ($c_n = h_{n,2}$). They were used to characterize certain elementary slices in Higgs branches of 4d $\mathcal{N} = 2$ rank 1 SCFTs. The quiver for $h_{n,k}$ is

$$\begin{array}{c}
1 \\
\boxed{} \\
| \\
\bigcirc \text{---} \bigcirc \text{---} \dots \text{---} \bigcirc \text{---} \bigcirc \text{---} \bigcirc \\
1 \qquad 1 \qquad \qquad 1 \qquad 1 \qquad 1
\end{array}
\quad (3.15)$$

with $\mathfrak{u}(n)$ global symmetry.

n	Beginning of the expansion of the PL
2	t^2 : $[2] + [0]$ t^3 : $(q + \frac{1}{q})[2]$ t^4 : $-[0]$ t^5 : $-(q + \frac{1}{q})([0] + [2])$
3	t^2 : $[11] + [00]$ t^3 : $q[20] + \frac{1}{q}[02]$ t^4 : $-[00] - [11]$ t^5 : $-q([01] + [12] + [20]) - \frac{1}{q}([02] + [10] + [21])$
4	t^2 : $[101] + [000]$ t^3 : $q[200] + \frac{1}{q}[002]$ t^4 : $-[000] - [020] - [101]$ t^5 : $-q([010] + [111] + [200]) - \frac{1}{q}([002] + [010] + [111])$

Table 5. ac_n refined PL. $[\dots]$ are the Dynkin labels for $SU(n)$.

	Beginning of the expansion of the PL
ag_2	t^2 : $[2] + [0]$ t^4 : $-[0] + q[3] + \frac{1}{q}[3]$ t^6 : $-(1 + q^2 + \frac{1}{q^2})[0] - [2] - [4]$
cg_2	t^2 : $[2] + [0]$ t^3 : $q[3] + \frac{1}{q}[3]$ t^4 : $-[0] + q[3] + \frac{1}{q}[3]$ t^5 : $-(q + \frac{1}{q})([1] + [3])$

Table 6. ag_2 and cg_2 refined PL. $[\dots]$ are the Dynkin labels for $SU(2)$.

Along a similar line of logic, we expect the generalization of ac_n and ag_2 a two parameter family of singularities that we call $\bar{h}_{n,k}$, with $a_2 = \bar{h}_{n,1}$, $ac_n = \bar{h}_{n,2}$ and $ag_2 = \bar{h}_{2,3}$. The quiver for $\bar{h}_{n,k}$ is

$$\begin{array}{c}
\begin{array}{ccccccc}
1 & & & & & & 1 \\
\boxed{} & & & & & & \boxed{} \\
| & & & & & & | \\
\bigcirc & \text{---} & \bigcirc & \text{---} & \cdots & \text{---} & \bigcirc & \text{---} & \bigcirc & \text{---} & \bigcirc \\
1 & & 1 & & & & 1 & & 1 & & 1 \\
\hline
& & & & & & & & & & n
\end{array}
\end{array}
\tag{3.16}$$

where the global symmetry is also $\mathfrak{u}(n)$. The Coulomb branch is no longer an orbifold.

The HWGs for the singularities $h_{n,k}$ and $\bar{h}_{n,k}$ are

$$\text{HWG}[h_{n,k}] = \text{PE} \left[t^2 + \mu_1 \mu_{n-1} t^2 + (q \mu_1^k + q^{-1} \mu_{n-1}^k) t^{k+1} - \mu_1^k \mu_{n-1}^k t^{2k} \right] \quad (3.17)$$

$$\text{HWG}[\bar{h}_{n,k}] = \text{PE} \left[t^2 + \mu_1 \mu_{n-1} t^2 + (q \mu_1^k + q^{-1} \mu_{n-1}^k) t^{k+1} - \mu_1^k \mu_{n-1}^k t^{2k+2} \right] \quad (3.18)$$

where μ_i and q are the Dynkin fugacities of $\mathfrak{u}(n) \cong \mathfrak{su}(n) \times \mathfrak{u}(1)$. A highest weight variety for $h_{n,k}$ is $\mathbb{C} \times \mathbb{C}^2/\mathbb{Z}_k$, with equation $xy = z^k$. A highest weight variety for $\bar{h}_{n,k}$ is the threefold defined by the equation $xy = z^k w$ for $(x, y, z, w) \in \mathbb{C}^4$.

Unframed quivers. So far we have considered quivers with an explicit framing (flavor nodes). Magnetic quivers for higher dimensional supersymmetric gauge theories ($4d \mathcal{N} = 2$, $5d \mathcal{N} = 1$ and $6d \mathcal{N} = (1, 0)$ theories) usually arise from brane configurations, and are more conveniently written without framing. For unframed quivers, it is understood that a $U(1)$ node has to be ungauged on the long side [32, 52]. The quivers discussed in this section are summarized in both framed and unframed form in Table 1.

4 Branes

In this section we construct brane systems for the affine Grassmannian of classical groups consisting of NS5, D5, and D3 branes in Type IIB String Theory as first developed in [9], possibly in presence of an ON plane. The method of reading quivers from such brane systems, including quivers for transverse slices, is reviewed in Appendix A.

Affine Grassmannian. As discussed in Section 2, the affine Grassmannian $[\text{Gr}_G]$ of a group G consists of several connected components, one for each lowest dominant coweight Ω_I , see Table 2. Each connected component of the affine Grassmannian is infinite dimensional, as are the transverse slices $[\mathcal{W}_G]_\lambda$. The transverse slices $[\overline{\mathcal{W}_G}]_\lambda^\mu$ however are finite dimensional and can be constructed as a Coulomb branch⁸ of a quiver theory as discussed in Section 3. Every such quiver describes the low energy theory of a brane system, which can be obtained using simple rules (see Appendix A). The goal of this section however, is to turn this around and to generate the affine Grassmannian, or rather any $[\mathcal{W}_G]_\lambda$, from a brane system. For every component I in the affine Grassmannian a brane system is proposed whose phases correspond to the symplectic leaves of $[\mathcal{W}_G]_{\Omega_I}$. From this brane system all of $[\mathcal{W}_G]_{\Omega_I}$ can be constructed. Since the objective is to construct an infinite dimensional space, an infinite number of moduli (D3 branes) must be present in the brane system. To study the symplectic leaves of $[\mathcal{W}_G]_{\Omega_I}$ from bottom-up, we restrict the movements of almost every D3 brane and only turn on few moduli at a time, moving from one symplectic leaf of $[\mathcal{W}_G]_{\Omega_I}$ to another. Starting at the lowest leaf, i.e. all D3 branes rest at the origin, this process generates the transverse slices to the lowest leaf in the component at hand. This bottom-up construction solely uses Kraft-Procesi transitions [13–15] in brane systems, without the need to rely on the results of Section 3. As a result, the affine Grassmannian arises naturally in brane systems.

⁸Higgs branch constructions are possible but not discussed in this paper.

All other finite slices $\overline{[\mathcal{W}_G]_\lambda}^\mu$ in the affine Grassmannian are contained in the brane systems as (generically non-elementary) Kraft-Procesi transitions. Furthermore any $[\mathcal{W}_G]_\lambda$ may be constructed bottom-up from the proposed brane systems by first moving to the phase in the brane system which corresponds to $[\mathcal{W}_g]_{\Omega_I}^\lambda$, ignoring the already turned on D3 moduli, and proceeding with Kraft-Procesi transitions.

4.1 The A-type affine Grassmannian

The affine Grassmannian of $\mathrm{PSL}(n, \mathbb{C})$ consists of n connected components. We propose a brane system for each such component. More precisely, we propose a brane system for $[\mathcal{W}_{\mathrm{PSL}(n, \mathbb{C})}]_{\Omega_I}$ for every lowest dominant coweight Ω_I .

Component $0 \in \mathbb{Z}_n$ The component connected to the origin (component 0) is in fact the affine Grassmannian of $\mathrm{SL}(n, \mathbb{C})$. The proposed brane system for $[\mathcal{W}_{\mathrm{PSL}(n, \mathbb{C})}]_{[0, \dots, 0]}$ consists of n NS5 branes with an infinite number of D5 branes on both sides, and an infinite number of D3 branes extended between every neighbouring pair of D5 branes.

$$(4.1)$$

When drawing the brane system, we generally do not depict branes which are not essential to study the symplectic leaf at hand, i.e. we suppress those branes resting at the origin. Depicting the origin of $[\mathcal{W}_{\mathrm{PSL}(n, \mathbb{C})}]_{[0, \dots, 0]}$ and suppressing all irrelevant branes leads to the following:

$$(4.2)$$

For this brane system we read the empty quiver:

$$\begin{array}{ccccccc}
 & 0 & & 0 & & & 0 \\
 & \square & & \square & & & \square \\
 & | & & | & & & | \\
 & \circ & \text{---} & \circ & \text{---} & \cdots & \text{---} & \circ \\
 & 0 & & 0 & & & & 0
 \end{array} \tag{4.3}$$

i.e. the origin of $[\mathcal{W}_{PSL(n,\mathbb{C})}]_{[0,\dots,0]}$ corresponding to the lowest dominant coweight $\Omega_0 = [0, 0, \dots, 0]$.

Other components. The transverse slices to the lowest leaf in the remaining connected components of the affine Grassmannian of $PSL(n, \mathbb{C})$ can be constructed from a brane system where a single D5 is in one of the intervals between two neighbouring NS5 branes. For example, placing a D5 brane in the first interval we obtain the following brane system:

$$\begin{array}{c}
 \begin{array}{c}
 | \qquad | \qquad \qquad | \\
 \bullet \qquad \qquad \cdots \qquad \qquad \cdot \\
 \hline
 n \text{ NS5}
 \end{array}
 \end{array} \tag{4.4}$$

For this brane system we read the quiver:

$$\begin{array}{ccccccc}
 & 1 & & 0 & & & 0 \\
 & \square & & \square & & & \square \\
 & | & & | & & & | \\
 & \circ & \text{---} & \circ & \text{---} & \cdots & \text{---} & \circ \\
 & 0 & & 0 & & & & 0
 \end{array} \tag{4.5}$$

which represents the origin of $[\overline{\mathcal{W}_{PSL_n}}]_{[1,0,\dots,0]}$, corresponding to the lowest dominant coweight $\Omega_0 = [1, 0, \dots, 0]$.

The two brane systems in (4.2) and (4.4) contain an infinite number of D5 branes; however, they differ as the D5 brane depicted in (4.4) has a different linking number⁹ than any of the D5 branes in (4.2).

Quotients of $SL(n, \mathbb{C})$. For quotients $SL(n, \mathbb{C})/\mathbb{Z}_k$, where k divides n , k connected components make up its affine Grassmannian. The starting points for the respective components are those with a single D5 placed in the I -th interval satisfying the condition

$$I \bmod \frac{n}{k} = 0, \tag{4.6}$$

⁹All prescriptions for linking numbers are equivalent and can be used.

which has k solutions for $I \in \{0, \dots, n-1\}$.

Example: The possible starting intervals for a D5 (depicted by an \times) to be placed for a respective component of the affine Grassmannian of $\mathrm{SL}(6, \mathbb{C})/\mathbb{Z}_k$ are as follows:

$k = 6$	\times	\times	\times	\times	\times	
$k = 3$		\times		\times		
$k = 2$			\times			
$k = 1$						

(4.7)

Note that a brane system without a D5 in any interval corresponds to the component connected to the origin, the 0-th component, which is always present for any $\mathrm{SL}(n, \mathbb{C})/\mathbb{Z}_k$.

Identifying the component. Given a brane system for any slice in the affine Grassmannian of $\mathrm{PSL}(n, \mathbb{C})$, with n_l D5 branes in the l -th interval, there is a simple formula to compute which component the corresponding slice belongs to:

$$\sum_{l=1}^{n-1} l n_l \bmod n = I \quad , \quad (4.8)$$

where I labels the component. Now that we addressed the various components of the A-type affine Grassmannian, we can start exploring the stratification of each component.

Symplectic leaves, minimal transitions. In order to study the different leaves of a given transverse slice in the affine Grassmannian one can start turning on Coulomb branch moduli of the brane system. However, this has to be done in a systematic way in order to identify every leaf. One has to carefully turn on a ‘minimal’ amount of moduli in the following two ways.

In order to open up Coulomb branch directions, one needs to consider an interval of D5 branes that contains at least 2 NS5 branes. In order to open up a minimal direction, the D5 branes need to be the closest two D5 branes separated by at least two NS5 branes. This leaves two options:

1. Activating a D3 brane between two neighbouring D5 branes (i.e. there is no D5 brane between them) separated by p NS5 branes, where $p \geq 2$. This corresponds to the

transverse slice a_{p-1} .

$$\text{Diagram (4.9): } a_{p-1} \quad . \quad (4.9)$$

2. Activating a D3 brane between two D5 branes which have exactly 2 NS5 branes between them, with possibly $q \geq 0$ D5 branes between the two NS5 branes. This corresponds to a transverse slice A_{q+1} .

$$\text{Diagram (4.10): } A_{q+1} \quad . \quad (4.10)$$

Clearly (4.9) for $p = 2$ and (4.10) for $q = 0$ are the same transition, as $a_1 = A_1$.

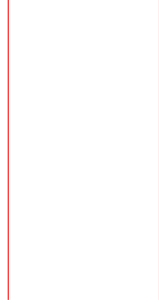
This allows a transition from one leaf to another. The quiver can be read from the brane system. Its Coulomb branch contains the moduli which are turned on, and the moduli space is the closure of the corresponding leaf. This is analysed in detail for rank 1 and 2 in the following two sections.

4.1.1 The A_1 affine Grassmannian

The affine Grassmannian for $\text{PSL}(2, \mathbb{C})$ has two connected components, corresponding to the two lowest dominant coweights, $[0]$ and $[1]$.

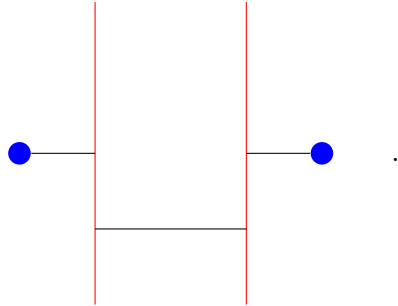
Component $0 \in \mathbb{Z}_2$ $[\mathcal{W}_{\text{PSL}(2, \mathbb{C})}]_{[0]}$, for the 0-th component of the affine Grassmannian of $\text{PSL}(2, \mathbb{C})$, which is the affine Grassmannian of $\text{SL}(2, \mathbb{C})$, is given by a brane system with infinitely many D3 branes which are free to move between two NS5 branes in the presence of D5 branes. The origin of $[\mathcal{W}_{\text{PSL}(2, \mathbb{C})}]_{[0]}$ is where all these infinitely many branes are coincident. Let us draw the two NS5 branes and suppress the infinitely many D3 branes

at the origin, as well as infinitely many D5 branes to the left and right.



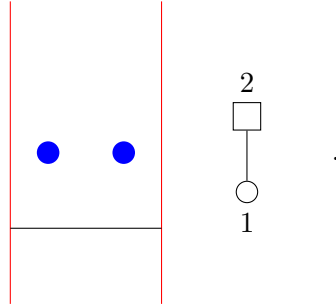
(4.11)

We move to the lowest non-trivial leaf by pulling a D3 brane from the stack of infinitely many branes at the origin and placing it between two D5 branes and letting it slide along the NS5 branes, corresponding to an A_1 transition:



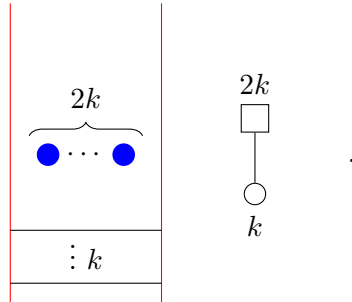
(4.12)

The stuck D3 branes between the two pairs of D5 and NS5 can be annihilated by a Hanany-Witten transition and we can read the quiver whose Coulomb branch is the closure of the leaf:



(4.13)

The only way to keep moving onto higher leaves in the affine Grassmannian is by repeating the same process. However, the D5 branes already placed between the NS5 branes make the transverse slices A_{2k-1} for the k -th transition of this type. A general leaf and the corresponding quiver are:



(4.14)

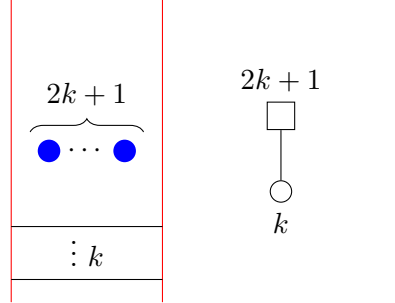
Which is indeed what we find in Section 3.

Component $1 \in \mathbb{Z}_2$ For the first connected component of $\mathrm{PSL}(2, \mathbb{C})$ we start with the following brane system:



(4.15)

Which depicts the origin of $[\mathcal{W}_{\mathrm{PSL}(2, \mathbb{C})}]_{[1]}$. The transverse slice for the k -th transition is A_{2k} while the brane system and quiver for the leaf are:



(4.16)

The quivers in (4.14) correspond to slices to the lowest leaf (origin) in the 0-th component of the affine Grassmannian, while the quivers in (4.16) correspond to slices to the lowest leaf in the 1-st component. The other slices, between any two leaves in a connected component, are realised as (generically non-minimal) Kraft-Procesi transitions [15] in the brane system. The form of the quiver is a framed A_1 quiver, or an SQCD theory with $U(k)$ gauge group and N flavors, satisfying $N \geq 2k$. k is the number of minimal slices between the two leaves, and N is even for slices in the 0-th component, while N is odd for slices in the 1-st component. In this way every good quiver of A_1 type is realised in one of the two brane systems corresponding to the two connected components of the affine Grassmannian of $\mathrm{SL}(2, \mathbb{C})$.

4.1.2 The A_2 affine Grassmannian

The affine Grassmannian of $\mathrm{PSL}(3, \mathbb{C})$ has 3 disconnected components.

Component $0 \in \mathbb{Z}_3$ The brane systems for the lower symplectic leaves and elementary slices between them for the component connected to the origin are depicted in Figure 14.

Component $1, 2 \in \mathbb{Z}_3$ The brane systems for the lower symplectic leaves and elementary slices between them for one of the components not connected to the origin are depicted in Figure 15. The brane system for the other component is related to the one depicted in Figure 15 by a \mathbb{Z}_2 action $x^6 \mapsto -x^6$, and we do not draw it.

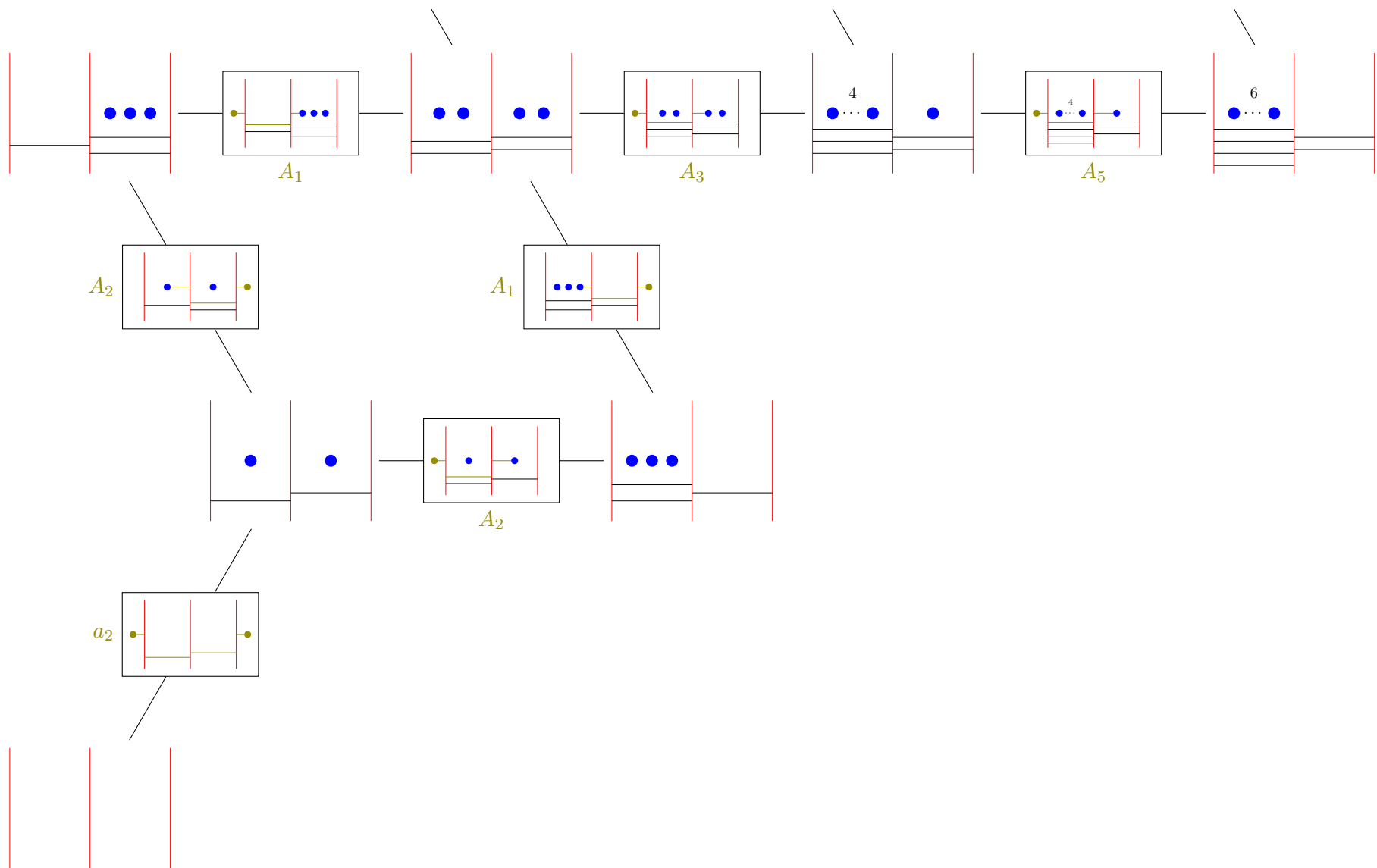


Figure 14. Brane depiction of the low dimensional leaves [and elementary slices between them] of $[\mathcal{W}_{\text{PSL}(3,\mathbb{C})}]_{[0,0]}$.

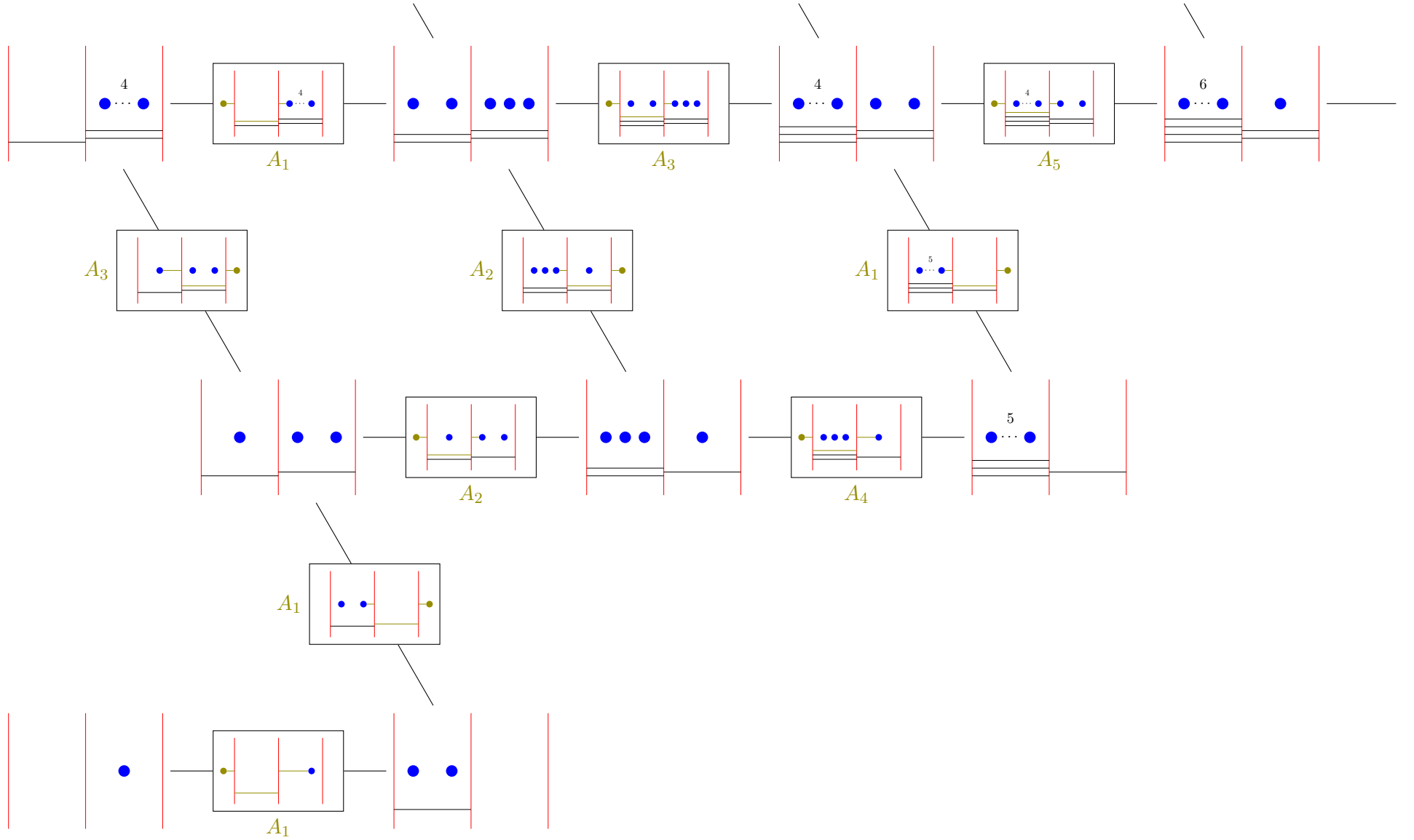


Figure 15. Brane depiction of the low dimensional leaves [and elementary slices between them] of $[\mathcal{W}_{\text{PSL}(3,\mathbb{C})}]_{[0,1]}$.

4.2 The B -type affine Grassmannian

For this setup, we require a $\widetilde{\text{ON}}^-$ plane. In the main text we always draw the full covering space and refer to half branes simply as branes.

Component $0 \in \mathbb{Z}_2$ The the affine Grassmannian of $\text{Spin}(2n+1, \mathbb{C})$ is the 0-th component of the affine Grassmannian of $\text{SO}(2n+1, \mathbb{C})$. The brane system for $[\mathcal{W}_{\text{SO}(2n+1, \mathbb{C})}]_{[0,0,\dots,0]}$ is proposed to be

(4.17)

Depicted at the origin, with all D3 branes and D5 branes suppressed. The quiver representing the origin is:

(4.18)

Component $1 \in \mathbb{Z}_2$ The brane system for the 1-st component of the affine Grassmannian of $\text{SO}(2n+1, \mathbb{C})$, is proposed to be

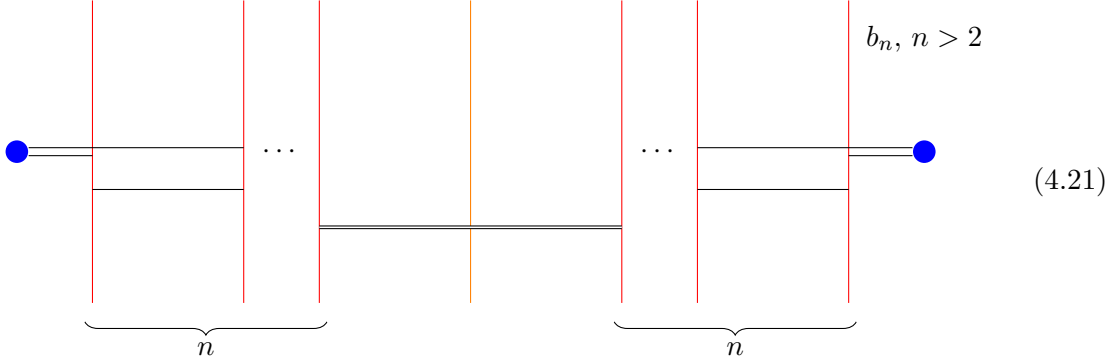
(4.19)

Depicted at the origin, with all D3 branes and D5 branes suppressed. The quiver representing the origin is:

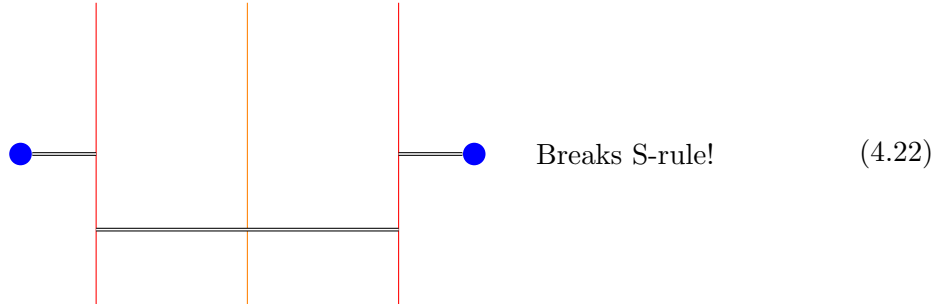
(4.20)

Which is indeed the quiver representing the origin of $[\mathcal{W}_{\text{SO}(2n+1, \mathbb{C})}]_{[1,0,\dots,0]}$.

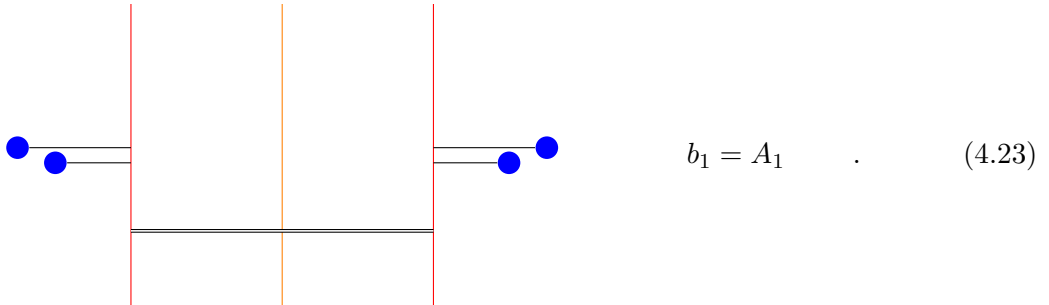
Minimal transitions. When activating D3 branes between D5 branes, one can follow the same procedure as for the A-type affine Grassmannian, when considering branes away from the ON (keeping in mind that in the covering space one has to move mirrors images alike). If however one wants to activate a D3 brane between a D5 brane and its image, in order to move the D3 brane along an NS5 brane and its image, one has to keep in mind the boundary conditions reviewed in Appendix A. The D3 brane ending on a D5 brane and its image needs to be accompanied by its own mirror image. The associated transition is b_n if the D5 branes are separated by n NS5 branes (and their mirror images).



In the case of $n = 1$ one has to be slightly more careful. If we attempt to move the D3 brane and its mirror along the NS5 brane we would obtain a set up breaking the S-rule:



We therefore need to include another D5 brane and its mirror image and can now perform a $b_1 = A_1$ transition:



Drawing the D5 branes at different vertical positions is purely for convenience. In (4.23) more D5 branes could be present between the NS5 and the $\widetilde{\text{ON}}^-$ plane leading to A_k transitions.

When dealing with the 1-st component for $\text{SO}(5, \mathbb{C})$, i.e. $n = 2$, one also has to be careful with the first transition. Activating a minimal number of moduli without breaking supersymmetry has to be done like this:

This transition is called ac_2 as it appears also in the type C affine Grassmannians, and we use the isomorphism $C_2 = B_2$. For $n > 2$ no new slices arise.

4.2.1 The B_1 affine Grassmannian

Component $0 \in \mathbb{Z}_2$ The affine Grassmannian of $\text{Spin}(3, \mathbb{C})$, i.e. component 0 of the affine Grassmannian of $\text{SO}(3, \mathbb{C})$, is given by the brane system:

depicted at the origin of $[\mathcal{W}_{\text{SO}(3, \mathbb{C})}]_{[0]}$. We can now move onto the lowest non-trivial leaf through a $b_1 = A_1$ transition as in (4.23). After a Hanany-Witten transition we can read off the quiver:

The only way to keep moving onto higher leaves in $[\mathcal{W}_{\text{SO}(3, \mathbb{C})}]_{[0]}$ is by repeating the same thing, however the D5 branes already placed between the NS5 branes make the transverse slices A_{2k-1} for the k -th transition of this type. A general leaf and the corresponding quiver

are:

$$(4.27)$$

Which completely agrees with the construction in Section 4.1.1.

Component $1 \in \mathbb{Z}_2$ For the second connected component of $\mathrm{SO}(3, \mathbb{C})$ we start with:

$$(4.28)$$

depicting the origin of $[\mathcal{W}_{\mathrm{SO}(3, \mathbb{C})}]_{[1]}$. The transverse slice for the k -th transition is A_{2k} and the brane system and quiver for the leaf are:

$$(4.29)$$

Which is again in agreement with Section 4.1.1.

4.2.2 The B_2 affine Grassmannian

Component $0 \in \mathbb{Z}_2$ Is in Figure 16.

Component $1 \in \mathbb{Z}_2$ Is in Figure 17.

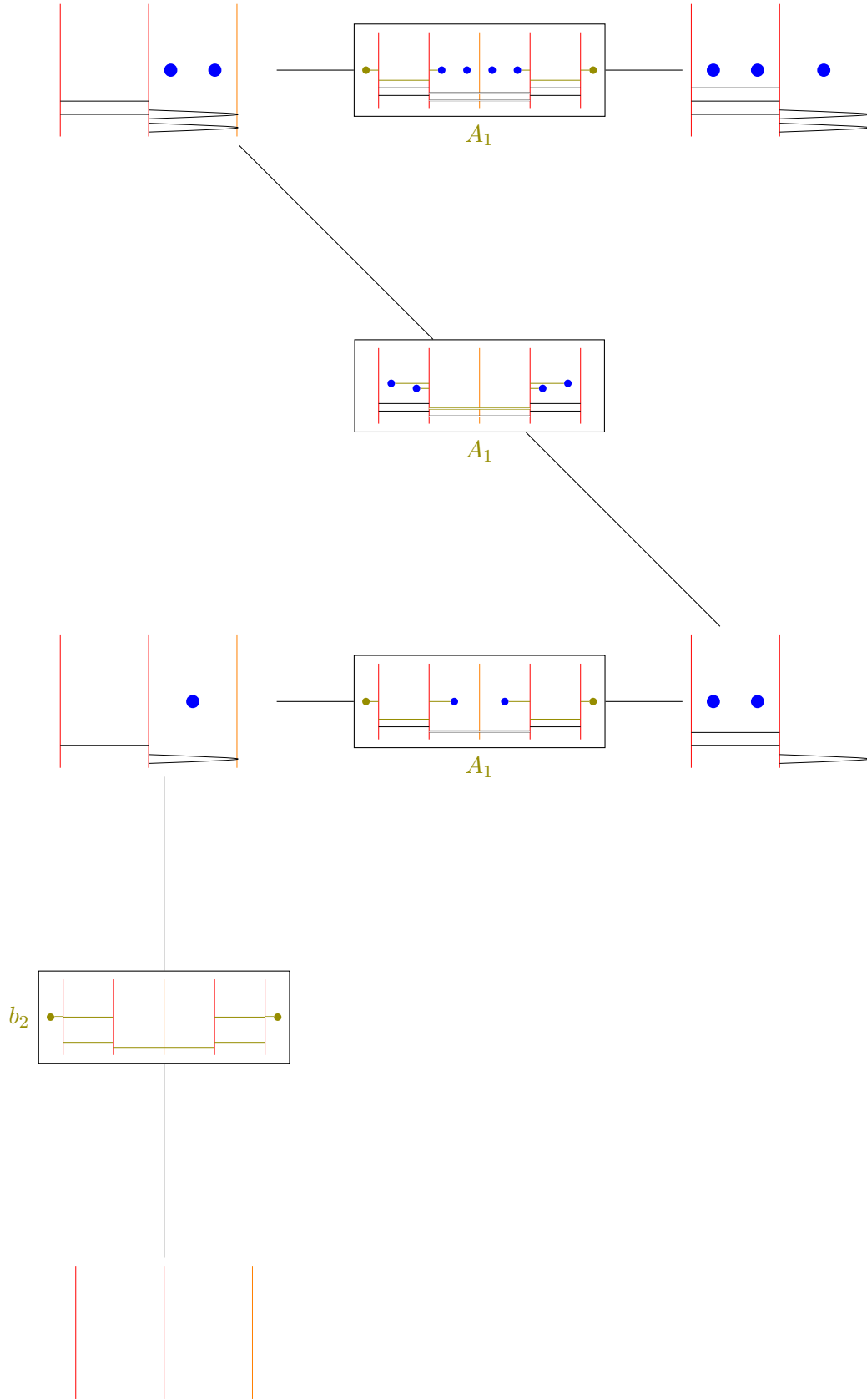


Figure 16. Brane depiction of the low dimensional leaves [and elementary slices between them] of $[\mathcal{W}_{\text{SO}(5,\mathbb{C})}]_{[0,0]}$.

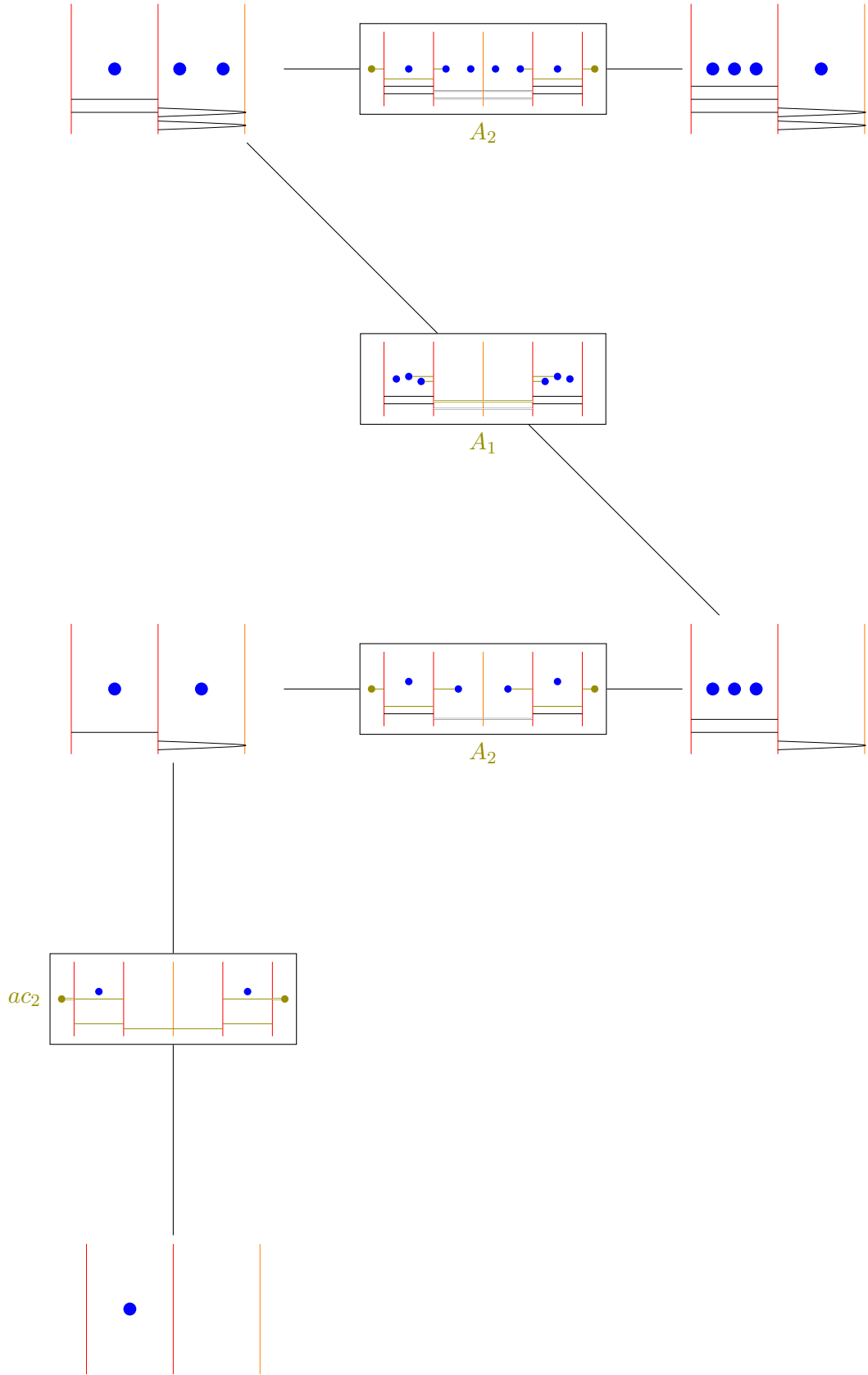


Figure 17. Brane depiction of the low dimensional leaves [and elementary slices between them] of $[\mathcal{W}_{\text{SO}(5,\mathbb{C})}]_{[1,0]}$.

4.3 The C -type affine Grassmannian

For this setup, we require a ON^+ plane. In the main text we draw the full covering space and refer to half branes simply as branes.

Component $0 \in \mathbb{Z}_2$ The brane system for the affine Grassmannian of $\text{Sp}(2n, \mathbb{C})$, i.e. the 0-th component of the affine Grassmannian of $\text{PSp}(2n, \mathbb{C})$, is proposed to be

Depicted is the origin of $[\mathcal{W}_{\text{PSp}(2n, \mathbb{C})}]_{[0, \dots, 0, 0]}$, with all D3 branes and D5 branes suppressed. The quiver representing the origin is:

Component $1 \in \mathbb{Z}_2$ The brane system for the 1-st component of the affine Grassmannian of $\text{PSp}(2n, \mathbb{C})$, is proposed to be

Depicted is the origin of $[\mathcal{W}_{\text{PSp}(2n, \mathbb{C})}]_{[0, \dots, 0, 1]}$, with all D3 branes and D5 branes suppressed. The quiver representing the origin is:

Minimal transitions. In the C -type brane systems, we may perform the same transitions as in the A -type case. Additionally there are two more minimal transitions:

$$\begin{array}{c}
 \text{Diagram (4.34): A brane system with vertical red lines and a central green line. Blue dots are on the outermost red lines. Horizontal lines connect the red lines, with a central segment crossing the green line. Labels include } c_n, n, \text{ and } \dots
 \end{array}
 \tag{4.34}$$

and

$$\begin{array}{c}
 \text{Diagram (4.35): A brane system similar to (4.34) but with a blue dot on the central green line. Labels include } ac_n, n, \text{ and } \dots
 \end{array}
 \tag{4.35}$$

For $n = 1$ there are transitions corresponding to Kleinian singularities studied in detail in the next section.

4.3.1 The C_1 affine Grassmannian

Component $0 \in \mathbb{Z}_2$ The affine Grassmannian of $\mathrm{PSp}(2, \mathbb{C})$ is given by the brane system:

$$\begin{array}{c}
 \text{Diagram (4.36): A brane system with three vertical lines: two red and one central green. A comma is placed to the right of the diagram.}
 \end{array}
 \tag{4.36}$$

depicted at the origin of $[\mathcal{W}_{\mathrm{PSp}(2, \mathbb{C})}]_{[0]}$. We can now move onto the lowest non-trivial leaf by activating a D3 brane between two D5 branes, which are mirror images, and moving the D3 brane along the NS5 branes, corresponding to a A_1 transition:

$$\begin{array}{c}
 \text{Diagram (4.37): A brane system with vertical red lines and a central green line. Blue dots are on the red lines. Horizontal lines connect the red lines, with a central segment crossing the green line.}
 \end{array}
 \tag{4.37}$$

After a Hanany-Witten transition we can read off the quiver:

$$\begin{array}{c}
 \text{[Diagram: Two vertical red lines, a central vertical green line, and a horizontal black line. Two blue dots are in the upper region, one in each side region.] \\
 \text{[Quiver: A square node labeled 2 connected to a circular node labeled 1.]}
 \end{array} . \quad (4.38)$$

The only way to keep moving onto higher leaves in the affine Grassmannian is by repeating the same thing, however the D5 branes already placed between the NS5 branes make the transverse slices A_{2k-1} for the k -th transition of this type. A general leaf and the corresponding quiver are:

$$\begin{array}{c}
 \text{[Diagram: Two vertical red lines, a central vertical green line, and a horizontal black line. Upper region: two groups of blue dots labeled k. Lower region: two vertical ellipses labeled k.] \\
 \text{[Quiver: A square node labeled 2k connected to a circular node labeled k.]}
 \end{array} . \quad (4.39)$$

This is in agreement with the construction in both Section 4.1.1 and 4.2.1.

Component $1 \in \mathbb{Z}_2$ For the second connected component for $\mathrm{PSp}(2, \mathbb{C})$ we start with:

$$\text{[Diagram: Two vertical red lines, a central vertical green line, and a single blue dot on the green line in the upper region.]} . \quad (4.40)$$

Depicting the origin of $[\mathcal{W}_{\mathrm{PSp}(2, \mathbb{C})}]_{[1]}$. The transverse slice for the k -th transition is A_{2k} and the brane system and quiver for the leaf are:

$$\begin{array}{c}
 \text{[Diagram: Two vertical red lines, a central vertical green line, and a horizontal black line. Upper region: three groups of blue dots labeled k. Lower region: two vertical ellipses labeled k.] \\
 \text{[Quiver: A square node labeled 2k + 1 connected to a circular node labeled k.]}
 \end{array} . \quad (4.41)$$

This is in agreement with the construction in both Section 4.1.1 and 4.2.1.

4.3.2 The C_2 affine Grassmannian

The two components are represented in Figures 18 and 19.

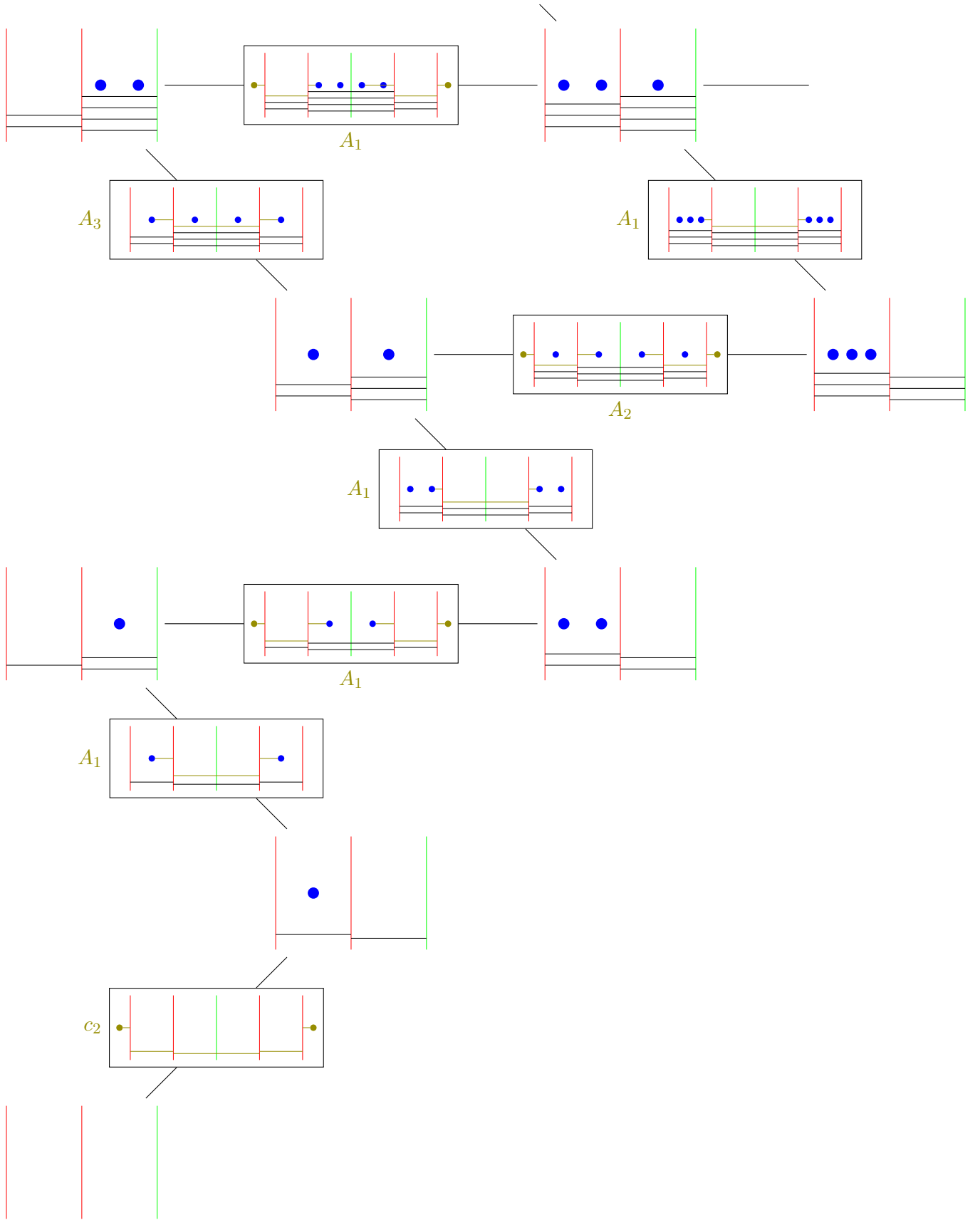


Figure 18. Brane depiction of the low dimensional leaves [and elementary slices between them] of $[\mathcal{W}_{\text{PSP}(4,\mathbb{C})}]_{[0,0]}$.

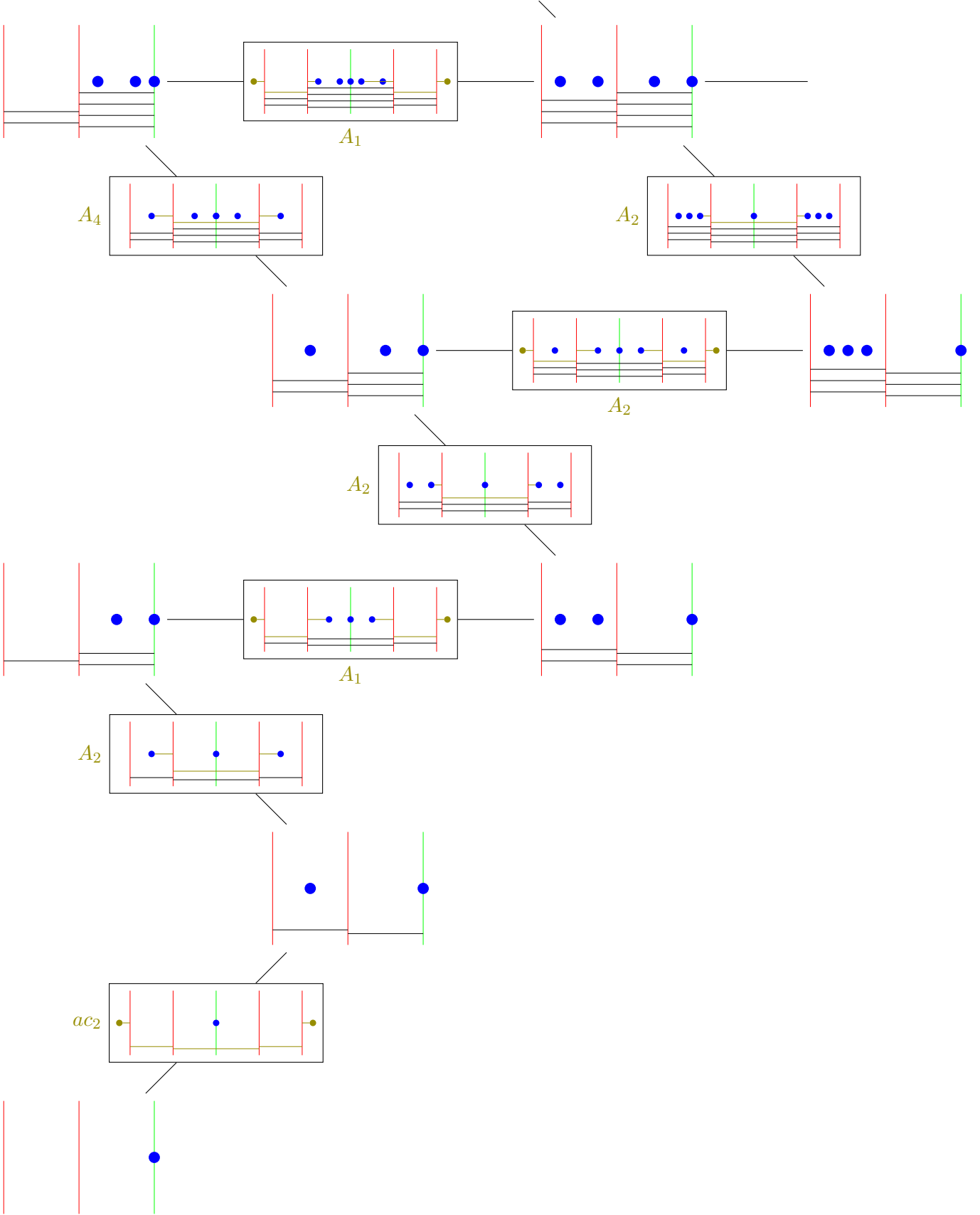


Figure 19. Brane depiction of the low dimensional leaves [and elementary slices between them] of $[\mathcal{W}_{\text{PSP}(4,\mathbb{C})}]_{[0,1]}$.

4.4 The D -type affine Grassmannian

For this setup, we require a ON^- plane. In the main text we draw the full covering space and refer to half branes simply as branes.

Component $(0, 0) \in \mathbb{Z}_2 \times \mathbb{Z}_2$ **or** $0 \in \mathbb{Z}_4$ The brane system for the affine Grassmannian of $\text{Spin}(2n, \mathbb{C})$, i.e. the $(0, 0)$ -th (for n even) or 0 -th component (for n odd) of the affine Grassmannian of $\text{PSO}(2n, \mathbb{C})$, is proposed to be

$$\underbrace{\quad \quad \quad}_n \quad \text{ON}^- \quad \underbrace{\quad \quad \quad}_n \quad (4.42)$$

Depicted is at the origin of $[\mathcal{W}_{\text{Spin}(2n, \mathbb{C})}]_{[0, 0, \dots, 0, 0, 0]}$, with all D3 branes and D5 branes suppressed. The quiver representing the origin is:

$$\begin{array}{c} 0 \quad 0 \quad 0 \\ \square \quad \square \quad \square \\ | \quad | \quad | \\ \circ \quad \circ \quad \circ \\ 0 \quad 0 \quad 0 \end{array} \quad \dots \quad \begin{array}{c} 0 \\ \square \\ | \\ \circ \\ 0 \end{array} \begin{array}{c} 0 \\ \circ \\ | \\ \square \quad 0 \end{array} \begin{array}{c} 0 \\ \circ \\ | \\ \square \quad 0 \end{array} \quad (4.43)$$

There are three more components.

Component $(1, 1) \in \mathbb{Z}_2 \times \mathbb{Z}_2$ **or** $2 \in \mathbb{Z}_4$

$$\underbrace{\quad \quad \quad}_n \quad \text{ON}^- \quad \underbrace{\quad \quad \quad}_n \quad (4.44)$$

Depicted at the origin of $[\mathcal{W}_{\text{Spin}(2n, \mathbb{C})}]_{[1,0,\dots,0,0,0]}$, with all D3 branes and D5 branes suppressed. The quiver representing the origin is:

$$(4.45)$$

Component $(1, 0) \in \mathbb{Z}_2 \times \mathbb{Z}_2$ **or** $1 \in \mathbb{Z}_4$

$$(4.46)$$

Depicted at the origin of $[\mathcal{W}_{\text{Spin}(2n, \mathbb{C})}]_{[0,0,\dots,0,1,0]}$, with all D3 branes and D5 branes suppressed. The quiver representing the origin is:

$$(4.47)$$

Component $(0, 1) \in \mathbb{Z}_2 \times \mathbb{Z}_2$ **or** $3 \in \mathbb{Z}_4$

$$(4.48)$$

Depicted at the origin of $[\mathcal{W}_{\text{Spin}(2n, \mathbb{C})}]_{[0,0,\dots,0,0,1]}$, with all D3 branes and D5 branes suppressed. The quiver representing the origin is:

$$(4.49)$$

Minimal transitions. In the D -type brane systems, we may perform the same transitions as in the A -type case. Additionally there is one more minimal transition:

$$(4.50)$$

4.4.1 The D_2 affine Grassmannian

There are four components:

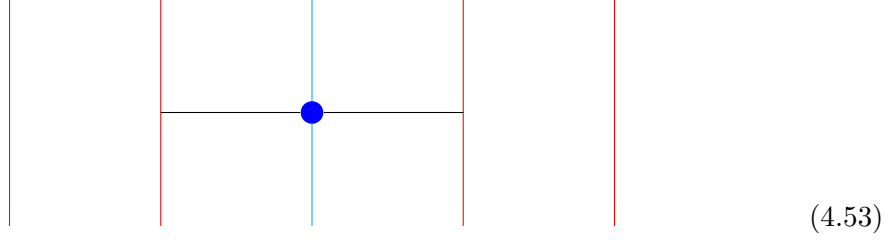
Component $(0,0) \in \mathbb{Z}_2^2$ This component is studied in Figure 20. The origin is

$$(4.51)$$

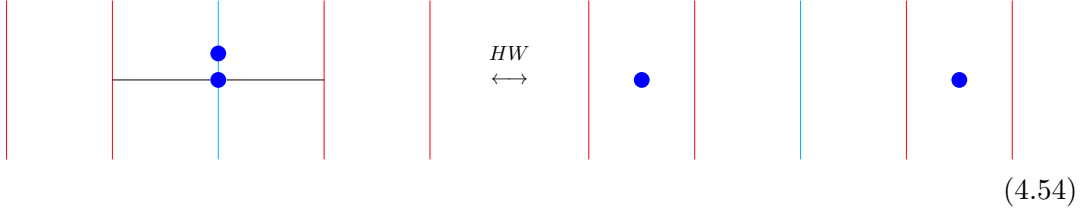
Component $(0,1) \in \mathbb{Z}_2^2$ This component is studied in Figure 21. The origin is

$$(4.52)$$

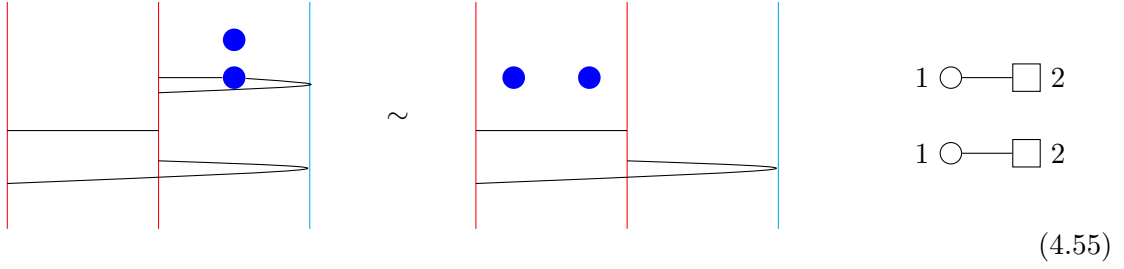
Component $(1, 0) \in \mathbb{Z}_2^2$ This component is studied in Figure 22. The origin is



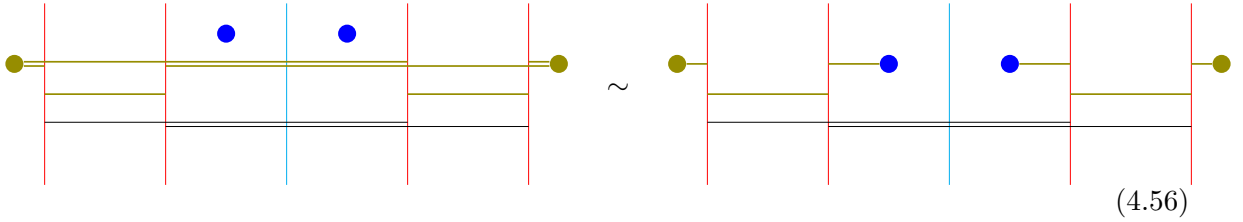
Component $(1, 1) \in \mathbb{Z}_2^2$ This component is studied in Figure 23. The origin is



Transition. While not strictly a Hanany-Witten transition, the following two brane webs are equivalent in that they depict the same leaf in the Coulomb branch:



In Figure 20 we use the representation on the left. Furthermore the following two transverse slices are equivalent and correspond to an A_1 transition:



The only difference between the two brane systems in (4.55) and (4.56) lies in their Higgs branch.

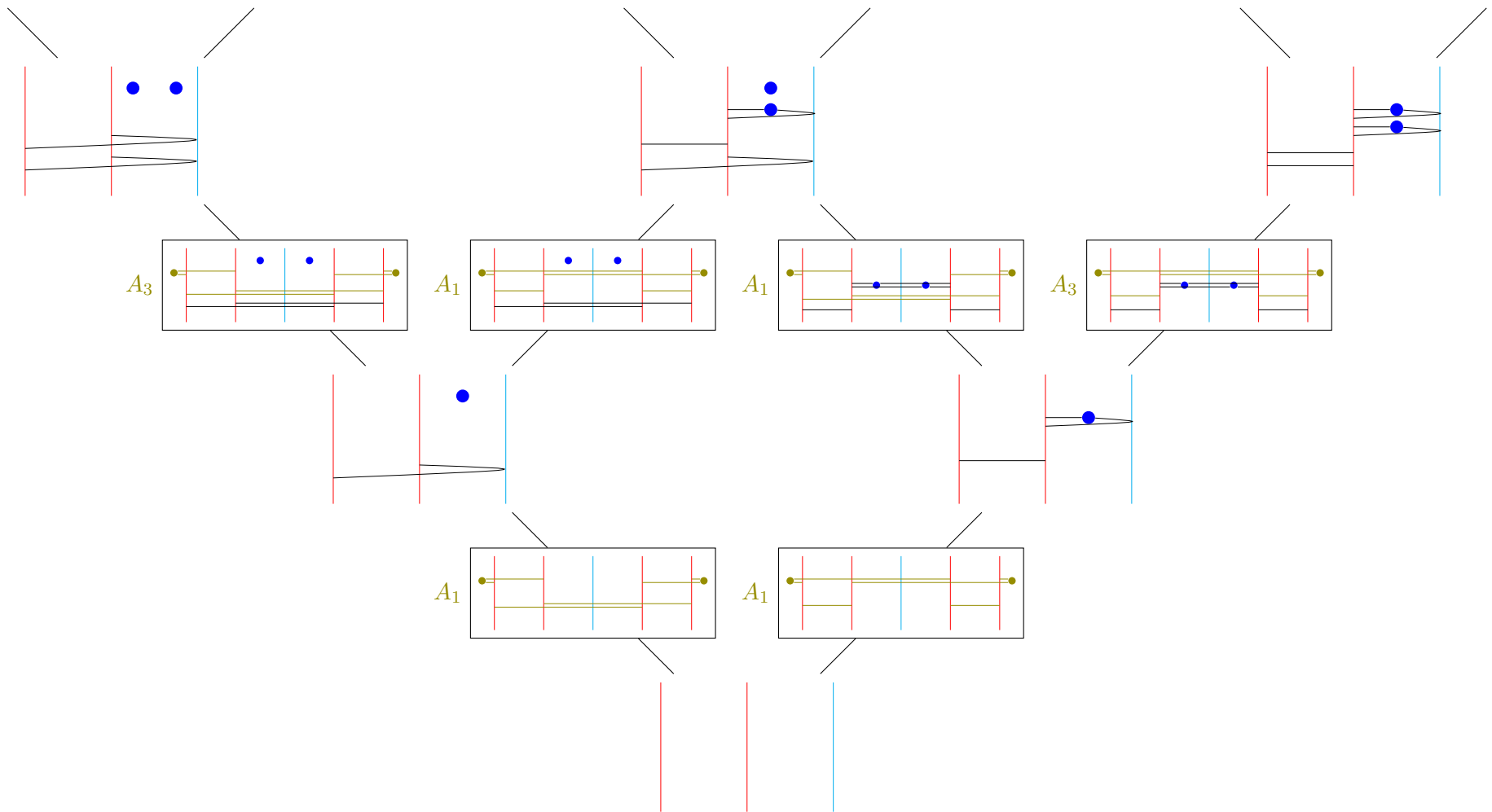


Figure 20. Brane depiction of the low dimensional leaves [and elementary slices between them] of $[\mathcal{W}_{\text{PSO}(4,\mathbb{C})}]_{[0,0]}$.

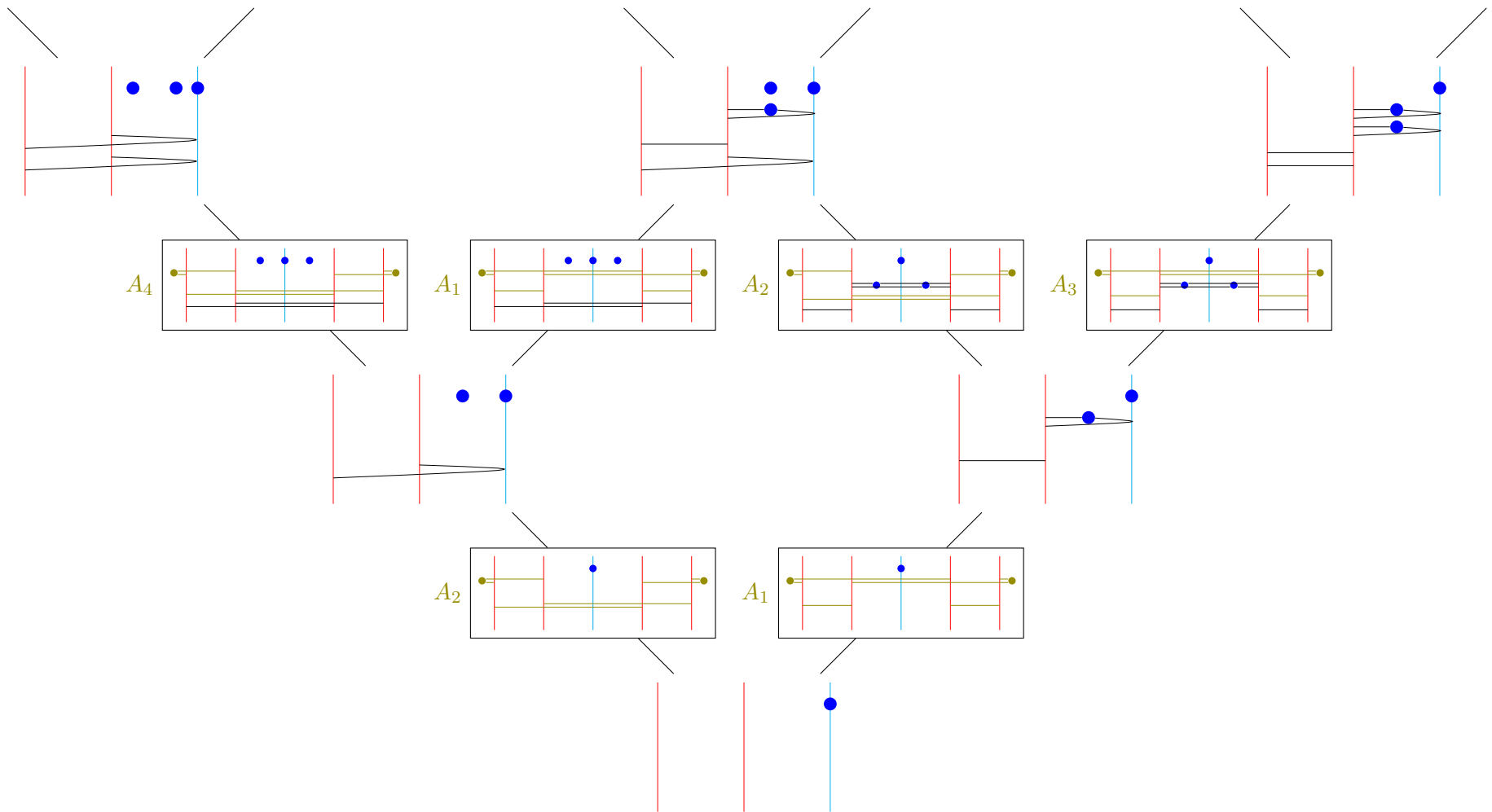


Figure 21. Brane depiction of the low dimensional leaves [and elementary slices between them] of $[\mathcal{W}_{\text{PSO}(4,\mathbb{C})}]_{[0,1]}$.

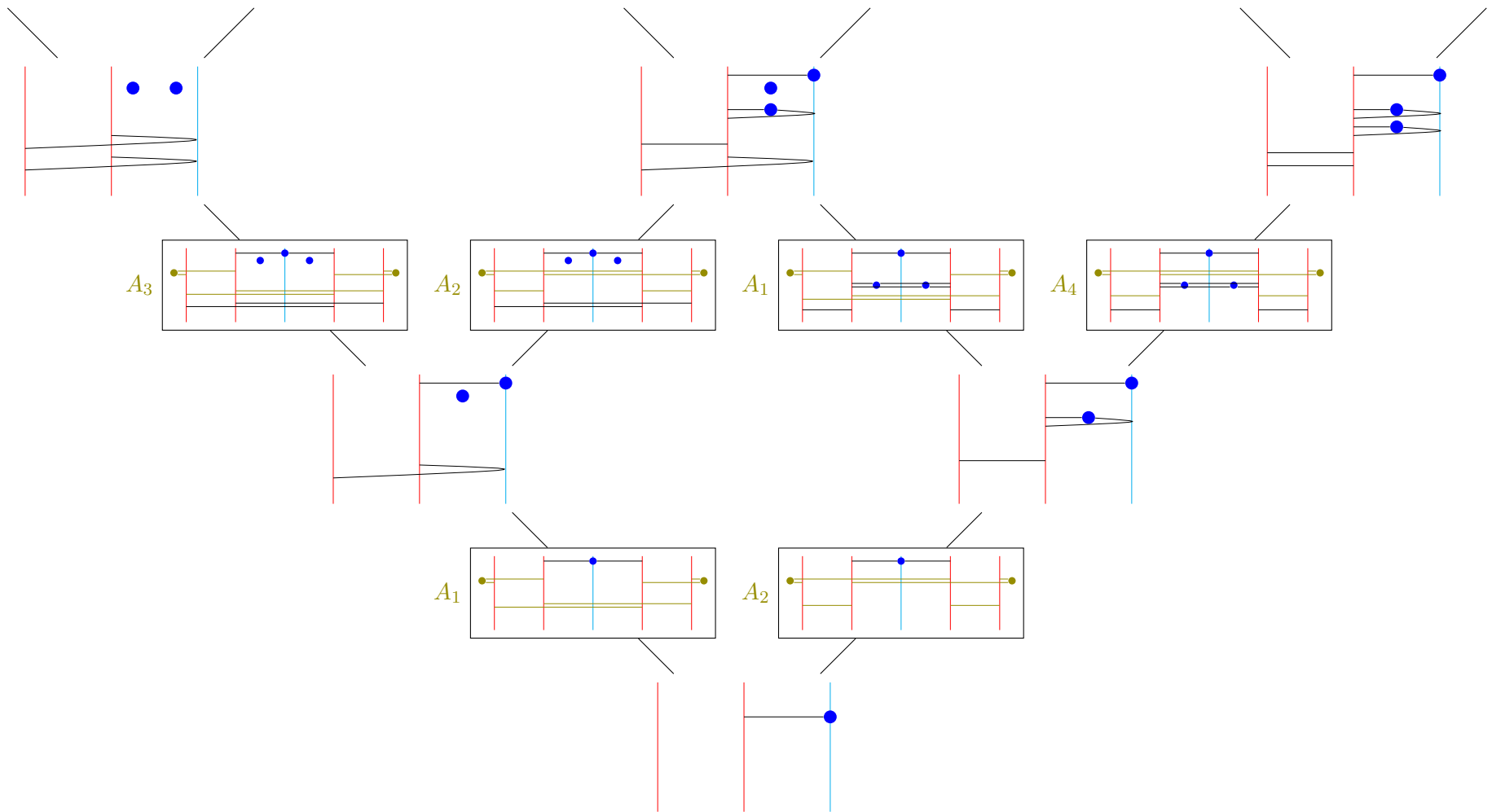


Figure 22. Brane depiction of the low dimensional leaves [and elementary slices between them] of $[\mathcal{W}_{\text{PSO}(4,\mathbb{C})}]_{[1,0]}$.

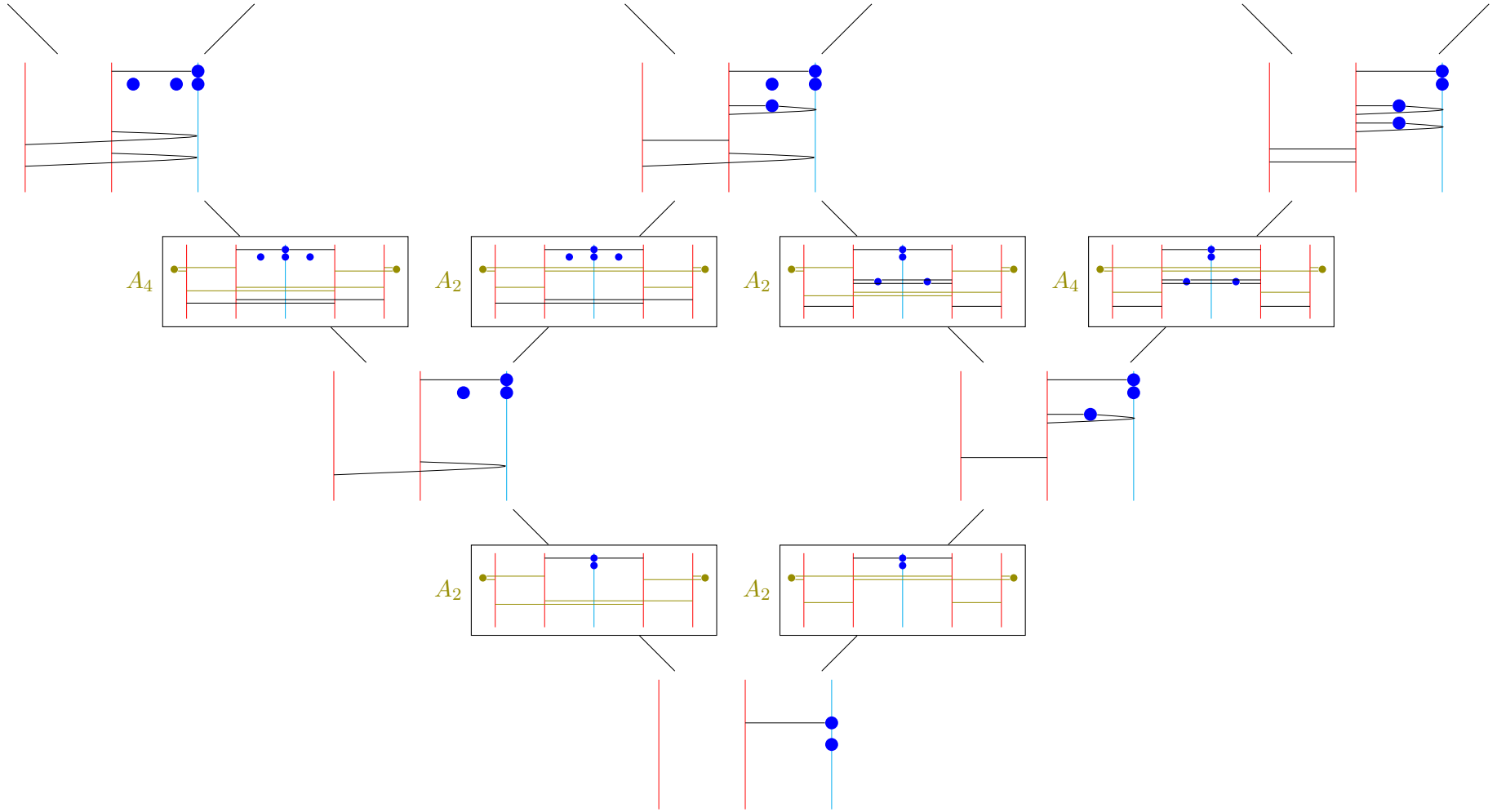


Figure 23. Brane depiction of the low dimensional leaves [and elementary slices between them] of $[\mathcal{W}_{\text{PSO}(4,\mathbb{C})}]_{[1,1]}$.

5 Quiver addition

5.1 Algorithm

In recent papers [15, 16, 32, 51–58], the notion of quiver subtraction was developed to obtain the Hasse diagram for symplectic singularities, and has been used in various scenarios [59–65]. In this section, we consider the reverse of this process: *quiver addition*. Aspects of this notion have been discussed in [60] for D -type Dynkin quivers. In this work, we show that the quiver addition algorithm presented below precisely reproduces the Hasse diagrams and quivers for the slices in the affine Grassmannian of any finite dimensional simple complex Lie group. For classical groups the quiver addition algorithm can be viewed as the quiver version of the brane constructions of Section 4, expressed in a way more suitable e.g. to teach a computer. For exceptional groups however no brane systems are known, and the quiver addition algorithm provides a simple but powerful way to obtain the Hasse diagram of any transverse slice in the affine Grassmannian. Before proceeding to quiver addition, let us review the procedure of quiver subtraction.

One way to obtain the Coulomb branch Hasse diagram of a quiver Q is to use quiver subtraction. In quiver subtraction one identifies an elementary slice with quiver D from Table 1 and subtracts it from Q following the algorithm given in [32, Appendix A] to produce a new quiver $Q' = Q - D$. We restrict to the case where a given elementary slice cannot be subtracted more than once consecutively.¹⁰ In this case, the Coulomb branch of Q' is the closure of a minimal degeneration of the highest leaf in the Coulomb branch of Q . One key point in the algorithm is that the balance of all the gauge nodes remains invariant during subtraction. If more than one quiver can be subtracted, the Hasse diagram bifurcates. As introduced above, we call the number of elementary slices which can be subtracted at any given step the disposition \mathfrak{D} of the leaf.

Conversely, to a given quiver one can generically add an infinite number of elementary quivers. However, if one imposes the restriction that *the Dynkin diagram formed by the gauge nodes remains invariant* then the number of possible slices allowed to be added becomes finite. We now discuss the algorithm.

Quiver addition algorithm. Let Q be a quiver of unitary gauge nodes forming a rank r finite Dynkin diagram with Cartan matrix $(C_{\mathfrak{g}})_{i,j=1,\dots,r}$. Let the ranks of the gauge nodes be $k_i \geq 0$, and the ranks of the flavors nodes be $N_i \geq 0$ for $i = 1, \dots, r$.¹¹

1. **Identification of the elementary quivers S to add.** Three kinds of elementary quivers can be added to Q .

- Define the subset of gauge nodes without any flavors

$$J_0 = \{j \in \{1, \dots, r\} \mid N_j = 0\} . \quad (5.1)$$

¹⁰If the same slice can be subtracted more than once, we are in the realm of affine Grassmannians of affine type, rather than finite type.

¹¹We emphasize that $k_i = 0$ is allowed, even when $N_i > 0$.

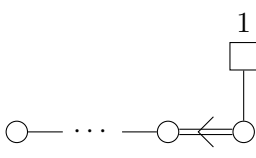
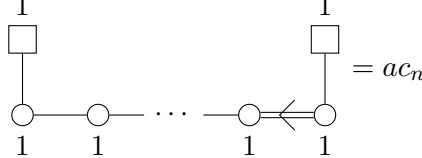
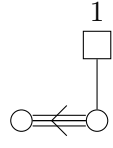
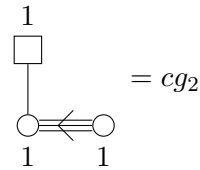
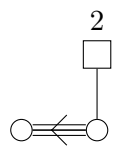
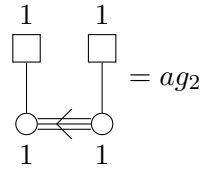
To this section of Q	One can add the following S
	
	
	

Table 7. Identification of the situations where the quivers for ac_n , cg_2 and ag_2 can be added. We insist on the fact that the flavor nodes must be exactly as indicated in the first column, and that there should be no flavorless gauge node connected to the portions of quiver drawn in the first column, so that quiver of the second column can be added.

The nodes labeled by J_0 form a union of connected Dynkin diagrams. For each connected Dynkin diagram, one can add the quiver S for the closure of the minimal nilpotent orbit (see Table 1).

- Consider the set of gauge nodes

$$J_1 = \{j \in \{1, \dots, r\} \mid N_j \geq 1 \text{ and } \forall j' \in \{1, \dots, r\}, N_{j'} \geq -(C_{\mathfrak{g}})_{j'j}\} \quad (5.2)$$

such that gauge node itself has flavours and also its connected neighbours have enough flavour. For each $j \in J_1$, one can add on that node the quiver for a Kleinian singularity A_{N_j+1} .

- If there is a subset of the gauge nodes which realize the quivers on the first column of Table 7 with *the flavors exactly as indicated*, and with *no flavorless gauge node connected to that subset*, then one can add the S in the second column.

2. Addition of the elementary quivers. The result of the addition of the elementary quiver S to Q is a quiver Q' with gauge nodes given by the Dynkin diagram specified by $(C_{\mathfrak{g}})_{i,j=1,\dots,r}$, where

- The ranks of the gauge groups k'_i are the sums of the ranks in Q and S.
- The flavors N'_i are given by the corresponding flavor in S if $k_i \neq k'_i$ and by rebalancing otherwise.

Note that the total number of flavors either stays the same or increases when a slice is added.¹² As we grow the Hasse diagram further, we reach a stage where all gauge groups have non-zero flavor nodes. Once this happens, the only slice that can be added are Kleinian A_k singularities. Hence, as the Hasse diagram grows, more and more Kleinian singularities populate the Hasse diagram. When all the nodes have flavors, the disposition is equal to the rank of the group, and can not decrease upon quiver addition.

5.2 Examples with simply laced quivers

Let us exemplify how the algorithm works in the case of good linear quivers. The set J_0 of unflavored nodes decomposes into smaller A -type diagrams, and for each such diagram, an a_n -type slice can be added.¹³ For instance, consider the following scenario:

$$\begin{array}{ccc}
 \begin{array}{c} \text{Can add } a_{m_1} \\ \begin{array}{c} \square \quad \square \\ | \quad | \\ \circ \quad \cdots \quad \circ \\ | \quad | \\ 1 \quad \cdots \quad 1 \\ \underbrace{\hspace{1cm}} \\ m_1 \end{array} \end{array} &
 \begin{array}{c} \text{Can add } a_{m_2} \\ \begin{array}{c} \square \quad \square \\ | \quad | \\ \circ \quad \cdots \quad \circ \\ | \quad | \\ 1 \quad \cdots \quad 1 \\ \underbrace{\hspace{1cm}} \\ m_2 \end{array} \end{array} &
 \begin{array}{c} \text{Can add } a_{m_3} \\ \begin{array}{c} \square \quad \square \\ | \quad | \\ \circ \quad \cdots \quad \circ \\ | \quad | \\ 1 \quad \cdots \quad 1 \\ \underbrace{\hspace{1cm}} \\ m_3 \end{array} \end{array} \\
 \downarrow & & \downarrow \\
 \begin{array}{c} \begin{array}{c} \circ \quad \cdots \quad \circ \quad \square \quad \circ \quad \cdots \quad \circ \quad \square \quad \circ \quad \cdots \quad \circ \quad \square \quad \circ \\ | \quad | \quad | \quad | \quad | \quad | \quad | \quad | \quad | \quad | \quad | \quad | \\ k_a \quad \cdots \quad k_b \quad k_c \quad k_d \quad \cdots \quad k_f \quad k_g \quad k_h \quad \cdots \quad k_i \quad k_j \\ \underbrace{\hspace{1cm}} \quad \underbrace{\hspace{1cm}} \quad \underbrace{\hspace{1cm}} \\ m_1 \quad m_2 \quad m_3 \end{array} \end{array}
 \end{array} \tag{5.3}$$

There are three possible slices one can add a_{m_1} , a_{m_2} , and a_{m_3} . For example, the result of adding the a_{m_2} slice produces:

$$\begin{array}{c}
 \begin{array}{c} \begin{array}{c} \circ \quad \cdots \quad \circ \quad \square \quad \square \quad \cdots \quad \square \quad \square \quad \cdots \quad \circ \quad \square \quad \circ \\ | \quad | \quad | \quad | \quad | \quad | \quad | \quad | \quad | \quad | \quad | \quad | \\ k_a \quad \cdots \quad k_b \quad k_c \quad k_{d+1} \quad \cdots \quad k_{f+1} \quad k_g \quad k_h \quad \cdots \quad k_i \quad k_j \\ \underbrace{\hspace{1cm}} \quad \underbrace{\hspace{1cm}} \quad \underbrace{\hspace{1cm}} \\ m_1 \quad m_2 \quad m_3 \end{array} \end{array}
 \end{array} \tag{5.4}$$

¹²Just like the number of D5 branes between NS5 branes stays the same or increases when moving upwards in the Hasse diagrams in Section 4

¹³The transition in the corresponding brane system is (4.9).

On the other hand the A -type Kleinian singularities can be added in the following situation:¹⁴

$$\begin{array}{ccc}
 \begin{array}{c} N_2+2 \\ \square \\ \circ \\ 1 \\ \downarrow \end{array} & \text{Can add } A_{N_2+1} & \\
 \begin{array}{c} N_1 \quad N_2 \quad N_3 \\ \square \quad \square \quad \square \\ \circ \quad \circ \quad \circ \\ \vdots \quad \vdots \quad \vdots \end{array} & \longrightarrow & \begin{array}{c} N_1-1 \quad N_2+2 \quad N_3-1 \\ \square \quad \square \quad \square \\ \circ \quad \circ \quad \circ \\ \vdots \quad \vdots \quad \vdots \end{array}
 \end{array} \tag{5.5}$$

which corresponds to nodes in the set J_1 .

Single unbalanced gauge group. As an illustration, we consider linear quivers with one unbalanced node, with imbalance $+1$. These quivers cover all cases of transverse slice to the lowest leaf in the components of $\text{Gr}_{\text{PSL}(N, \mathbb{C})}$ not connected to the trivial lattice. Quiver addition then reproduces the Hasse diagram and quivers for the transverse slices in these components of $\text{Gr}_{\text{PSL}(N, \mathbb{C})}$. Specifically, Figure 24 shows the first few leaves in the affine Grassmannian Hasse diagram of $\text{Gr}_{\text{PSL}(m_1+m_2+2, \mathbb{C})}$ for $m_1, m_2 \geq 6$ and lowest dominant coweight (see Table 2)

$$\Omega_{1+m_1} = [\underbrace{0 \dots 0}_{m_1} 1 \underbrace{0 \dots 0}_{m_2}]. \tag{5.6}$$

It is clear that for quivers where all gauge groups have non-zero ranks, the global symmetry is $A_{m_1} \times A_{m_2} \times \mathfrak{u}(1)$. As a feature of Hasse diagrams, the non-abelian part of the global symmetry is given by the two slices directly connected to the origin. Note, since m_1 and m_2 can be different, the Hasse diagram becomes less symmetric as one moves away from the bottom.

We observe that in the Hasse diagram of $\text{Gr}_{\text{PSL}(m_1+m_2+2, \mathbb{C})}$, if we keep the leaves where only the ranks of the first m_1 gauge nodes are non zero, then the resulting diagram is finite and is the Hasse diagram of the nilpotent orbits of $\mathfrak{sl}(m_1 + 1, \mathbb{C})$.

Non-linear $D_N, E_{6,7,8}$ quivers. The treatment is almost identical to the A -type affine Grassmannians except for the novelty that one may add d_n, e_6, e_7, e_8 elementary slices. For A -type affine Grassmannian, we mentioned how n unflavored gauge groups between two flavored gauge groups allow the addition of an a_n slice. We can now generalize this by considering the subset of n flavorless gauge nodes that are bounded by flavored gauge nodes. Then, one is allowed to add the elementary slice that is the closure of the minimal nilpotent orbit of \mathfrak{g}_n , where \mathfrak{g}_n is the finite Dynkin diagram in the shape of the unflavored

¹⁴The transition in the corresponding brane system is (4.10).

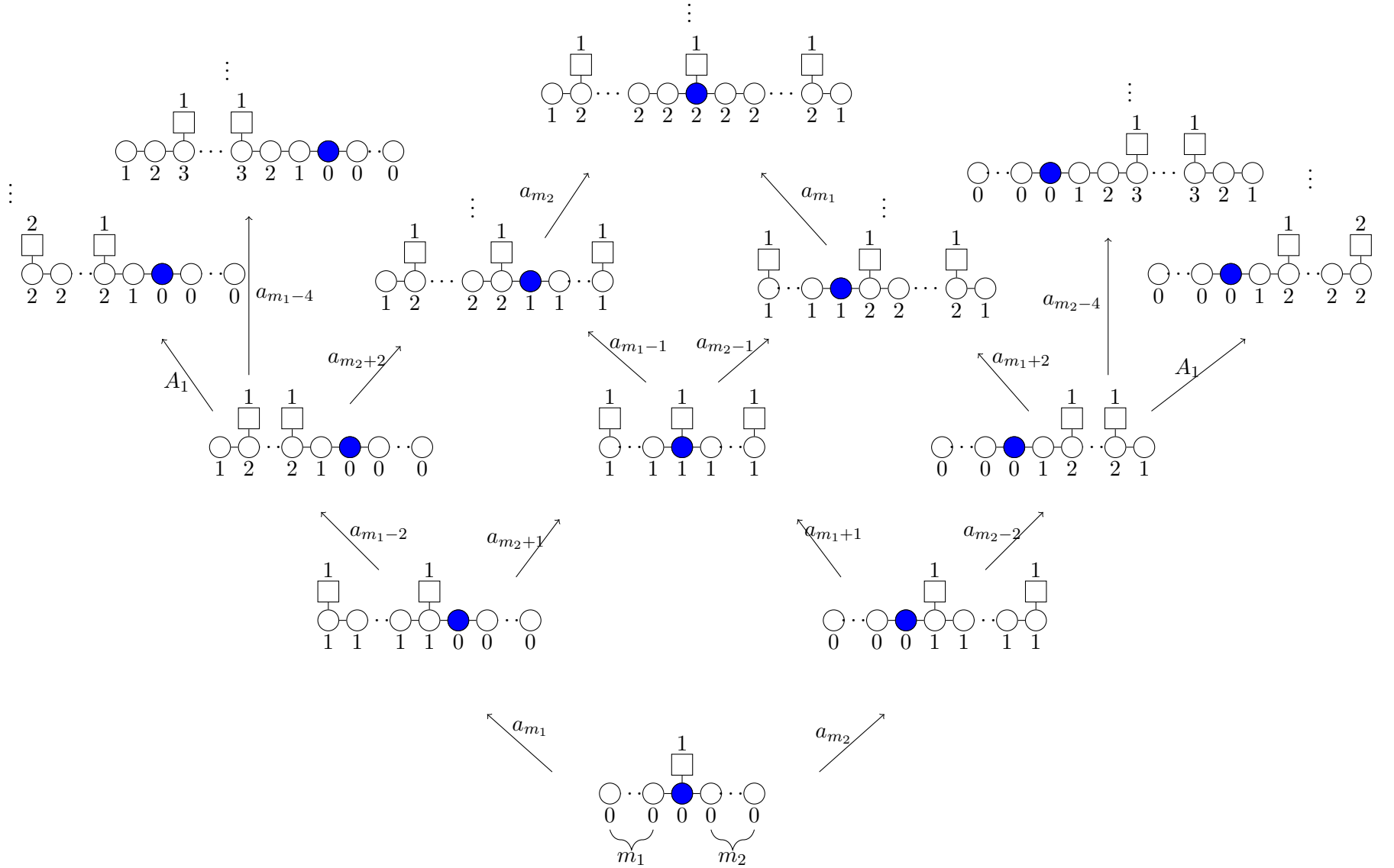


Figure 24. Hasse diagram for the first orbits in the component of $\text{Gr}_{\text{PSL}(m_1+m_2+2, \mathbb{C})}$ corresponding to the lowest coweight $\Omega_{1+m_1} = [0 \dots 0 \underbrace{1}_{m_1} 0 \dots 0]$ for $m_1, m_2 \geq 6$. Blue nodes represent unbalanced gauge groups.

gauge nodes. Let us demonstrate this with some slices of E_6 affine Grassmannian:

add a_5

(5.7)

Here, we can add a a_5 slice to the nodes that make up a a_5 finite Dynkin diagram in the red box.

add d_5

(5.8)

Here, we can add a d_5 slice to the nodes that make up a d_5 finite Dynkin diagram in the red box.

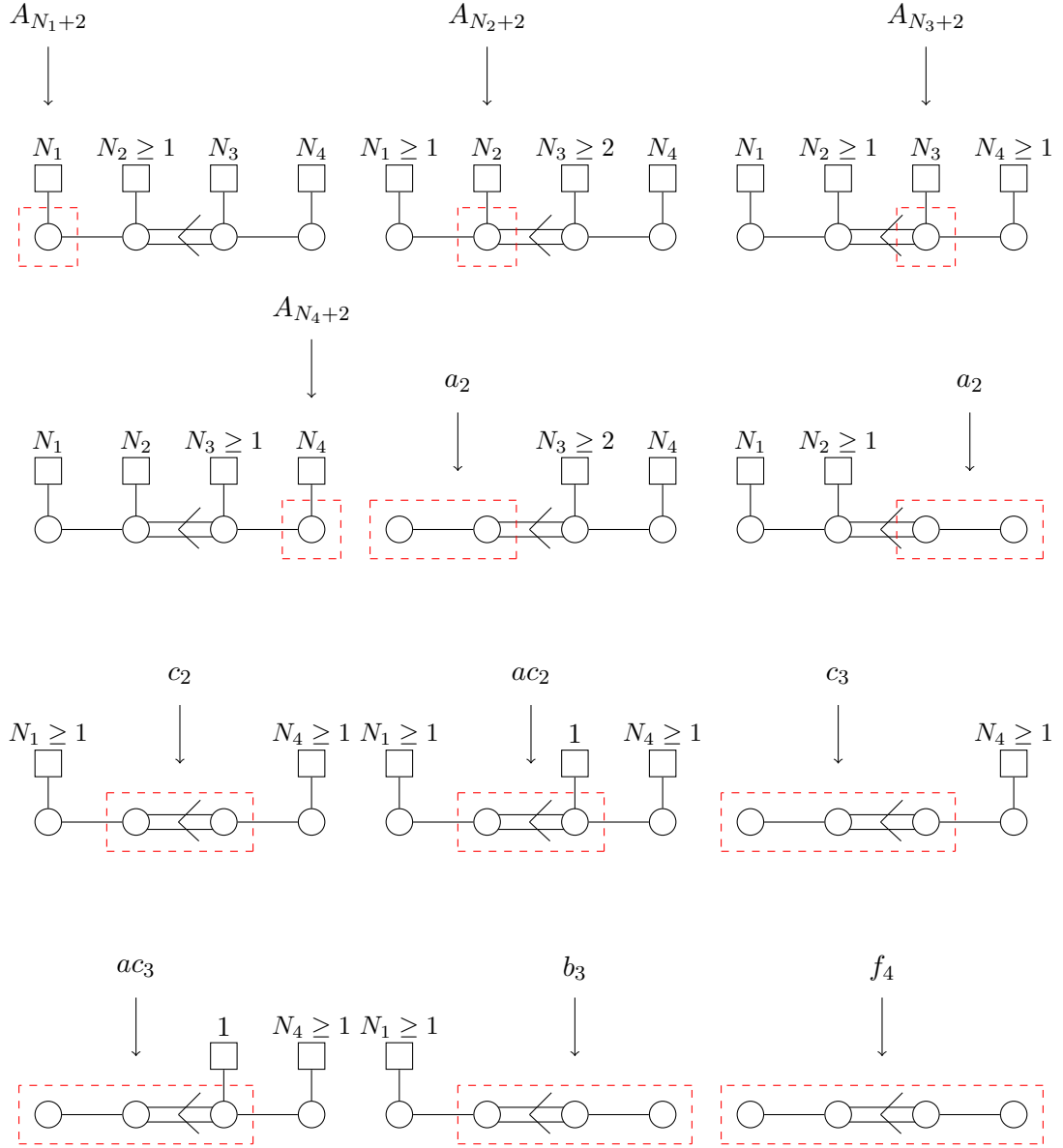


Figure 25. Quiver addition rules regarding slices in the affine Grassmannian of F_4 . We just illustrate step 1 of the algorithm, as once the slices to be added are identified, step 2 is straightforward. The red boxes indicate where the quivers for the slices, which can be found in Table 1, have to be added. When no condition is written on a flavor node rank N_i , it means that it can take any value $N_i \geq 0$.

where

$$x^\lambda = \prod_{i=1}^r x_i^{\langle \lambda, \alpha_i^\vee \rangle} \quad (6.3)$$

and r is the rank of G .

The Hilbert series $\text{HS}_{G,\lambda}^\mu$ of a (finite dimensional) transverse slice $\overline{[\mathcal{W}_G]_\lambda}^\mu = [\mathcal{W}_G]_\lambda \cap [\text{Gr}_G]^\mu$ approximates the Hilbert series for the infinite dimensional transverse slice (6.2),

and this approximation gets better when μ gets large. More precisely,

$$\lim_{\langle \rho, \mu \rangle \rightarrow \infty} \text{HS}_{G,\lambda}^\mu(t; x) = \text{HS}_{G,\lambda}(t; x), \quad (6.4)$$

where ρ is the Weyl vector. In this equation, $\text{HS}_{G,\lambda}^\mu$ can be computed using the monopole formula on the quiver \mathbf{Q}_λ^μ . When μ gets larger, the ranks of the gauge nodes in \mathbf{Q}_λ^μ increase while the imbalance stays fixed. In the remainder of this section, we elaborate on the appearance of new generators in the chiral ring when these ranks increase, focusing on two examples with $G = \text{Sp}(4, \mathbb{C})$ and $\lambda = 0$ and $\lambda = \varpi_2$ respectively.

The case $\lambda = 0$. By means of the Hilbert series, we are studying the moduli space generators and the relations between them. Let us consider slices in the affine Grassmannian of G where all gauge groups are balanced (i.e. slices to the origin, $\lambda = 0$). If all the generators appear at order t^2 in the Hilbert series, the Coulomb branch is the closure of a nilpotent orbit of G [67]. However, by increasing the ranks of the gauge groups, whilst maintaining the balance, new generators show up at higher orders.

For example, let us consider slices of the $G = \text{Sp}(4, \mathbb{C})$ affine Grassmannian for $\lambda = [0, 0]$:

Slices of $[\text{Gr}_{\text{Sp}(4, \mathbb{C})}]_{\lambda=0}$	PL[HS]	Slices of $[\text{Gr}_{\text{Sp}(4, \mathbb{C})}]_{\lambda=0}$	PL[HS]
 $\begin{array}{cc} 1 & 0 \\ \square & \square \\ & \\ \bigcirc & \bigcirc \\ & \swarrow \\ 1 & 1 \end{array}$	$[2, 0]_{C_2} t^2 + \dots$	 $\begin{array}{cc} 1 & 2 \\ \square & \square \\ & \\ \bigcirc & \bigcirc \\ & \swarrow \\ 2 & 3 \end{array}$	$[2, 0]_{C_2} t^2 + [2, 0]_{C_2} t^4 + \dots$
 $\begin{array}{cc} 0 & 2 \\ \square & \square \\ & \\ \bigcirc & \bigcirc \\ & \swarrow \\ 1 & 2 \end{array}$	$[2, 0]_{C_2} t^2 + \dots$	 $\begin{array}{cc} 0 & 4 \\ \square & \square \\ & \\ \bigcirc & \bigcirc \\ & \swarrow \\ 2 & 4 \end{array}$	$[2, 0]_{C_2} t^2 + [2, 0]_{C_2} t^4 + \dots$
 $\begin{array}{cc} 2 & 0 \\ \square & \square \\ & \\ \bigcirc & \bigcirc \\ & \swarrow \\ 2 & 2 \end{array}$	$[2, 0]_{C_2} t^2 + [2, 0]_{C_2} t^4 + \dots$	 $\begin{array}{cc} 3 & 0 \\ \square & \square \\ & \\ \bigcirc & \bigcirc \\ & \swarrow \\ 3 & 3 \end{array}$	$[2, 0]_{C_2} t^2 + [2, 0]_{C_2} t^4 + [2, 0]_{C_2} t^6 + \dots$

(6.5)

where the first few terms of the PL of the Hilbert series are written, giving the quantum numbers of the generators of the Coulomb branch. In general, one starts with the affine Dynkin quiver of C_2 which contributes $[2, 0]t^2$ for the generators. Once all gauge nodes increase their rank by 1, a generator transforming in $[2, 0]t^4$ is added. This pattern persists

for any addition of 1 to all gauge nodes, and we see the quivers in the blue boxes are precisely those where new generators in the adjoint representation appear. In general, for the quiver

$$\begin{array}{ccc}
 1+x & 0 \\
 \square & \square \\
 | & | \\
 \bigcirc & \bigcirc \\
 1+x & 1+x
 \end{array}
 \quad (6.6)$$

one finds

$$\text{PL} \left[\text{HS}_{\text{Sp}(4, \mathbb{C}), \lambda=[0,0]}^{\mu=[1+x,0]} \right] = \sum_{i=0}^x [2,0]_{C_2} t^{2(1+i)} + O(t^{2(2+x)}) = [2,0]_{C_2} t^2 \frac{1-t^{2+2x}}{1-t^2} + O(t^{2(2+x)}). \quad (6.7)$$

As $x \rightarrow \infty$, we see the Coulomb branch Hilbert series takes the following form:

$$\text{HS}_{\text{Sp}(4, \mathbb{C}), [0,0]} \text{PE} \left[[2,0]_{C_2} \frac{t^2}{1-t^2} \right]. \quad (6.8)$$

In this equation, it is understood that $[2,0]_{C_2}$ stands for a character whose variables participate in the plethystic exponential. Explicitly, using fundamental weight fugacities x_i of C_2 , this is

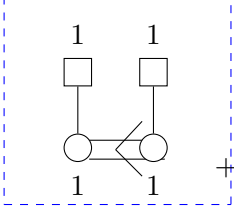
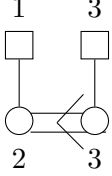
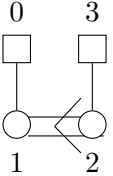
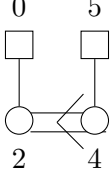
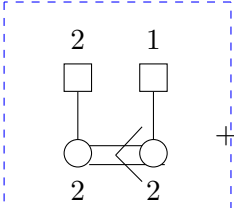
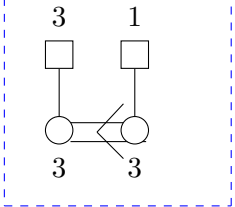
$$\text{HS}_{\text{Sp}(4, \mathbb{C}), [0,0]}(t; x_i) = \text{PE} \left[\left(x_1^2 + x_2 + \frac{x_2^2}{x_1^2} + \frac{x_1^2}{x_2} + 2 + \frac{x_2}{x_1^2} + \frac{x_1^2}{x_2^2} + \frac{1}{x_2} + \frac{1}{x_1^2} \right) \frac{t^2}{1-t^2} \right] \quad (6.9)$$

This reproduces the limit (6.4).

The reasoning behind this is as follows: if one increases the rank of *all* the gauge groups, then new generators appear. This is most easily seen in the cases of algebras of type A and C where the comarks are all equal to 1. If we increase all the ranks by 1, then the number of new generators is the dimension of the adjoint representation. For type A and C and all nodes balanced, we are able to simultaneously increase the rank of all gauge groups by 1 and at the same time maintaining a fully balanced quiver. Since the balance is maintained, the new generators transform always in the adjoint representation. Each time this is done, a new set of generators in the adjoint appears at higher and higher order. One can consider repeating this counting process for other Lie algebras, but since some comarks are > 1 , the situations is more involved and is left for future work.

The cases $\lambda \neq 0$. If $\lambda \neq 0$, the quiver is unbalanced. However, the total number of generators is still an integer multiple of the dimension of the adjoint representation of G ,

but with generators spread over different orders of t . Consider $\lambda = [0, 1]$ for $G = \text{Sp}(4, \mathbb{C})$:

Slices of $[\text{Gr}_{\text{Sp}(4, \mathbb{C})}]_{\lambda=[0,1]}$	PL[HS]	Slices of $[\text{Gr}_{\text{Sp}(4, \mathbb{C})}]_{\lambda=[0,1]}$	PL[HS]
	$([2]_{A_1} + [0]_{A_1})t^2 + (q + q^{-1})[2]_{A_1}t^3 + \dots$		$([2]_{A_1} + [0]_{A_1})t^2 + (q + q^{-1})[2]_{A_1}t^3 + ([2]_{A_1} + [0]_{A_1})t^4 + (q + q^{-1})[2]_{A_1}t^5 + \dots$
	$([2]_{A_1} + [0]_{A_1})t^2 + (q + q^{-1})[2]_{A_1}t^3 + \dots$		$([2]_{A_1} + [0]_{A_1})t^2 + (q + q^{-1})[2]_{A_1}t^3 + ([2]_{A_1} + [0]_{A_1})t^4 + (q + q^{-1})[2]_{A_1}t^5 + \dots$
	$([2]_{A_1} + [0]_{A_1})t^2 + (q + q^{-1})[2]_{A_1}t^3 + ([2]_{A_1} + [0]_{A_1})t^4 + (q + q^{-1})[2]_{A_1}t^5 + \dots$		$([2]_{A_1} + [0]_{A_1})t^2 + (q + q^{-1})[2]_{A_1}t^3 + ([2]_{A_1} + [0]_{A_1})t^4 + (q + q^{-1})[2]_{A_1}t^5 + ([2]_{A_1} + [0]_{A_1})t^6 + (q + q^{-1})[2]_{A_1}t^7 + \dots$

(6.10)

Due to the overbalanced gauge node, the global symmetry is now $\mathfrak{su}(2) \times \mathfrak{u}(1)$ with $[]_{A_1}$ and q Dynkin labels respectively. Compared with (6.5), we see that the total number of generators (at all orders of t combined) remains the same. However, due to the unbalanced gauge node, some generators appear at higher orders and acquire non-trivial $\mathfrak{u}(1)$ charge. The precise irreducible representations for these generators depend on which node of the balanced quiver it is connected to [68]. This easily generalizes to $\lambda = [0, \lambda_2]$ such that in the large rank limit, we can once again derive the freely generated Hilbert series:

$$\begin{aligned}
 \text{HS}_{\text{Sp}(2), [0, \lambda_2]}(t) &= \text{PE} \left[\sum_{i=1}^{\infty} (\dim([2]_{SU(2)}) + 1) t^{2i} + 2 \dim([2]_{SU(2)}) t^{2i + \lambda_2} \right] \\
 &= \text{PE} \left[\sum_{i=1}^{\infty} 4t^{2i} + 6t^{2i + \lambda_2} \right]
 \end{aligned} \tag{6.11}$$

and refining with x_i and q , the fundamental weight fugacities of $\mathfrak{su}(2) \times \mathfrak{u}(1)$, yields:

$$\text{HS}_{\text{Sp}(2), [0, \lambda_2]}(t; x_i, q) = \text{PE} \left[\frac{(2 + x^2 + \frac{1}{x^2})t^2 + (q + \frac{1}{q})(1 + x^2 + \frac{1}{x^2})t^{2 + \lambda_2}}{1 - t^2} \right]. \tag{6.12}$$

This agrees with (6.2). A similar analysis can be made for any coweight λ and any group G .

Observation about number of generators. We have the following generalization of the observations above. Take a slice $\overline{[\mathcal{W}_G]_\mu}^\lambda$ in the affine Grassmannian of a group G , with global symmetry $G' \subset G$. The adjoint representation, identified with the Lie algebra, is decomposed as

$$\mathfrak{g} \mapsto \underbrace{\mathfrak{g}'}_{\text{appears at } t^2} + \underbrace{R'}_{\text{appears at higher orders}} \quad (6.13)$$

where R' is a (possibly reducible) representation of G' . In the Hilbert series of $\overline{[\mathcal{W}_G]_\mu}^\lambda$, \mathfrak{g}' appears at t^2 while irreducible representations in R' appear at higher orders of t . The only further sets of generators (if there are any) are in the same representations $\mathfrak{g}' + R'$ but appear at higher orders in t , shifted by a fixed integer. The total number of generators is hence an integer multiple of the dimension of G . One could say that the adjoint of G is “stretched” over higher orders.

6.2 A note on Infinity

The affine Grassmannian is infinite dimensional, and this aspect pervades through all parts of this paper, in which we met infinite Hasse diagrams, configurations with infinitely many branes, Hilbert series with infinitely many generators. However in all those cases, these infinite quantities do not represent a problem, because they can be approached in a controlled way by finite quantities. In our language, this translates into equalities of the type

$$\lim_{N \rightarrow \infty} \mathcal{C}^{3d} \left(\begin{array}{c} \square^{2N} \\ \circlearrowleft_N \end{array} \right) = \text{Gr}_{\text{SL}(2\mathbb{C})}. \quad (6.14)$$

The affine Grassmannian appears here as a controlled limit of finite dimensional Coulomb branches. The reason why the limit (6.14) makes sense is because each term in the sequence is a subset of the next term:

$$\mathcal{C}^{3d} \left(\begin{array}{c} \square^{2N} \\ \circlearrowleft_N \end{array} \right) \subset \mathcal{C}^{3d} \left(\begin{array}{c} \square^{2(N+1)} \\ \circlearrowleft_{N+1} \end{array} \right). \quad (6.15)$$

This property is the reason why we can build the bottom part of the Hasse diagrams of the infinite dimensional affine Grassmannian using only data from the finite dimensional Coulomb branches corresponding to transverse slices. In algebraic geometry, this is the main idea behind the construction of so-called *ind-schemes*, of which the affine Grassmannian is a prime example.

All the infinite quantities that appear in this paper can be regularized that way. For instance, the brane setup (4.1) should be seen as the limit

$$\lim_{N \rightarrow \infty} \left(\begin{array}{c} \text{Diagram of brane setup} \end{array} \right) \quad (6.16)$$

where the fundamental property that the system for a given N is included into the system for $N + 1$ is again satisfied. On that diagram, we can now compute the linking number of the D5 branes at finite N to be $N - (N - 1) - N + (N - 1) = 0$, independent of N . Therefore in the infinite limit, the D5 branes also have linking number 0. On the other hand, if one adds a D5 brane between the two NS5 branes in (6.16), its linking number is equal to $N - N - (N - 1) + N = 1$ for all N , and therefore is 1 in the limit, as claimed below the brane system (4.4).

Finally, the same logic is behind the formulas for the Hilbert series as infinite products (6.2) obtained as a limit (6.4), and underlies the observations about the generators made in the previous subsection.

7 Outlook

In this paper we explore the Hasse diagrams and transverse slices of various affine Grassmannians, using both quivers and branes. Every slice in the affine Grassmannian, specified by two dominant coweights $\lambda \leq \mu$, of a finite dimensional simple group G is the Coulomb branch of a good framed quiver in the shape of the Dynkin diagram of G . The coweight μ (in coweight basis) is the framing, while λ is the imbalance. For classical groups Kraft-Process transitions in brane systems naturally reproduce Hasse diagram of the affine Grassmannian and all transverse slices. Quiver subtraction proves effective in the realm of the affine Grassmannian. A new notion called *quiver addition* is introduced. Asking for the reverse of quiver subtraction in the sense that for a quiver Q we take an ‘addable’ quiver S and produce a new quiver Q' , such that $Q' = Q - S$ leads to an infinite number of possibilities. When we limit to slices in the affine Grassmannian however, we have a finite number of possibilities. Starting with a coweight, quiver addition produces the entire Hasse diagram of slices to this coweight. This agrees perfectly with the brane construction.

‘Ugly’ and ‘bad’ quivers. Of course quivers, as well as brane systems, are not limited to ‘good’ theories. Theories which have a negative imbalance have Coulomb branches dubbed *generalized affine Grassmannian slices* [12], which are also specified by two coweights, but the lower coweight, λ , is not required to be dominant, i.e. the imbalance is allowed to be negative. Quivers and brane systems for these generalized slices are easily produced, and

the Hasse diagram may be obtained using quiver subtraction or Brane moves. It would be nice to explore these theories in the future.

Other brane systems. We expect that for many brane systems consisting of Dp , NS5, and $D(p+2)$ branes (with $p \leq 6$), and more general systems, there exists a corresponding slice in the affine Grassmannian (provided that every gauge group in the effective theory has enough flavors). We hope to explore brane systems, other than the D3, NS5, and D5 systems in this paper, in the future.

Relation to nilpotent orbits and $T_\rho^\sigma[G]$ theories. Quivers for slices in the affine Grassmannian of A -type and $T_\rho^\sigma[SU]$ theories coincide. They are the good framed linear quivers. For other groups this is not the case. While the construction for T_ρ^σ theories for other classical groups uses O3 orientifold planes and linear orthosymplectic quivers, the construction for affine Grassmannian slices uses ON planes and Dynkin shape unitary quivers. The moduli spaces only coincide in few cases, and are related through quotients in few more. Exploring the relationship between T_ρ^σ theories and slices in the affine Grassmannian are left for future work.

Symplectic duality. The quivers associated to slices in the affine Grassmannian for simply laced groups also possess a Higgs branch. Their Hasse diagrams are simply obtained from *inversion* [57]. It could be interesting to ask for some notion of the symplectic dual of the entire affine Grassmannian.

Relation to other work. We expect there to be many other interesting lines of research involving the affine Grassmannian in physics, such as in the context of little strings [69, 70], or domain walls [71].

Acknowledgements

AH would like to extend special thanks to Jacob Matherne for explaining basic concepts about the affine Grassmannian, and for email exchange together with Santiago Cabrera, where early versions of the main topic of this paper were conceived. We are grateful to Alex Weekes for helping us understand the mathematical literature and for vital insights. Furthermore we would like to thank Travis Schedler for many helpful discussions throughout the years. AB would like to thank Daniel Juteau for many profitable exchanges. The work of AB, JFG, AH and ZZ is supported by STFC grant ST/P000762/1 and ST/T000791/1. The work of MS is supported by the National Thousand-Young-Talents Program of China, the National Natural Science Foundation of China (grant no. 11950410497), and the China Postdoctoral Science Foundation (grant no. 2019M650616).

A Branes, ON Planes and Quivers

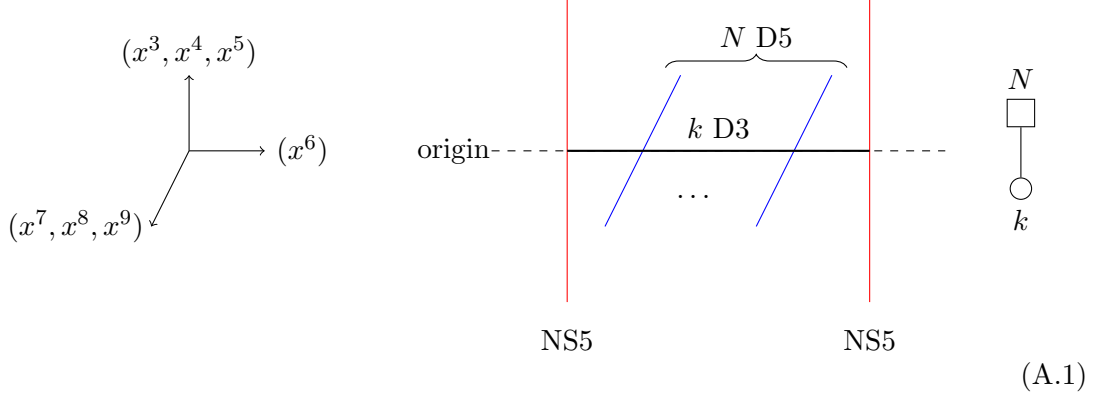
In this appendix we review allowed configurations of branes in the presence of ON planes. We construct brane systems of NS5 branes, D5 branes and D3 branes in Type IIB String

	x^0	x^1	x^2	x^3	x^4	x^5	x^6	x^7	x^8	x^9
NS5	x	x	x	x	x	x				
D3	x	x	x				x			
D5	x	x	x					x	x	x
ON	x	x	x	x	x	x				

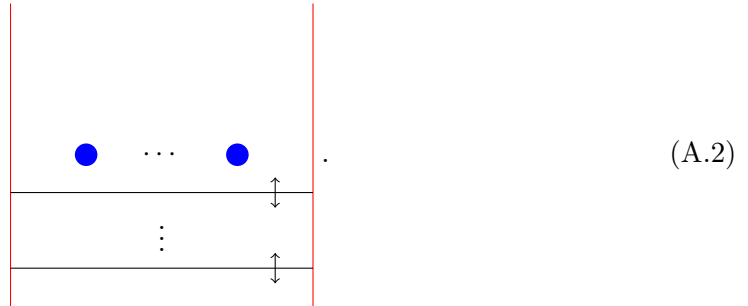
Table 8. Type IIB set up. The 'x' mark the spacetime directions spanned by the various branes and, if present, the ON plane. All NS5 branes are localized at the same value of (x^7, x^8, x^9) . All D5 branes are localized at the same value of (x^3, x^4, x^5) .

Theory as first developed in [9], with the addition of ON planes. The space-time extension of the branes are collected in Table 8.

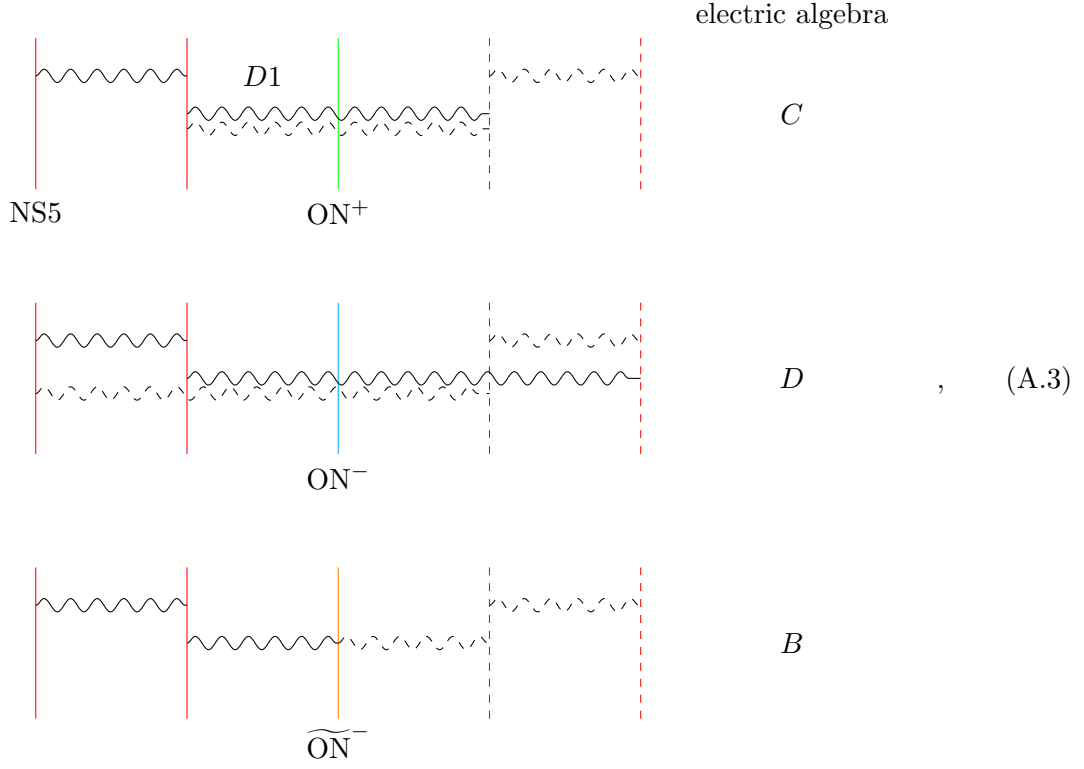
The low energy theory on the world-volume of D3 branes suspended between NS5 branes is a $3d \mathcal{N} = 4$ quiver gauge theory, where D5 branes provide flavour nodes. For example, the following set up:



We will suppress the (x^7, x^8, x^9) direction from now on and draw D5 branes as \bullet . The position of D3 branes along the NS5 branes, as depicted in (A.2), correspond to Coulomb branch moduli:

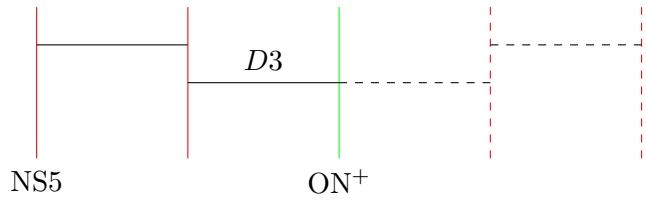
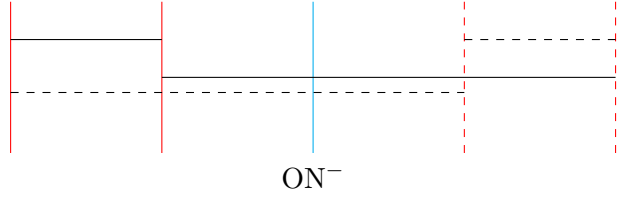
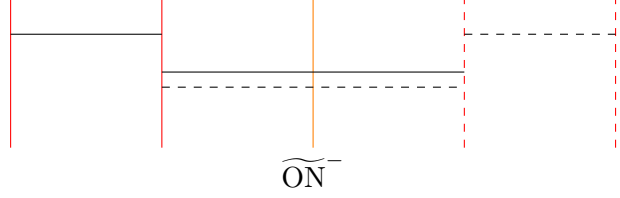


Including ON planes. The gauge group on the world-volume of a stack of NS5 branes on top of an ON plane is given by the allowed D1 branes (and their mirror images) ending on NS5 branes and their mirror images. This is analogous to stacks of D3 branes on top of O3 planes with fundamental strings stretched between them, studied in [72]. The allowed D1 states and the corresponding gauge/electric algebra on the world-volume of the NS5 branes are:



where dashed lines correspond to mirror images (in the main text we use solid lines).

The endpoints of D3 branes play the role of magnetic monopoles on the world-volume of the NS5 branes, and the D3 branes play the role of roots of the GNO dual/magnetic algebra [73]. The allowed D3 states and corresponding magnetic algebras are:

	magnetic algebra	quiver type
 <p>NS5 ON⁺</p>	B	C
 <p>ON⁻</p>	D	D
 <p>$\widetilde{\text{ON}}^-$</p>	C	B

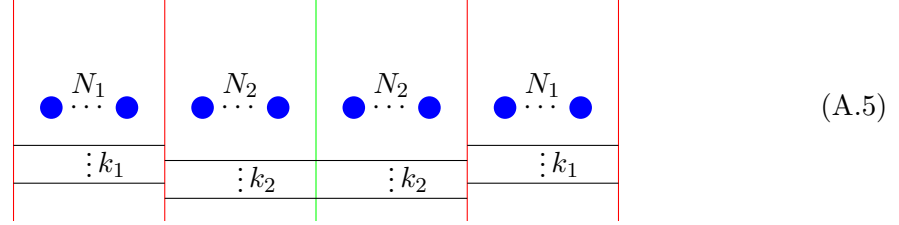
(A.4)

However, the quiver representation of the low energy theory on the world-volume of D3 branes suspended between NS5 branes in presence of an ON plane is not in the form of the Dynkin diagram associated to the magnetic algebra of the ON plane given in (A.4). Rather, D3 branes corresponding to a short root of the magnetic algebra will produce a gauge node which is a long node in the quiver and vice versa, as pointed out in [74]. The quiver type is also indicated in (A.4).

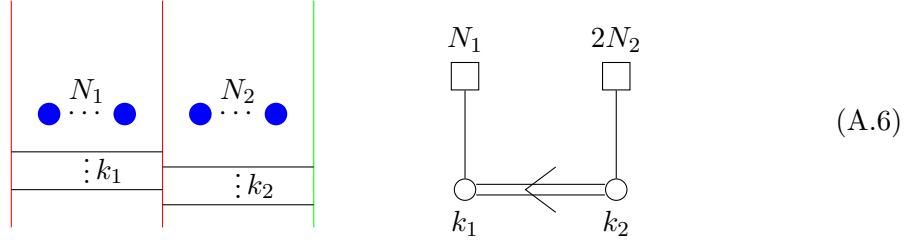
Reading the quiver. In the following, and in the main text, we denote both a brane and its mirror image with a solid line. A stack of k D3 branes between two NS5 branes away from an ON leads to a $U(k)$ gauge node in the corresponding quiver, as depicted in (A.1). The presence of an ON plane does not have an effect on the type of gauge groups in the quiver (they remain unitary), but one has to use the following rules to read the shape of the quiver:

A.1 ON^+

In the presence of an ON^+ we can study the following brane system. (D3 branes are drawn away from the origin for clarity)

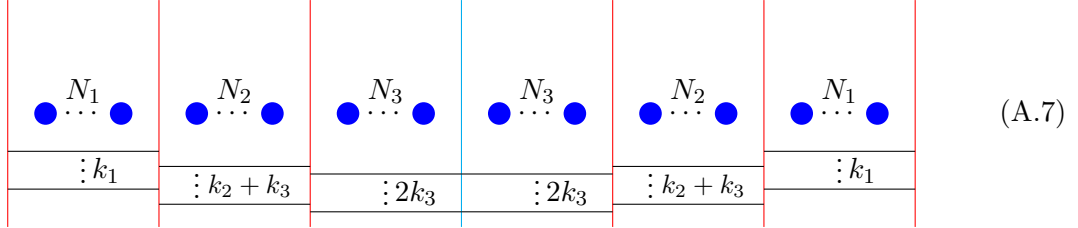


We can restrict to the physical system, move onto the Coulomb branch, and read the corresponding quiver:

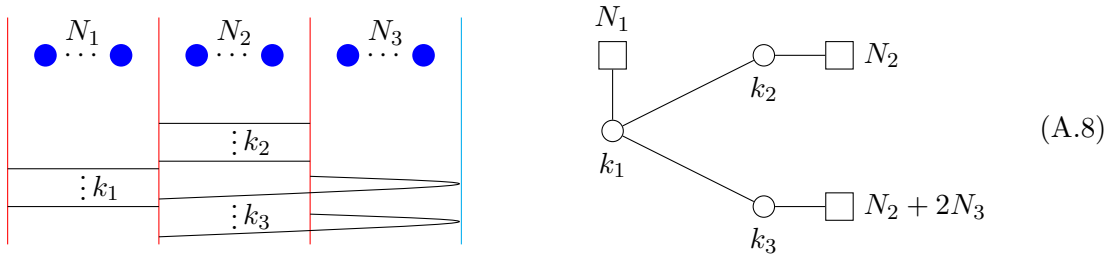


A.2 ON^-

In the presence of an ON^- we can study the following brane system.



In order to move onto the Coulomb branch and read a quiver from the brane system, one has to be careful. For a general system, where $N_3 > 0$, there will be several quivers one can read, depending on boundary conditions. This is investigated in detail in [75] and we only state the possibilities here. The first option is the most natural one, identified in the literature before [76]:



The second option is obtained, when one of the $2k_3$ D3 branes crossing the ON^- ends on one of the N_3 D5 branes instead of NS5 branes. This leads to a different possibility of

breaking the D3 branes along the NS5 branes, and provides a different electric quiver (The horizontal separation of D5 branes is only for ease of reading):

(A.9)

One can keep going in this way. Overall there are $\min\{N_3 + 1, k_3 + 1\}$ possibilities, labelled by $l \in \{0, \dots, \min\{N_3, k_3\}\}$:

(A.10)

Note that in order to transition between two leaves, whose closure is described by two quivers with different l in (A.10), one needs to move onto a lower leaf which appears in the stratification of both spaces.

A.3 $\widetilde{\text{ON}}^-$

In the presence of an $\widetilde{\text{ON}}^-$ we can study the following brane system.

(A.11)

We can restrict to the physical system and read the corresponding quiver:

(A.12)

A.4 Leaf Closures and Transverse Slices in Brane Systems

In this section we investigate how to not only to identify the low energy theory living on D3 branes in a brane system, but how to analyse the stratification of its moduli space using branes. For a given brane system there are various distinct phases, which correspond to the symplectic leaves that make up its moduli space. In the following we will only consider Coulomb branch phases. For an analysis of the full moduli space, including a brane perspective, see [57]; we repeat what is needed for this paper in the following. Let \mathcal{C} be the Coulomb branch of the low energy theory living on the brane system. For every symplectic leaf $\mathcal{L} \subset \mathcal{C}$ there is a Coulomb phase \mathcal{P} in the brane system. From the phase \mathcal{P} we can read a quiver \mathbf{Q} , whose Coulomb branch $\mathcal{C}(\mathbf{Q}) = \overline{\mathcal{L}}$ is the closure of the symplectic leaf \mathcal{L} corresponding to the phase \mathcal{P} . The phases of the brane system are distinguished, by how many branes coincide at the origin, i.e. how many massless states are present in the field theory when on the leaf \mathcal{L} on its Coulomb branch. Let us look at the example of $U(2)$ with 4 fundamental hypers. The Hasse diagram of its Coulomb branch is straightforwardly computed, e.g. through quiver subtraction:

$$\begin{array}{c} \bullet \\ A_3 \\ \bullet \\ A_1 \\ \bullet \end{array} \begin{array}{l} \mathcal{L}_c \\ \\ \mathcal{L}_b \\ \\ \mathcal{L}_a \end{array} \quad \text{for} \quad \mathcal{C} \left(\begin{array}{c} 4 \\ \square \\ \circ \\ 2 \end{array} \right) \quad (\text{A.13})$$

Where we labelled the leaves by \mathcal{L}_i , $i = a, b, c$. The three distinct Coulomb phases of the brane system are:

$$\begin{array}{ccc} \mathcal{P}_a & \mathcal{P}_b & \mathcal{P}_c \end{array} \quad (\text{A.14})$$

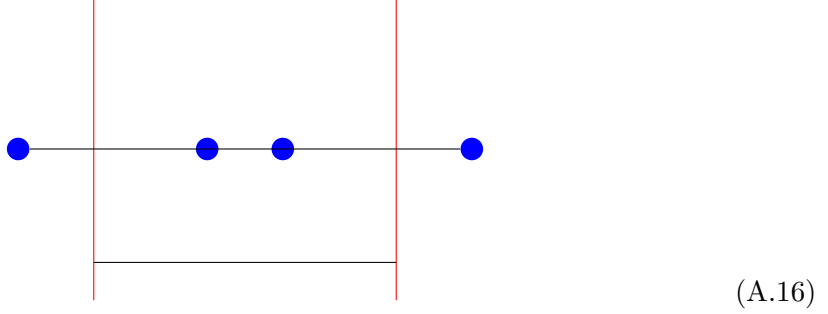
The quiver for the most general Coulomb phase, \mathcal{P}_c , is easily read off. It is the theory itself:

$$\mathbf{Q}_c = \begin{array}{c} 4 \\ \square \\ \circ \\ 2 \end{array} \quad (\text{A.15})$$

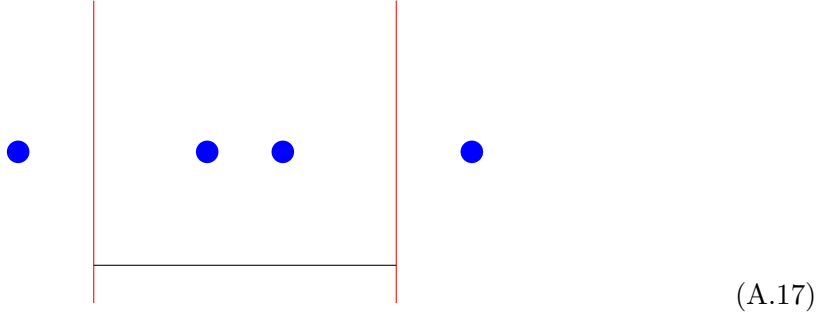
The quiver not only describes the phase \mathcal{P}_c , but also the possibility of the D3 branes moving to the origin. It is a quantum field theory in its own right with a moduli space

consisting of several leaves. Hence its Coulomb branch is not the leaf \mathcal{L}_c itself, but the closure of the leaf $\overline{\mathcal{L}}_c$, or in other words, the transverse slice from the origin, \mathcal{L}_a , to the leaf \mathcal{L}_c .

The quiver for the phase \mathcal{P}_b is more tricky to work out. There is one D3 brane resting at the origin. We first have to make this D3 brane end on D5 branes rather than NS5 branes. This can be done through a Hanany-Witten transition. The resulting brane system is:



Now we have to ignore the possibility of the D3 brane, which is supposed to rest at the origin, to move along the NS5 branes. We do this by simply not drawing it:



Now we can read a quiver from this brane system:

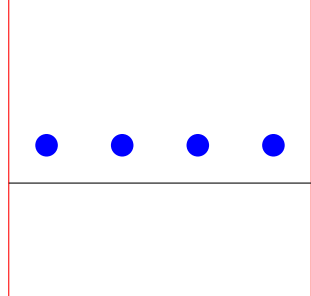
$$Q_b = \begin{array}{c} 2 \\ \square \\ | \\ \circ \\ 1 \end{array} \quad (A.18)$$

The Coulomb branch of Q_b is the closure $\overline{\mathcal{L}}_b$.

The quiver associated to \mathcal{P}_a , the origin, is trivial:

$$Q_a = \begin{array}{c} 0 \\ \square \\ | \\ \circ \\ 0 \end{array} \quad (A.19)$$

The quivers we have computed represent closures of the leaves. This corresponds to transverse slices from the origin \mathcal{L}_a to the leaf \mathcal{L}_i in question. We can also obtain a quiver for any other transverse slice. The remaining non-trivial slice for our theory is the one from \mathcal{L}_b to \mathcal{L}_c , we refer to the corresponding quiver as $Q_{b->c}$. We can obtain the quiver from the brane system in the following way: Comparing the two phases \mathcal{P}_b and \mathcal{P}_c we have to ignore the modulus which is turned on in both phases. We achieve this by simply not drawing the D3 brane in question; one can think of it as sending the D3 brane off to infinity ¹⁵. The resulting brane system is:


(A.20)

From which a quiver is easily read off:

$$Q_{b->c} = \begin{array}{c} 4 \\ \square \\ | \\ \circ \\ 1 \end{array}$$
(A.21)

The Coulomb branch of this quiver is the transverse slice from \mathcal{L}_b to \mathcal{L}_c .

Of course none of these quivers are new, as they are exactly the quivers involved in quiver subtraction. The point of this exercise was to show, how all transverse slices of the Coulomb branch show up as transitions in the brane system.

In Section 4 we propose brane systems whose Coulomb branch is the transverse slice to the lowest leaf in a connected component of the affine Grassmannian of a classical group. This space is infinite dimensional reflected in the fact that we have an infinite amount of D3 branes present in the brane system. We fix all but a finite amount of D3 branes to be at the origin, in order to study the symplectic leaves the space is made up of from bottom up. For every such leaf we look at the corresponding phase in the brane system and obtain the quiver whose Coulomb branch is the closure of the leaf. Furthermore one can associate a quiver to a transition between any two phases in the brane system. Every good quiver in shape of a classical Dynkin diagram appears this way in one of the brane systems.

¹⁵We have two instances of ignoring a D3 brane by not drawing it: Either fixing it to remain at the origin, or sending it to infinity. When computing the quiver associated to the transition between two non-trivial phases of the brane system, one in general has to use both.

References

- [1] A. Beauville and Y. Laszlo, *Conformal blocks and generalized theta functions*, *Communications in mathematical physics* **164** (1994) 385–419.
- [2] S. Kumar, M. Narasimhan and A. Ramanathan, *Infinite grassmannians and moduli spaces*, *Math. Ann* **300** (1994) 41–75.
- [3] A. Beauville, Y. Laszlo and C. Sorger, *The picard group of the moduli of-bundles on a curve*, *Compositio Mathematica* **112** (1998) 183–216.
- [4] G. Pappas and M. Rapoport, *Twisted loop groups and their affine flag varieties*, *Advances in Mathematics* **219** (2008) 118–198.
- [5] C. Sorger, *Lectures on moduli of principal g -bundles over algebraic curves*, *ICTP Lecture Notes* 3.
- [6] A. Beilinson and V. Drinfeld, “Quantization of hitchin’s integrable system and hecke eigensheaves.”
- [7] V. Ginzburg, *Perverse sheaves on a loop group and langlands’ duality*, *arXiv preprint alg-geom/9511007* (1995) .
- [8] I. Mirković and K. Vilonen, *Geometric langlands duality and representations of algebraic groups over commutative rings*, *Annals of mathematics* (2007) 95–143.
- [9] A. Hanany and E. Witten, *Type IIB superstrings, BPS monopoles, and three-dimensional gauge dynamics*, *Nucl. Phys.* **B492** (1997) 152–190, [[hep-th/9611230](#)].
- [10] A. Malkin, V. Ostrik and M. Vybornov, *The minimal degeneration singularities in the affine Grassmannians*, *arXiv Mathematics e-prints* (May, 2003) math/0305095, [[math/0305095](#)].
- [11] J. Kamnitzer, B. Webster, A. Weekes and O. Yacobi, *Yangians and quantizations of slices in the affine grassmannian*, *Algebra & Number Theory* **8** (2014) 857–893.
- [12] A. Braverman, M. Finkelberg and H. Nakajima, *Coulomb branches of 3d $\mathcal{N} = 4$ quiver gauge theories and slices in the affine Grassmannian*, *Adv. Theor. Math. Phys.* **23** (2019) 75–166, [[1604.03625](#)].
- [13] H. Kraft and C. Procesi, *Minimal singularities in GL_n* , *Inventiones mathematicae* **62** (1980) 503–515.
- [14] H. Kraft and C. Procesi, *On the geometry of conjugacy classes in classical groups*, *Commentarii Mathematici Helvetici* **57** (Dec, 1982) 539–602.
- [15] S. Cabrera and A. Hanany, *Branes and the Kraft-Procesi Transition*, *JHEP* **11** (2016) 175, [[1609.07798](#)].
- [16] S. Cabrera and A. Hanany, *Branes and the Kraft-Procesi transition: classical case*, *JHEP* **04** (2018) 127, [[1711.02378](#)].
- [17] J. de Boer, K. Hori, H. Ooguri, Y. Oz and Z. Yin, *Mirror symmetry in three-dimensional theories, $SL(2, \mathbb{Z})$ and D-brane moduli spaces*, *Nucl. Phys. B* **493** (1997) 148–176, [[hep-th/9612131](#)].
- [18] S. A. Cherkis and A. Kapustin, *Singular monopoles and supersymmetric gauge theories in three-dimensions*, *Nucl. Phys. B* **525** (1998) 215–234, [[hep-th/9711145](#)].
- [19] D. Tong, *Three-dimensional gauge theories and ADE monopoles*, *Phys. Lett. B* **448** (1999) 33–36, [[hep-th/9803148](#)].

- [20] M. Finkelberg, *Double affine grassmannians and coulomb branches of 3d $n=4$ quiver gauge theories*, in *Proceedings of the International Congress of Mathematicians*, World Scientific, 2017. DOI.
- [21] H. Nakajima and A. Weekes, *Coulomb branches of quiver gauge theories with symmetrizers*, [1907.06552](#).
- [22] A. Braverman, M. Finkelberg et al., *Pursuing the double affine grassmannian, i: Transversal slices via instantons on a_k -singularities*, *Duke Mathematical Journal* **152** (2010) 175–206.
- [23] S. Cremonesi, A. Hanany and A. Zaffaroni, *Monopole operators and Hilbert series of Coulomb branches of 3d $\mathcal{N}=4$ gauge theories*, *JHEP* **01** (2014) 005, [[1309.2657](#)].
- [24] H. Nakajima, *Towards a mathematical definition of Coulomb branches of 3-dimensional $\mathcal{N}=4$ gauge theories, I*, *Adv. Theor. Math. Phys.* **20** (2016) 595–669, [[1503.03676](#)].
- [25] M. Bullimore, T. Dimofte and D. Gaiotto, *The Coulomb Branch of 3d $\mathcal{N}=4$ Theories*, *Commun. Math. Phys.* **354** (2017) 671–751, [[1503.04817](#)].
- [26] H. Nakajima, *Questions on provisional Coulomb branches of 3-dimensional $\mathcal{N}=4$ gauge theories*, *arXiv e-prints* (Oct, 2015) arXiv:1510.03908, [[1510.03908](#)].
- [27] A. Braverman, M. Finkelberg and H. Nakajima, *Towards a mathematical definition of Coulomb branches of 3-dimensional $\mathcal{N}=4$ gauge theories, II*, *Adv. Theor. Math. Phys.* **22** (2018) 1071–1147, [[1601.03586](#)].
- [28] H. Nakajima, *Introduction to a provisional mathematical definition of Coulomb branches of 3-dimensional $\mathcal{N}=4$ gauge theories*, [1706.05154](#).
- [29] J. Kamnitzer, D. Muthiah, A. Weekes and O. Yacobi, *Reducedness of affine grassmannian slices in type a* , *Proceedings of the American Mathematical Society* **146** (2018) 861–874.
- [30] D. Muthiah and A. Weekes, *Symplectic leaves for generalized affine grassmannian slices*, *arXiv preprint arXiv:1902.09771* (2019) .
- [31] A. Weekes, *Generators for coulomb branches of quiver gauge theories*, *arXiv preprint arXiv:1903.07734* (2019) .
- [32] A. Bourget, S. Cabrera, J. F. Grimminger, A. Hanany, M. Sperling, A. Zajac et al., *The Higgs mechanism — Hasse diagrams for symplectic singularities*, *JHEP* **01** (2020) 157, [[1908.04245](#)].
- [33] A. Beauville, *Symplectic singularities*, *Inventiones mathematicae* **139** (2000) 541–549.
- [34] J. R. Stembridge, *The partial order of dominant weights*, *Advances in Mathematics* **136** (1998) 340–364.
- [35] Y. Ito, T. Okuda and M. Taki, *Line operators on $S^1 \times \mathbb{R}^3$ and quantization of the Hitchin moduli space*, *JHEP* **04** (2012) 010, [[1111.4221](#)].
- [36] J. Gomis, T. Okuda and V. Pestun, *Exact Results for 't Hooft Loops in Gauge Theories on S^4* , *JHEP* **05** (2012) 141, [[1105.2568](#)].
- [37] B. Assel and A. Sciarappa, *On monopole bubbling contributions to 't Hooft loops*, *JHEP* **05** (2019) 180, [[1903.00376](#)].
- [38] B. Assel, S. Cremonesi and M. Renwick, *Quantized Coulomb branches, monopole bubbling and wall-crossing phenomena in 3d $\mathcal{N}=4$ theories*, *JHEP* **04** (2020) 213, [[1910.01650](#)].
- [39] G. Segal, *Loop groups*, in *Arbeitstagung Bonn 1984*, pp. 155–168. Springer, 1985.

- [40] U. Görtz, *Affine springer fibers and affine deligne-lusztig varieties*, in *Affine flag manifolds and principal bundles*, pp. 1–50. Springer, 2010.
- [41] X. Zhu, *An introduction to affine Grassmannians and the geometric Satake equivalence*, *arXiv e-prints* (Mar., 2016) arXiv:1603.05593, [[1603.05593](#)].
- [42] P. Baumann and S. Riche, *Notes on the geometric satake equivalence*, in *Relative aspects in representation theory, Langlands functoriality and automorphic forms*, pp. 1–134. Springer, 2018.
- [43] T. Richarz, *Notes: Basics on affine grassmannians*, https://timo-richarz.com/wp-content/uploads/2020/02/BoAG_02.pdf, accessed November 2020.
- [44] P. Achar, *Lecture: Introduction to affine grassmannians and the geometric satake equivalence*, Notes taken by Jose Simental, https://web.northeastern.edu/iloseu/Achar_lectures.html, accessed November 2020.
- [45] J. C. Brunson, *Matrix Schubert varieties for the affine Grassmannian*. PhD thesis, Virginia Tech, 2014.
- [46] A. Kapustin and E. Witten, *Electric-Magnetic Duality And The Geometric Langlands Program*, *Commun. Num. Theor. Phys.* **1** (2007) 1–236, [[hep-th/0604151](#)].
- [47] E. Witten, *Geometric Langlands And The Equations Of Nahm And Bogomolny*, [0905.4795](#).
- [48] D. Juteau, *Modular representations of reductive groups and geometry of affine grassmannians*, *arXiv preprint arXiv:0804.2041* (2008) .
- [49] D. Gaiotto and E. Witten, *S-Duality of Boundary Conditions In $N=4$ Super Yang-Mills Theory*, *Adv. Theor. Math. Phys.* **13** (2009) 721–896, [[0807.3720](#)].
- [50] A. Hanany and R. Kalveks, *Highest Weight Generating Functions for Hilbert Series*, *JHEP* **10** (2014) 152, [[1408.4690](#)].
- [51] A. Bourget, J. F. Grimminger, A. Hanany, M. Sperling, G. Zafrir and Z. Zhong, *Magnetic quivers for rank 1 theories*, *JHEP* **09** (2020) 189, [[2006.16994](#)].
- [52] A. Bourget, S. Giacomelli, J. F. Grimminger, A. Hanany, M. Sperling and Z. Zhong, *S-fold magnetic quivers*, *JHEP* **02** (2021) 054, [[2010.05889](#)].
- [53] S. Cabrera and A. Hanany, *Quiver Subtractions*, *JHEP* **09** (2018) 008, [[1803.11205](#)].
- [54] S. Cabrera, A. Hanany and M. Sperling, *Magnetic quivers, Higgs branches, and 6d $N=(1,0)$ theories*, *JHEP* **06** (2019) 071, [[1904.12293](#)].
- [55] S. Cabrera, A. Hanany and M. Sperling, *Magnetic quivers, Higgs branches, and 6d $N=(1,0)$ theories — orthogonal and symplectic gauge groups*, *JHEP* **02** (2020) 184, [[1912.02773](#)].
- [56] A. Hanany and R. Kalveks, *Quiver Theories and Hilbert Series of Classical Slodowy Intersections*, *Nucl. Phys. B* **952** (2020) 114939, [[1909.12793](#)].
- [57] J. F. Grimminger and A. Hanany, *Hasse diagrams for 3d $\mathcal{N} = 4$ quiver gauge theories — Inversion and the full moduli space*, *JHEP* **09** (2020) 159, [[2004.01675](#)].
- [58] A. Bourget, J. F. Grimminger, A. Hanany, M. Sperling and Z. Zhong, *Magnetic Quivers from Brane Webs with $O5$ Planes*, *JHEP* **07** (2020) 204, [[2004.04082](#)].
- [59] J. Rogers and R. Tatar, *Moduli space singularities for 3d $\mathcal{N} = 4$ circular quiver gauge theories*, *JHEP* **11** (2018) 022, [[1807.01754](#)].

- [60] J. Rogers and R. Tatar, D_n Dynkin quiver moduli spaces, *J. Phys. A* **52** (2019) 425401, [[1902.10019](#)].
- [61] J. Eckhard, S. Schäfer-Nameki and Y.-N. Wang, *Trifectas for T_N in 5d*, *JHEP* **07** (2020) 199, [[2004.15007](#)].
- [62] C. Closset, S. Schafer-Nameki and Y.-N. Wang, *Coulomb and Higgs Branches from Canonical Singularities: Part 0*, *JHEP* **02** (2021) 003, [[2007.15600](#)].
- [63] M. van Beest, A. Bourget, J. Eckhard and S. Schafer-Nameki, *(Symplectic) Leaves and (5d Higgs) Branches in the Poly(go)nesian Tropical Rain Forest*, *JHEP* **11** (2020) 124, [[2008.05577](#)].
- [64] M. van Beest, A. Bourget, J. Eckhard and S. Schafer-Nameki, *(5d RG-flow) Trees in the Tropical Rain Forest*, [2011.07033](#).
- [65] C. Closset, S. Giacomelli, S. Schäfer-Nameki and Y.-N. Wang, *5d and 4d SCFTs: Canonical Singularities, Trinions and S-Dualities*, [2012.12827](#).
- [66] A. E. Barns-Graham, *Much ado about nothing: The superconformal index and Hilbert series of three dimensional $\mathcal{N} = 4$ vacua*. PhD thesis, Cambridge U., DAMTP, 2018. 10.17863/CAM.35266.
- [67] Y. Namikawa, *A characterization of nilpotent orbit closures among symplectic singularities*, *Mathematische Annalen* **370** (2018) 811–818.
- [68] S. Cabrera, A. Hanany and A. Zajac, *Minimally Unbalanced Quivers*, *JHEP* **02** (2019) 180, [[1810.01495](#)].
- [69] N. Haouzi and C. Schmid, *Little String Origin of Surface Defects*, *JHEP* **05** (2017) 082, [[1608.07279](#)].
- [70] N. Haouzi and C. Schmid, *Little String Defects and Bala-Carter Theory*, [1612.02008](#).
- [71] C. Bachas, J. Hoppe and B. Pioline, *Nahm equations, $N=1^*$ domain walls, and D strings in $AdS(5) \times S(5)$* , *JHEP* **07** (2001) 041, [[hep-th/0007067](#)].
- [72] A. Hanany and J. Troost, *Orientifold planes, affine algebras and magnetic monopoles*, *JHEP* **08** (2001) 021, [[hep-th/0107153](#)].
- [73] P. Goddard, J. Nuyts and D. I. Olive, *Gauge Theories and Magnetic Charge*, *Nucl. Phys.* **B125** (1977) 1–28.
- [74] S. Cremonesi, G. Ferlito, A. Hanany and N. Mekareeya, *Coulomb Branch and The Moduli Space of Instantons*, *JHEP* **12** (2014) 103, [[1408.6835](#)].
- [75] A. Bourget, J. F. Grimminger, A. Hanany, R. Kalveks, M. Sperling and Z. Zhong, *A Tale of N Cones, to appear*.
- [76] G. Ferlito and A. Hanany, *A tale of two cones: the Higgs Branch of $Sp(n)$ theories with $2n$ flavours*, [1609.06724](#).